EXPLORATIONS OF DOMAIN WALLS AND HALF QUANTUM VORTICES IN UNCONVENTIONAL SUPERCONDUCTORS

BY

DAVID GEORGE FERGUSON

DISSERTATION

Submitted in partial fulfillment of the requirements
for the degree of Doctor of Philosophy in Physics
in the Graduate College of the
University of Illinois at Urbana-Champaign, 2011

Urbana, Illinois

Doctoral Committee:

Professor Michael Stone, Chair
Professor Paul M. Goldbart, Director of Research
Professor Raffi Budakian
Professor John Stack

Abstract

Most known superconductors are characterized by spin-singlet superconducting order. An exception is Sr_2RuO_4, for which evidence is accumulating in favor of superconducting order of spin-triplet character, specifically of the equal-spin type of pairing and, furthermore, which may exibit spontaneously broken time reversal symmetry. Triplet superconductors have been proposed to host half quantum vortices, whereas superconductors with spontaneously broken time-reversal symmetry are proposed to admit domain walls that separate regions of opposing chirality. Thus—in addition to conventional vortices—the topological structure of the unconventional superconducting order of Sr_2RuO_4 may allow for at least two additional topologically stable defects. This thesis explores aspects of two unconventional topological defects: In Part I of the thesis we focus on domain walls, and in Part II we turn to half quantum vortices.

In Part I, via a general phenomenological and symmetry based approach, we derive an effective description of superconductivity that spontaneously breaks time reversal symmetry, in terms of the relevant topological coordinates for domain walls and vortices. One of the key consequences expected of broken time-reversal symmetry superconductivity is that in its ground state the system should exhibit chiral currents of charge that are localized near the core of any domain wall and near the boundaries of the sample. However, signatures of such currents, in the form of magnetic fields, have not been observed in Sr_2RuO_4, to date, despite considerable efforts. In this thesis, we explore alternative magnetic signatures of the existence of walls between domains of opposing chirality. We show that, in the limit in which the superconducting system is taken to have in-plane rotational invariance, a

domain wall that is translationally invariant along the z axis (which runs perpendicular to the aforementioned planes) and includes an isolated bend through an angle Θ is accompanied by a nonintegral magnetic *bend flux* of value $\big((\Theta/\pi)+n\big)\Phi_0$, with integral n, that penetrates the superconductor and is localized near the bend. We find this result to be independent of the magnitude of chiral-charge currents that are predicted to flow along the core of domain walls. On the basis of this specialized result and its generalization to cases of discrete crystalline symmetry, we note that the observation of localized, nonintegral flux penetrating a z-axis surface (detected, e.g., via scanned-probe magnetic imaging) can potentially be interpreted in terms of the presence of bent walls between domains of opposing chirality, and hence would be suggestive of the existence of time-reversal symmetry-breaking superconductivity.

In Part II of this thesis we consider half quantum vortices. We begin by developing a classification of the topologically stable line and point defects that are allowed for layered superconductors having triplet equal-spin pairing, under various assumptions about the structure of the superconducting pairing. Here, the central result is that, in contrast to the case of bulk superfluid ^{3}He, half quantum vortices are shown to exist for both the time-reversal symmetry broken *and* time-reversal intact forms of superconducting order. Then, after introducing the structure of the London free energy that effectively describes the energetics of half quantum vortices in such systems, we study the influence of sample geometry on the stability of half quantum vortices, finding that half quantum vortices are expected to be stable for a range of parameters that is wider than previously expected.

An "annular," ring-shaped, geometry is useful in the experimental study of topological line defects such as half quantum vortices because such a geometry is expected to yield a discrete family of low-energy "fluxoid" states in which the superconducting order parameter winds around the annulus as it would around the line defect. Recently, evidence for half integer fluxoid states (the fluxoid analog of half quantum vortices) has been obtained in experiments on mesoscopic, ring-shaped samples of Sr_2RuO_4, using cantilever torque magnetometry [30]. We briefly review the experimental technique and the experimental results

that have emerged from its application to Sr_2RuO_4. We then discuss two possible scenarios for the theoretical interpretation of the observed half integer fluxoid behavior: a half quantum vortex scenario, and a wall vortex scenario. We find the first scenario to be more consistent with the observations, and we suggest further experiments that could provide even more stringent tests of the consistency of this exciting, half quantum vortex scenario.

For Teagan and Kieran and especially my wife and partner Loretta

Acknowledgments

This thesis research is the culmination of my graduate studies at University of Illinois Urbana Champaign. During my time at Illinois I have received brilliant instruction, participated in inspiring collaborations, and made many great friends. The Department of Physics at Illinois is truly a special institution and I will always remember it fondly. I would like to acknowledge a number of people who played an integral role in the completion of this thesis. Firstly, I would like to express my deep gratitude to my adviser, teacher, and collaborator Prof. Paul M. Goldbart. Without his guidance and support this thesis would not have been possible. One of the many advantages of being Paul's student is that you have the good fortune of being introduced to the full range of Paul's research interests. Often, I have found that inspiration for an idea comes from an unexpected direction. In addition to proposing many interesting research projects, I am grateful that Paul has encouraged me to develop and pursue my own wide range of research interests. I am also very appreciative of Paul's commitment to a close collaboration between theoretical and experimental work. My scientific career was forever changed when Paul said the words: "there is some interesting data that I think it would be fun for us to have look at...;" which leads into my next acknowledgement. I would also like to express my deep gratitude and thanks to Joonho Jang and Prof. Raffi Budakian, whose exceptional and fascinating experimental work provided the inspiration for this thesis, and from whose collaboration I have gained so much. It has also been my honor and pleasure to collaborate with my good friend Dr. Victor Vakaryuk. One of the scientific ethics that I feel Victor has helped me more fully appreciate can be summarized as follows: "Is there a simpler explanation?" Finally, I would also like to take this opportunity to thank

Prof. Tony Leggett, whose thoughtful and principled approach to scientific inquiry has been an inspiration to me.

There are many people over the years to whom I owe a debt of gratitude. To all, you have my love and thanks. I would especially like to thank Loretta, Kieran, and Teagan for their love and support. I would also like to thank my Dad for advising me a long time ago to: "Listen carefully, and then think it through for yourself."

Table of Contents

Part I

Domain Walls

Chapter 1

Introduction to domain walls

Recently, there has been developing excitement regarding the nature of the superconducting state of the crystalline compound Sr_2RuO_4 [49]. This is because, as in superfluid ^{3}He, the superconductivity has been proposed to be unconventional, having Cooper pairs of the triplet type [63, 25, 58]. However, questions remain concerning the structure of the pairing state (see, e.g., Refs. [83, 60]) and, in particular, whether half quantum vortices can be energetically stabilized, and whether the superconductivity does indeed spontaneously break time-reversal symmetry, and would thus form a chiral state [48, 80, 31]. An analysis of the existence and stability of half quantum vortices from both the theoretical and experimental perspective, is the subject of Part II of this thesis. In the current part of the thesis we will study aspects of time reversal symmetry breaking superconductivity.

Whether or not the superconducting order of Sr_2RuO_4 is chiral is a particularly vexing question [31]. This is because various probes detect signatures of time reversal symmetry breaking that are coincident with the superconducting transition [48, 80, 32]. However the theoretical prediction (see e.g. [52]) that such chiral states would exhibit chiral charge-currents localized near the boundaries of the sample, has not been verified experimentally, to date, despite considerable efforts [8, 33, 23]. Moreover, if the superconductivity of Sr_2RuO_4 spontaneously breaks time-reversal symmetry then—in addition to vortices—domain walls that separate regions of opposing chirality would enter as a new topological feature of the theory [76]. Analogous to sample edges, domain walls are also predicted to exhibit chiral charge-currents localized near the core of domain walls [76, 52]. However, similarly to edge currents, no obvious magnetic signatures of such domain wall currents have been observed,

to date, in scanning magnetic imagining of Sr_2RuO_4 [8, 33, 23]. These magnetic imaging observations are thus consistent with either the absence of time reversal symmetry breaking or with proposals that suggest that the chiral charge currents that flow along edges and domain wall cores are significantly reduced (see e.g. [43, 4, 31, 60]) with respect to the estimate of Ref. [52].

For *conventional* superconductivity, the phenomenological and symmetry based approaches of London [47] and of Ginzburg and Landau [19] predated the formulation of the microscopic theory, due to Bardeen, Cooper, and Schrieffer [6]. For *unconventional* superconductors, including those in which time-reversal symmetry is spontaneously broken, it is likewise possible to make progress phenomenologically [76, 70, 54]. This is the approach that we adopt in this part of the thesis, as we explore certain specific features of time-reversal symmetry-broken states: (i) the possibility that there are walls between domains of opposing chirality, (ii) the threading of these walls by magnetic flux, and (iii) the fact that this flux may penetrate in nonintegral amounts [69, 67]. Lack of flux quantization has also been discussed in related settings, such as superfluid condensates of ionized hydrogen [5], as well as time-reversal symmetry-broken superconductors that feature spin-polarization [78], disclinations [77], or intersecting grain-boundaries between crystallites [68].

Our central result of this part of the thesis is as follows: nonintegral multiples of the superconducting quantum of magnetic flux penetrate time-reversal symmetry-breaking superconductors, localized near individual bends in walls between chiral domains. We first obtain this result via an effective description in terms of domain walls and vortices, which shows that (in the special case of the crystallographically in-plane rotationally invariant limit) a domain wall that is translationally invariant along the z-axis and bends through an angle Θ is accompanied by a net flux (which we term "bend flux") of $\big((\Theta/\pi) + n\big)\Phi_0$, localized in the bend region, for arbitrary integral n (see Fig. 1.1), independent of the magnitude of chiral-charge currents that are predicted to flow along the core of domain walls. If the rotational symmetry is broken down to discrete tetragonal symmetry, our central result

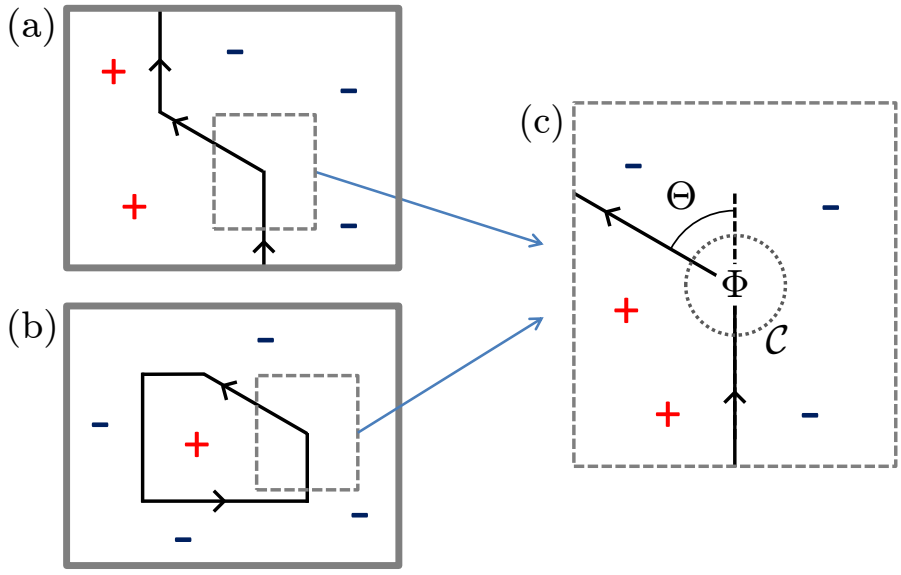

Figure 1.1: (a) and (b) schematically depict two rectangular samples of a chiral superconductor that with spontaneously broken time-reversal symmetry. The two samples are assumed to be infinite and translationally invariant along the z axis (out of plane) direction. Domain walls (oriented black lines) traverse these samples following locally straight paths, except for in isolated regions where they bend. The domain walls separate the chiral superconductor into regions of positive (+) and negative (−) chirality. The orientation of the domain walls are defined in such a way that a closed domain wall loop would circulate a positive chiral region in a counter-clockwise sense [see also Eq. (3.9)]. (a) depicts a domain wall that originates and terminates on the superconductors boundary (thick gray box). (b) depicts a domain wall loop. Two regions—one in each sample—are assumed to be locally identical. These regions are indicated by dashed gray boxes. (c) shows a blowup of this region. In this region the domain wall has a single bend of angle Θ, measured counter-clockwise relative to the orientation of the domain wall. The bend is surrounded by a contour $\mathcal{C}$ that is many penetration depths away from the bend. In the two regions where the contour crosses the domain wall, it is assumed that the contour follows locally identical paths (see Fig. 5.2 and Sec. 5.3). In this work we show that a nonintegral amount of flux Φ penetrates through the contour $\mathcal{C}$, independent of the magnitude of chiral-charge currents that are predicted to flow along the core of domain walls.

remains valid for the particular case of a domain wall bent through $\pi/2$ radians. We generalize these results to the situation in which gauge transformations and rotations about the z-axis are degenerate transformations of the maximally chiral superconducting order (i.e., are transformations that have equivalent impacts). Due to chiral-charge currents that flow along domain wall cores, small deformations of any contour that surround a domain wall bend can alter the amount of flux through the contour. Thus, to arrive at a unique value of "bend flux" for an individual bend in a domain wall, we consider particular contours with the following property: In each of the two regions where the contour crosses the domain wall, the domain wall must follow locally identical paths (see Fig. 1.1 and Fig. 5.2). For such contours $\oint dx_a g^{-1}_{ab} J_b$ is equal to zero. Here $\boldsymbol{g}$ is the superfluid density tensor and $\boldsymbol{J}$ is the current density. As we discuss in the last paragraph of Sec. 5.3, fluxoid quantization in conventional superconductors [46] would imply that the flux through such contours would be integral, i.e., would be equal to an integer multiple of Φ_0, and would not depend upon the bend angle. Thus, the existence of bend flux depends in an essential way on the unconventional nature of the superconductivity.

As "bend flux" is independent of the magnitude of the chiral currents that flow along domain wall cores, it is perhaps useful to regard bend flux as a robust magnetic signature of time reversal symmetry breaking, alternate to the magnetic signatures of the chiral currents themselves. In particular, our specialized and more general results indicate that observations of localized, nonintegral flux penetrating a z-axis surface (e.g., via scanned-probe magnetic imaging), could potentially be interpreted in terms of the presence of bent walls separating domains of opposing chirality, and hence would be suggestive of the existence of time-reversal symmetry-breaking superconductivity. Alternatively, if localized nonquantized flux is not observed to penetrate a z-axis surface, this would suggest that either (i) domain walls are not present, or (ii) domain walls are present, but are arranged in a parallel array and thus are not bent.

This part of the thesis is organized as follows. In chapter 2 we review the structure

of the Ginzburg-Landau order parameter appropriate for unconventional superconductivity with broken time-reversal symmetry, along with the corresponding Ginzburg-Landau free-energy functional. We assume that microscopic effects such as multiple electronic energy bands [7], spin-orbit interactions [21], and chiral currents [52], can be incorporated, self consistently, into the Ginzburg-Landau functional by choosing the appropriate values for the various material dependent coefficients. In Chapter 3 we analyze this free energy via an extension of the London limit, in which we exchange the Ginzburg-Landau order-parameter description for a reduced description in terms of the collection of spatially varying "phase-like" fields that for homogeneous configurations would parametrize the space of equilibrium states. The extension amounts to taking the limit in which the domain walls are vanishingly thin, compared with the London penetration depth. (It should be noted that Heeb and Agterberg, in Ref. [22], attach a different meaning to the term "extended London limit.") Taking this limit enables us to focus on the structure and implications of the topological excitations of the order parameter, which have the form of vortices and domain walls, and to relate the densities of these excitations to singularities in the phase-like fields. In Chapter 4 we return to the free energy, expressing it in terms of these excitation densities, and in Chapter 5 we use this framework to determine the spatial distribution of magnetization associated with domain-wall topological excitations, specifically walls that contain bends. In this chapter we also show that the thin-domain-wall limit is not essential, nor is it essential for the Ginzburg-Landau expansion of the free energy to be valid, in the sense that our central result—the threading of bent domain walls by nonintegral amounts of magnetic flux—continue to hold, even when these restrictions are relaxed. In Chapter 6 we consider three experimental settings in which nonintegral flux may be observed; positive results in any one of them would provide evidence for the existence of time-reversal symmetry-breaking superconductivity. At the end of the thesis in Chapter 12 we summarize the key results of Part I and II and their implications. Some technical details are relegated to a pair of appendices.

Chapter 2

Phenomenological theory of unconventional superconductivity

In this chapter we describe the phenomenological theory of superconductivity, on which our analysis is rooted. This approach is based on the notion of an appropriate superconducting order parameter, along with general symmetry considerations, and thus can be explored independently of any specific microscopic details. The order parameter transforms under the full symmetry group of the physical system, and thus provides a representation of this symmetry group. (It is common, in the context of planar superconductors, for the point-group aspect of this symmetry to be the tetragonal group D_{4h}, reflecting the underlying electronic and atomic structure of the crystalline material.) For Sr_2RuO_4, the material on which we shall focus, it is known that, for a range of temperatures close to the superconducting transition temperature T_c, the superconducting properties are nearly isotropic with respect to rotations about the z-axis [51, 13] (i.e., the direction perpendicular to the RuO_2 planes), and is only weakly tetragonal about this axis. Although, accordingly, the initial focus of our analysis will be on the isotropic limit (which we term the in-plane rotationally or $SO(2)_z$-invariant limit), we do subsequently address the cases in which the symmetry is lowered to the discrete group D_{4h} (and also, parenthetically, the group D_{6h}). At the outset, we therefore retain generality by determining the representation furnished by the superconducting order parameter appropriate to D_{4h} symmetry, motivated by the relevance of this group to Sr_2RuO_4.

We now determine the appropriate representation of the superconducting order parameter, bearing in mind the foregoing symmetry considerations. This choice of representation is made according to the following three simplifying assumptions: (i) The ground state of

the superconducting order should transform trivially under lattice translations. Thus, at the lengthscales relevant for a phenomenological description such as the one used here, the ground state of the superconducting order is translationally invariant. (ii) The representation of the symmetry group should be irreducible. This is justified in the case of Sr_2RuO_4 as, in the absence of an applied magnetic field, only one superconducting transition seems to be observed. (Recent experiments on Sr_2RuO_4 under uniaxial pressure do, however, indicate the possibility of a second transition [35].) (iii) The representation should allow for the possibility that the superconducting state spontaneously breaks time-reversal symmetry. This would require that the dimension of the representation be greater than unity. Taken together, these assumptions fix the order parameter to transform according to the Γ_5 representation [70], which is two-dimensional[1]. Accordingly, the order parameter is the complex-valued, two-component field $\eta_a(\boldsymbol{r})$, where the index a runs through the corresponding basis functions of the representation (i.e., X and Y) which, in general, depends on the three-dimensional position vector $\boldsymbol{r}$. To simplify our analysis, we consider superconducting states that are translationally invariant along the z-axis, thus rendering the physical problem effectively two-dimensional. Provided we apply external magnetic fields that are oriented along the z direction (i.e., $\boldsymbol{H} = H\hat{\boldsymbol{z}}$), this is an option, owing to the intrinsic translational invariance of the system along the z direction. These requirements, taken together, then dictate that the appropriate Ginzburg-Landau free energy functional governing the Γ_5 representation is given by [76, 70]

$$F'[\eta'] = \int d^2r' \big\{ \mathcal{K}'_{abcd} \, (D'_a \eta'_b)^* (D'_c \eta'_d) - \mathcal{A} \, \eta'^*_a \, \eta'_a + \frac{1}{2} \mathcal{B}'_{abcd} \, \eta'^*_a \, \eta'^*_b \, \eta'_c \, \eta'_d + \frac{1}{8\pi} |(\boldsymbol{\nabla}' \times \boldsymbol{A}') - \boldsymbol{H}'|^2 \big\}. \tag{2.1}$$

Here, two-dimensional summations are implied over the repeated indices a, b, c, d, and the covariant derivative is defined via $\boldsymbol{D}' := \boldsymbol{\nabla}' - 2\pi i \boldsymbol{A}'/\Phi_0$, where Φ_0 is the superconducting flux quantum $hc/2e$.

[1] We do not need to specify whether the representation is Γ_5^+ or Γ_5^-, for which the basis functions transform respectively as $\{XZ, YZ\}$ or $\{X, Y\}$. The results of the present work apply to both cases.

In Eq. (2.1) the primed variables are dimensionful. We now define relevant scales of length and energy, and use them to introduce convenient dimensionless variables, which we use throughout the remainder of this thesis and which we write without primes. As a first step, for the coefficient tensors $\mathcal{K}'$ and $\mathcal{B}'$ we define the dimensionful scale factors $\tilde{\mathcal{K}}$ and $\tilde{\mathcal{B}}$, which we then use to construct the dimensionless tensors $\mathcal{K} := \mathcal{K}'/\tilde{\mathcal{K}}$ and $\mathcal{B} := \mathcal{B}'/\tilde{\mathcal{B}}$. In the in-plane rotationally invariant limit, symmetry considerations dictate that $\mathcal{K}$ and $\mathcal{B}$ can be parametrized in the following way:

$$\mathcal{B}_{abcd} = I_{ac}I_{bd} + \frac{\sigma}{2}M^{\delta}_{ac}M^{\delta}_{bd}, \qquad \mathcal{K}_{abcd} = I_{ac}I_{bd} + \mu E_{ac}E_{bd} + \frac{\tau}{2}M^{\delta}_{ac}M^{\delta}_{bd}, \tag{2.2}$$

where a summation from 1 to 2 is implied over the repeated index δ, and the three real parameters $\{\sigma, \mu, \tau\}$ are, in principle, temperature dependent, and the constant tensors $\{\boldsymbol{I}, \boldsymbol{E}, \boldsymbol{M}^1, \boldsymbol{M}^2\}$ are defined via

$$\boldsymbol{I} := \begin{pmatrix} 1 & 0 \\ 0 & 1 \end{pmatrix}, \qquad \boldsymbol{E} := \begin{pmatrix} 0 & 1 \\ -1 & 0 \end{pmatrix}, \tag{2.3}$$

$$\boldsymbol{M}^1 := \begin{pmatrix} 1 & 0 \\ 0 & -1 \end{pmatrix}, \qquad \boldsymbol{M}^2 := \begin{pmatrix} 0 & 1 \\ 1 & 0 \end{pmatrix}. \tag{2.4}$$

The choice of tensor decomposition in Eq. (2.2) is motivated by the observation that under $\mathrm{SO}(2)_z$ rotations $\boldsymbol{I}$ and $\boldsymbol{E}$ each transform trivially, whereas the pair $\{\boldsymbol{M}^1, \boldsymbol{M}^2\}$ mix. If the symmetry were not $\mathrm{SO}(2)_z$ but D_{4h}, the coefficients of the $\boldsymbol{M}^1\boldsymbol{M}^1$ and $\boldsymbol{M}^2\boldsymbol{M}^2$ terms may be unequal; however, for D_{6h} symmetry they would remain the same.

We choose a natural scale for the order parameter, viz., $\eta_0 = (\mathcal{A}/\tilde{\mathcal{B}})^{1/2}$, and use it to make the definition $\eta := \eta'/\eta_0$. We then define the two lengthscales: (i) the penetration depth $\lambda := \Phi_0/(32\pi^3\eta_0^2\tilde{\mathcal{K}})^{1/2}$, which characterizes the lengthscale for variations of the magnetic field; and (ii) the coherence length $\xi := (\tilde{\mathcal{K}}/\mathcal{A})^{1/2}$, which characterizes the lengthscale for variations in the amplitude of the order parameter. We then scale all lengths by λ, via

$(\boldsymbol{r}, \boldsymbol{\nabla}, \boldsymbol{D}) := (\boldsymbol{r}'/\lambda, \lambda\boldsymbol{\nabla}', \lambda\boldsymbol{D}')$. We also make the conventional definition of the Ginzburg-Landau parameter $\kappa := \lambda/\xi$. Next, we define the dimensionless vector potential $\boldsymbol{A}$, applied magnetic field $\boldsymbol{H}$, and magnetic flux Φ via $(\boldsymbol{A}, \boldsymbol{H}, \Phi) := (2\pi\lambda\boldsymbol{A}'/\Phi_0, 2\pi\lambda^2\boldsymbol{H}'/\Phi_0, 2\pi\Phi'/\Phi_0)$. We note that, with this choice of units, a flux equal to a flux quantum has the dimensionless value 2π. As a final step in the construction of the dimensionless variables we choose as a scale for the free-energy density the value $f_0 = 2\tilde{\mathcal{K}}\eta_0^2/\lambda^2$, using which we arrive at the dimensionless free energy via $F := F'/\lambda^2 f_0$. It will be convenient for us to separate contributions to the dimensionless free-energy density into two groups: the "London type" terms $f_{\rm L}$ and the and potential terms $f_{\rm P}$, respectively defined via

$$f_{\rm L} = \frac{1}{2}\mathcal{K}_{abcd}(D_a\eta_b)^*(D_c\eta_d) + \frac{1}{2}|(\boldsymbol{\nabla}\times\boldsymbol{A}) - \boldsymbol{H}|^2, \tag{2.5}$$

$$f_{\rm P} = \frac{1}{2}\kappa^2(-\eta_a^*\eta_a + \frac{1}{2}\mathcal{B}_{abcd}\eta_a^*\,\eta_b^*\,\eta_c\,\eta_d), \tag{2.6}$$

so that

$$F[\eta] = \int d^2r\{f_{\rm L} + f_{\rm P}\}. \tag{2.7}$$

One way in which F differs from the conventional Ginzburg-Landau free energy is that the tensors $\mathcal{K}$ and $\mathcal{B}$ allow for a larger number of material-dependent parameters, the latter free energy having only a single such parameter, viz., κ. It is possible to estimate these additional parameters under the assumptions of weak coupling and a cylindrical Fermi surface [85], and this results in the following values: $(\mu, \tau, \sigma) = (0, 1, 1)$. However, due to the presence in Sr_2RuO_4 of effects such as multiple electronic energy bands [7], spin-orbit interactions [21], and chiral currents [52], the parameters of a Ginzburg-Landau theory that incorporates such effects self-consistently are expected to be modified from their weak-coupling values, perhaps significantly. Thus, we shall not limit our analysis to the weak-coupling values of these parameters.

In the chapter that follows, we analyze the potential terms of the phenomenological free energy, Eq. (2.6), and, specifically, review how its structure leads to both vortices and

domain walls. In particular, we derive the vortex and domain-wall densities in terms of the "phase-like" variables; in the subsequent chapter, Chapter 4, we construct the effective free energy in terms of topological variables, such as the vortex and domain-wall densities.

Chapter 3

Topological field configurations

As is well known, for many purposes, the state of an ordered phase can be adequately specified via an order-parameter field that takes values lying in the subspace of degenerate homogeneous equilibrium states $\mathcal{R}$ (see, e.g., Ref. [53]). If, as an example, different regions of a sample were to adopt distinct such values, it can—depending on the structure of the order parameter—be possible for the system to become trapped into order-parameter configurations that possess topologically stable defects [53]. These are spatially varying configurations of the order parameter that cannot be removed via local deformations. The framework of homotopy groups of $\mathcal{R}$ enables one to identify and classify the possible topologically stable defects.

As is also well known (see, e.g., Refs. [28, 72, 62, 61]), there can be a rich interplay between the topological features of the (bosonic) order-parameter fields that describe ordered phases and the qualitative character of any fermionic particles moving in the presence of such order-parameter fields. However, in the present work we shall only consider the topological features of the appropriate order-parameter field, leaving for future work the analysis of its implications for the motion of fermions.

To determine $\mathcal{R}$ for the present problem, we follow the standard approach (see, e.g., Ref. [70]) and analyze the structure of the potential terms of Eq. (2.1). To simplify the analysis, it is useful to parametrize the two complex fields of the superconducting order parameter $\boldsymbol{\eta} = (\eta_X, \eta_Y)$ in terms of four real fields $\{|\eta|, \theta, \gamma, \beta\}$ that transform simply under

the operations of the symmetry group:

$$\boldsymbol{\eta} \quad = |\eta| e^{i\theta} \boldsymbol{R}^{\gamma} \cdot \begin{pmatrix} \cos(\beta/2) \\ i \sin(\beta/2) \end{pmatrix}, \tag{3.1}$$

$$\boldsymbol{R}^{\gamma} \quad := \begin{pmatrix} \cos\gamma & -\sin\gamma \\ \sin\gamma & \cos\gamma \end{pmatrix}. \tag{3.2}$$

Now, elements of the product group $\mathrm{U}(1) \times \mathrm{SO}(2)_z$ of gauge transformations and z-axis rotations can be parametrized via a phase angle θ' and a rotation angle γ'. Under such elements, the order parameter $\boldsymbol{\eta}$ transforms as

$$\boldsymbol{\eta}(|\eta|, \theta, \gamma, \beta) \to \boldsymbol{\eta}(|\eta|, \theta + \theta', \gamma + \gamma', \beta); \tag{3.3}$$

under time reversal, $\boldsymbol{\eta}$ transforms as

$$\boldsymbol{\eta}(|\eta|, \theta, \gamma, \beta) \to \boldsymbol{\eta}(|\eta|, -\theta, \gamma, -\beta). \tag{3.4}$$

Thus, we see that the parametrization of $\boldsymbol{\eta}$, Eq. (3.1), is given in terms of an amplitude $|\eta|$ and phase θ that are similar to those used in conventional superconductivity, but also two angular variables, γ and β, that respectively characterize the additional nontrivial $\mathrm{SO}(2)_z$ and time-reversal structure associated with the version of unconventional order under consideration [1]. In terms of the parametrization given in Eq. (3.1), the potential terms (2.6) become

$$f_{\mathrm{P}} = -\frac{\kappa^2}{2}|\eta|^2 + \frac{\kappa^2}{4}|\eta|^4 + \frac{1}{8L^2}|\eta|^4 \cos^2\beta, \tag{3.5}$$

in which we have introduced the dimensionless length $L = \sigma^{-1/2}/\kappa$, which will turn out to determine the domain-wall width. As required by $\mathrm{SO}(2)_z$ and time-reversal invariance, these

[1] This choice of parametrization is similar to that used in Ref. [67], in which the aforementioned additional structure of the order is parametrized by the scalar fields α and χ via $\boldsymbol{\eta} \propto \boldsymbol{R}^{-\alpha/2} \cdot \big(\cos(\chi + \pi/4), i \sin(\chi + \pi/4)\big)$.

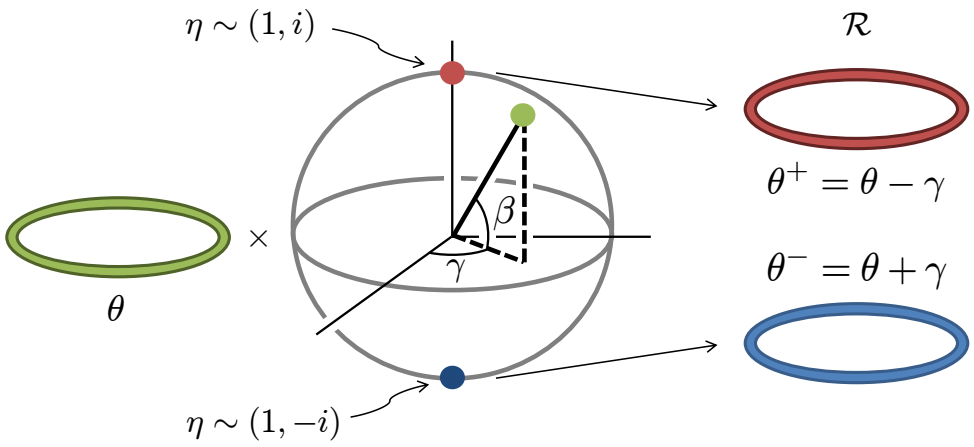

Figure 3.1: Visualizations of the order parameter space. In the standard London limit, in which $\kappa \to \infty$, the order parameter is restricted to the coset space of configurations with local structure isomorphic to $S^1 \times S^2$ [see the discussion following Eq. (3.5)]. When, in addition, the Ginzburg-Landau parameter σ of Eq. (2.2) is positive, the north and south poles of the sphere become free-energy minima, and are thus energetically preferred, relative to the equator. In the thin domain-wall limit (i.e., $L \to 0$), which we term the extended London limit, this preference is extreme. In this latter case, the coset space describing degenerate minimum-energy configurations becomes $S^1 \times \{+, -\}$.

potential terms are independent of γ, as well as being even functions of β. If the symmetry were reduced to D_{4h}, there would be the possibility of an additional term, proportional to $|\eta|^4 \cos(4\gamma) \cos^2(\beta)$. In the present setting, to achieve the standard London limit, in which the magnitude of the order parameter $|\eta|$ is fixed at unity, we take the *joint* limit $(\kappa, \sigma) \to (\infty, 0)$, keeping L fixed. In this limit, the local structure of the order-parameter space can be visualized as being the product of (i) a circle, corresponding to the gauge degree of freedom θ, and (ii) an open subset of a sphere corresponding to the angular variables $\{\gamma, \beta\}$) (see Fig. 3.1).[2]

The parameters (θ, γ) and $(\theta + \pi, \gamma + \pi)$ give identical values of the order parameter [see Eq. (3.1)], and therefore correspond to physically identical configurations.

As we aim to discuss states having time-reversal symmetry breaking, we have assumed

[2]The global structure of this order parameter space is that of a twisted $U(1)$ bundle (see e.g., [71]).

the Ginzburg-Landau parameter σ [defined in Eq. (2.2)] to be positive as, for sufficiently weak $\mathrm{SO}(2)_z$ symmetry-breaking, this favors states in which $\beta = \pm\pi/2$. These states are related by time-reversal symmetry, and can be visualized as lying at the poles of the order-parameter sphere (see Fig. 3.1). In these states, the order parameter takes the form

$$\boldsymbol{\eta}|_{\beta=\pm\pi/2} = |\eta| e^{i(\theta \mp \gamma)} \frac{1}{\sqrt{2}} \begin{pmatrix} 1 \\ \pm i \end{pmatrix}. \tag{3.6}$$

If, across the entire system, the state had chirality $\beta = \pi/2$, only a single, position dependent, phase field would be required to describe low-energy excitations away from equilibrium (and, similarly, if the state had only chirality $\beta = -\pi/2$). On the other hand, to describe low-energy excitations featuring both chiralities, as well as the "domain walls" between them (through which β changes between $\pm\pi/2$), a pair of position-dependent phase fields, $\theta(\boldsymbol{r})$ and $\gamma(\boldsymbol{r})$, is required. It will often be convenient to exchange these fields for the pair

$$\theta^{\pm}(\boldsymbol{r}) := \theta(\boldsymbol{r}) \mp \gamma(\boldsymbol{r}). \tag{3.7}$$

From Eq. (3.5) we can see that within a domain of maximally positive (or maximally negative) β, the free energy does not depend on θ^+ (or θ^-), and this remains true even after weak $\mathrm{SO}(2)_z$ symmetry-breaking terms are included in f_{P}. Consequently, the subspace of energy-degenerate homogeneous equilibrium states is disconnected, being composed, topologically, of two circles, which exchange under time-reversal, i.e. $\mathcal{R} = S^1 \times \{+, -\}$ (see Fig. 3.1). This order-parameter space combines two of the most familiar order-parameter spaces: the S^1 of conventional superconductivity/superfluidity, and the $\{+, -\}$ of Ising magnetism.

In general, to analyze the topological structure of order parameters, we consider their homotopy groups $\pi_n(\mathcal{R})$ associated with $\mathcal{R}$. For the specific case of $\mathcal{R} = S^1 \times \{+, -\}$, since each connected piece is isomorphic to S^1 the first homotopy group $\pi_1(\mathcal{R}) \cong \mathbf{Z}$. This implies that a domain of a given chirality can exhibit vortex singularities, as, e.g., in the case of

conventional superconductivity. As the space $\mathcal{R}$ is topologically disconnected, the zeroth homotopy group is also nontrivial, i.e., $\pi_0(\mathcal{R}) \cong \mathbf{Z}_2$; this implies the possibility of domain walls, which separate regions of opposing chirality. (Domain walls are common features of systems in which the order parameter is discrete as in the Ising case.) The $\mathbf{Z}_2$ value of π_0 indicates that domain walls annihilate one another. We remind the reader that order parameters for which $\pi_n(\mathcal{R})$ is nontrivial support topological defects of co-dimension $n+1$. Thus, in the effectively two-dimensional (real) space that we are considering, vortices are points and domain walls are lines.

The domain walls and vortices determine the *qualitative* structure of order-parameter field configurations; e.g., vortices in a domain of positive or negative chirality correspond to topological singularities in $\theta^+(\boldsymbol{r})$ or $\theta^-(\boldsymbol{r})$. In particular, when there are a total of $N^\pm$ vortices at positions $\{\boldsymbol{R}_\nu^\pm\}_{\nu=1}^{N^\pm}$ having vorticities $\{q_\nu^\pm\}_{\nu=1}^{N^\pm}$ interior to the positive- (or negative-) chirality domain, the singularities of $\theta^\pm$ can be characterized by the local *vortex density (scaler) fields* ρ^+_v and $\rho^-_{\rm v}$, which are defined via

$$2\pi\rho^\pm_{\rm v}(\boldsymbol{r}) := E_{ab}\nabla_a\nabla_b\theta^\pm(\boldsymbol{r}) = 2\pi\sum_{\nu=1}^{N^\pm} q_\nu^\pm\delta(\boldsymbol{r}-\boldsymbol{R}_\nu^\pm). \tag{3.8}$$

Here and elsewhere in this thesis, the Dirac delta functions δ are are softened on an appropriate lengthscale; for vortices it is the vortex core diameter.

Domain walls also have implications, but for the qualitative structure of $\beta(\boldsymbol{r})$. In two spatial dimensions, domain walls are lines, and a collection of N then can be characterized by specifying their trajectories $\{\boldsymbol{R}_n(s)\}_{n=1}^N$ as functions of an arclength parameter $-s_n \leq s \leq s_n$. By requiring, in addition, that the unit vector normal to the domain wall $\hat{n}_a(s)$, which is related to the domain wall trajectory via

$$\hat{n}_a(s) = (\cos\phi(s), \sin\phi(s))_a = -E_{ab}\,\partial_s R_b(s), \tag{3.9}$$

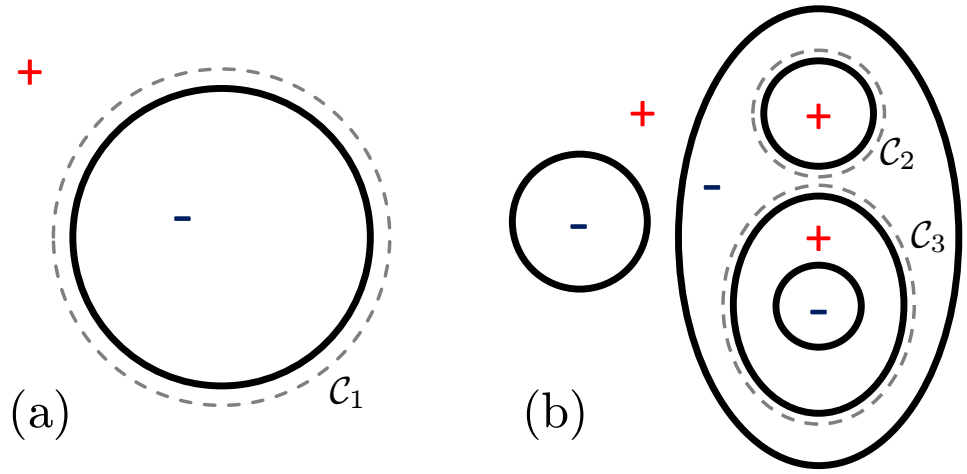

Figure 3.2: (a) A large region of positive chirality having an internal-island domain of negative chirality. As the positive-chirality region is multiply connected, the winding of θ^+ around the contour $\mathcal{C}_1$ is an independent topological variable. (b) Six, connected chiral regions (including the exterior, positive-chirality region). For every multiply connected chiral region, there is an independent topological variable associated with each non-contractible loop. As an example, the multiply connected negative-chirality region has two independent, non-contractible loops $\mathcal{C}_2$ and $\mathcal{C}_3$. Each of these loops is associated with an independent winding number for θ^-.

point from the negative towards the positive chiral domain, the sense of the vector tangent to the domain wall, $\partial_s \boldsymbol{R}(s)$, is determined. It is natural to associate the locations of the domain walls with the zeros of the field $\beta(\boldsymbol{r})$; for a given set of domain walls, the equilibrium form of $\beta(\boldsymbol{r})$ interpolates smoothly—with a solitonic form whose thickness is then the domain wall width—between regions in which it is essentially uniform and equal either to $\pi/2$ or to $-\pi/2$. Such structure can be characterized via a *domain-wall density (vector) field* $\boldsymbol{\rho}_{\rm dw}$, defined via

$$\boldsymbol{r}ho_{\rm dw} := \frac{1}{2}\boldsymbol{\nabla}\sin\beta_{\rm dw}(\boldsymbol{r}) \approx \sum_{n=1}^{N}\int_{-s_n}^{s_n} ds\,\hat{\boldsymbol{n}}(s)\,\delta(\boldsymbol{r}-\boldsymbol{R}_n(s)). \tag{3.10}$$

Here, the delta function is softened on the lengthscale of the domain-wall width. We shall make use of the vortex and domain wall densities given in Eqs. (3.8,3.10) in Sec. 4 in the construction of an effective free energy for the topological variables.

It should be recognized, however, that these densities do not, by themselves, fully specify

the topological structure of the order-parameter field. To see this, note, e.g., that a single island chiral domain affects the topology of the surrounding domain by rendering it multiply connected. Thus, to fully specify the topological structure of the $\theta^+(\boldsymbol{r})$ and $\theta^-(\boldsymbol{r})$ fields—in addition to specifying the location and vorticity of the individual vortices that lie within the respective domains—the global winding of of $\theta^+(\boldsymbol{r})$ or $\theta^-(\boldsymbol{r})$ must be specified around a loop that encircles each island (see Fig. 3.2a). To generalize to chiral domain structures that involve islands within islands, we note that to fully specify the topological structure of each positive (negative) connected chiral domain region, one must specify the winding of the θ^+ (θ^-) field around each independent non-contractible loop of that region (see Fig. 3.2b)[3].

In the remainder of this chapter we explain the connection between the $\gamma(\boldsymbol{r})$ field on a single domain-wall loop surrounding an island and the determination of the global freedom to wind possessed by the multiply-connected region exterior to the island. We also examine various situations involving individual chiral-domain islands, chosen to illustrate the physical roles played by the $\gamma(\boldsymbol{r})$ field. Before doing this, we remark that on any domain-wall line $\boldsymbol{R}(s)$ (i.e., a locus of points on which $\beta = 0$), the order parameter takes the form

$$\boldsymbol{\eta}|_{\beta=0} = |\eta| e^{i\theta} \begin{pmatrix} \cos\gamma \\ \sin\gamma \end{pmatrix}. \tag{3.11}$$

Thus we see that the field γ evaluated along a domain wall trajectory $\boldsymbol{R}(s)$, defines an angular variable $\Gamma(s) := \gamma\big(\boldsymbol{R}(s)\big)$ for each value of the arclength parameter s. We furthermore see that the function $\Gamma(s)$ determines the structure of the order parameter along the domain wall-line, specifically via the planar vector $(\cos\Gamma(s), \sin\Gamma(s))$.

To illustrate the physical role played by $\Gamma(s)$, we begin by considering the special case of a simply-connected chiral domain, bordered by a domain wall, and thus interior to a

[3]We note that for weak coupling and specular reflection, the condition at the sample boundary requires $\beta = 0$ (see, e.g., Ref. [70]), and thus, for a finite sample, all regions can be considered to be surrounded by domain-wall loops. However, the coupling between Γ and the normal direction of either the surface or the domain wall is generically different, which can result in distinct equilibrium orientations of Γ for each of these cases (see, e.g. [52]).

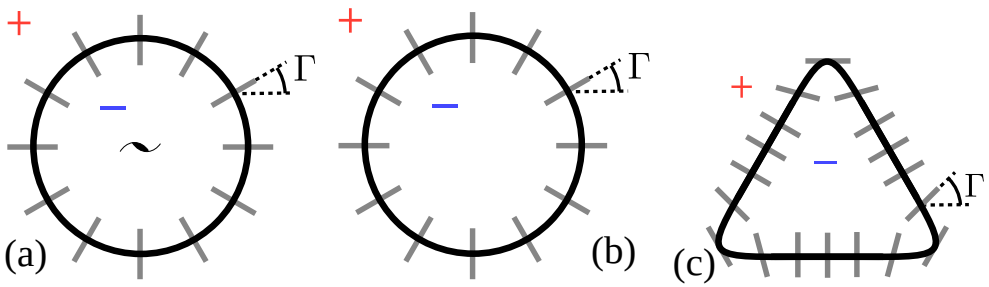

Figure 3.3: Three types of domain wall loops (black lines). The gray line segments intersecting the domain wall indicate the local direction of the planar vector $(\cos\Gamma(s), \sin\Gamma(s))$ (i.e., the strongest-pairing direction). Each loop is characterized by the three winding numbers (n_+, n_-, n_γ) [see Eq. (3.12,3.14)]: (a) $(-1, 1, 1)$; (b) $(-2, 0, 1)$; and (c) $(1, 0, -1/2)$. These domain wall loops are topologically equivalent to vortices with the following properties (a) singly quantized and rotationally invariant; (b) coreless and rotationally invariant; and (c) singly quantized and coreless.

larger surrounding region of opposing chirality. Two topological numbers (n_θ, n_γ), defined as follows, characterize the winding of the order parameter along paths that lie near to the domain wall:

$$2\pi n_\theta := \oint_{\rm dw} d\theta\,, \tag{3.12}$$

$$2\pi n_\gamma := \oint_{\rm dw} d\Gamma\,, \tag{3.13}$$

where "dw" indicates that the line integrals are evaluated along the domain wall, and the orientation of these integrals is taken to be counterclockwise. From Eq. (3.7), we see that (n_θ, n_γ) provide the same information as the two topological numbers (n_+, n_-), defined via

$$2\pi n_\pm := \oint_{\rm dw} d\theta^\pm\,; \tag{3.14}$$

specifically, $n_\pm = n_\theta \mp n_\gamma$. We note that n_θ and n_γ are either both integral or both half integral [so that $\boldsymbol{\eta}$ is single-valued; see Eq. (3.11)], and thus that n_+ and n_- are both integral.

For the sake of definiteness, we consider a domain of negative chirality that constitutes a simply-connected island within a larger, positive chiral domain. The positive domain is then

rendered multiply connected; see Figs. 3.2 and 3.3. Each of the winding numbers (n_+, n_-, n_γ) corresponds to a distinct physical property:

- The winding number n_+ of the exterior (positive) domain essentially determines, via $\Phi_{\rm tot} = \Phi_0 n_+$, the total flux $\Phi_{\rm tot}$ through an area that extends beyond the region bounded by the domain wall by a few penetration depths.

- The winding number n_- of the interior (negative) domain is the net number of vortices in the interior domain; if $n_- = 0$ then the domain-wall loop can be coreless, i.e., there is no topological requirement that there exist locations where $|\eta|$ vanish.

- Whether or not the winding number n_γ is unity determines whether or not the superconducting order can be rotationally invariant around a circular domain wall.

Importantly, as we previously noted in this chapter, by specifying the vorticial content in the interior and exterior domains, the interior winding number *is* uniquely determined, whereas the exterior winding number *is not*. However, if in addition to the vorticial content, the value of n_γ is specified, the winding of the exterior domain is also determined. In the particular case under consideration, $n_+ = n_- - 2n_\gamma$.

Thus, n_γ plays a dual role, determining both the total flux $\Phi_{\rm tot}$, via its influence on n_+ as well as whether or not the superconducting order can be rotationally invariant.

We pause to make two remarks concerning issues of energetics. First, as a domain wall has finite energy-cost per unit length, to reduce its energy a domain wall loop may shrink in size. When viewed on a lengthscale much larger than the domain size, a small domain wall loop appears topologically equivalent to a vortex [27], and thus provides an alternative description of the various vortex structures that can occur in superconductors with broken time-reversal symmetry (see, e.g., Refs. [73, 22, 65]). Second, in the limit in which the free energy is rotationally invariant and κ is large, energy considerations prefer domain-wall loops that are singly quantized (i.e., contain flux Φ_0), rotationally invariant, and coreless. However, owing to the linear relationship between n_+, n_-, and n_γ, these preferences cannot

all be simultaneously satisfied. Compromise order-parameter configurations result from this frustration; we show in Fig. 3.3 examples of the three types of vortices that satisfy two of the three preferences. Which particular type of vortex is preferred, energetically, will depend on the details of the parameters in the Ginzburg-Landau theory.

To illustrate this frustration and the dual physical role played by n_γ, we now consider two of the three small domain-wall loops that are favored energetically in the extreme London limit. In this limit, energetic considerations allow only coreless vortices, e.g., $n_- = 0$, and this implies that $\Phi_{\rm tot} = -2\Phi_0 n_\gamma$. Thus we see that, in the extreme London limit, if we also impose rotational invariance, namely $n_\gamma = 1$, we effect the magnetic properties of the vortex, requiring the vortex to be doubly quantized (i.e., contain $2\Phi_0$ of flux) and fixing the sense of the magnetic flux. Conversely, if we fix the vortex to be singly quantized then, in the extreme London limit, the vortex would not be rotationally invariant. This interplay between the rotational and magnetic structure, perpetrated by the dual nature of the γ field, underpins the central results of this work.

So far, we have established that, when taken together with vorticial content, n_γ fixes the *overall* winding of the order parameter along a non-contractible loop within a multiply-connected chiral domain. However, to describe the *local* structure of a domain wall [see Eq. (3.11)], it is necessary to specify the local value of γ [viz. $\Gamma(s)$] along the domain wall. As we shall see in Secs. 4 and 5.2, the local behavior of $\Gamma(s)$ also plays a role in determining the flux that penetrates through the domain wall locally [69, 67]. Thus, in order to develop a *local* description of the superconductor, the natural degree of freedom to use—for specifying the additional topological structure afforded by the presence of multiply-connected regions—is $\Gamma(s)$ rather than n_γ.

In the following chapter, by starting with the Ginzburg-Landau free energy, we construct an effective local free energy in terms of the topological variables. Specifically, we show that, in addition to the vortex density and domain wall density, the free energy depends on a third set of topological variables, viz., the value of $\Gamma(s)$ along domain walls.

Chapter 4

Effective free energy in terms of topological descriptors and the extended London limit

The aim of this chapter is to begin with the description of the superconducting system in terms of a Ginzburg-Landau free-energy functional dependent on the order-parameter field, and to derive from it a reduced description in terms of the vortex and domain-wall densities and $\Gamma(s)$ along domain walls. In this reduced description, the focus is on the dependence of the free energy on the topological variables [i.e., the locations of the vortices and domain wall, as well as $\Gamma(s)$]. The presumption is that the degrees of freedom associated with exciting the order parameter *around* the state of minimum free energy within a fixed topological sector [defined via the locations of the vortices and domain walls and $\Gamma(s)$] have been eliminated, either by integrating them out or by setting them to their stationary values. For a numerical implementation of the latter procedure applied to superconductivity in Sr_2RuO_4, see Ref. [24]. In this thesis, our aim is to proceed analytically, a task that is eased by our working in a particular limiting regime, an elaboration of the standard London limit that we term the "extended London limit." We remind the reader that the standard London limit amounts to assuming that the Ginzburg-Landau parameter κ tends to infinity, which enforces the condition $|\eta| = 1$. To pass to the extended London limit we make the additional assumption that the width of domain walls, which is controlled by the parameter L, tends to zero. In this limit, the domain wall becomes vanishingly thin, compared with the penetration depth.

We begin with the Ginzburg-Landau free energy, Eq. (2.5), and first pass to the standard London limit. From Eq. (3.5), we see that in this limit the order-parameter amplitude $|\eta|$ is energetically prohibited from departing from unity; inserting the corresponding form of

the order parameter [i.e., Eq. (3.1) but with $|\eta| = 1$] into Eq. (2.5), making the definition $(\Delta\Theta)_{ai} := (\nabla_a\theta - A_a, \nabla_a\gamma, \nabla_a\beta)_i$, and dropping constant terms arising from the potential terms, we arrive at the unconventional superconducting free energy $F_{\rm L}$ corresponding to the London free energy for conventional superconductivity, i.e.,

$$
\begin{aligned}
F_{\rm L}[\theta,\gamma,\beta,\boldsymbol{A},\boldsymbol{H}] = \int d^2r \Big\{ \frac{1}{2} K_{abcd}\, \Xi_{bidj}\, (\Delta\Theta)_{ai}\, (\Delta\Theta)_{cj} + \frac{1}{8L^2}\cos^2\beta + \frac{1}{2}|(\boldsymbol{\nabla}\times\boldsymbol{A}) - \boldsymbol{H}|^2 \Big\}, \\
\xi_{ai} := \quad R^{\gamma}_{ab}(iI_{bc}, -E_{bc}, iM^1_{bc})_i(\cos\beta, i\sin\beta)_c, \qquad (4.1) \\
\Xi_{aibj} := \quad \frac{1}{2}(\xi^*_{ai}\xi_{bj} + \xi^*_{bj}\xi_{ai}),
\end{aligned}
$$

where repeated indices $i, j, \ldots$ are summed from 1 to 3. Because in this free energy, the coefficient Ξ is contracted with a tensor that is symmetric under time reversal, we have adopted a form for Ξ that is manifestly symmetric under time reversal. In general, the supercurrent density $\boldsymbol{J}(\boldsymbol{r})$ is given by $-\delta F_{\rm sc}/\delta\boldsymbol{A}(\boldsymbol{r})$ and, continuing within the London limit, we see that it has the form

$$
\begin{aligned}
J_a \quad &= g_{ab}(\nabla_b\theta - A_b) + \mathcal{J}_a, && (4.2)\\
\mathcal{J}_a \quad &:= -\sin\beta\,\nabla_a\gamma + \frac{1}{4}(2\mu\cos\beta\, E_{ab} + \tau\mathcal{M}^{\gamma}_{ab})\nabla_b\beta, && (4.3)\\
\mathcal{M}^{\gamma}_{ab} \quad &:= R^{\gamma}_{ac}R^{\gamma}_{bd}M^1_{cd} = \begin{pmatrix} -\sin 2\gamma & \cos 2\gamma \\ \cos 2\gamma & \sin 2\gamma \end{pmatrix}_{ab}, && (4.4)\\
g_{ab} \quad &:= I_{ab} + \frac{1}{2}\tau\cos\beta\mathcal{M}^{\gamma-\pi/4}_{ab}\,. && (4.5)
\end{aligned}
$$

Note the occurrence of the unconventional contribution $\boldsymbol{\mathcal{J}}$ to the supercurrent, which includes currents that are localized near domain walls [76]. This contribution is manifestly odd under time reversal (which is evident because each term is odd in β).

We now proceed to take the *extended* London limit, in which domain walls are controlled to be thin compared with the penetration depth. We begin by noting that the term arising from $f_{\rm P}$ that remains in the free-energy density in the London limit is $\cos^2(\beta)/8L^2$, and that

this term contributes positively for any value of of $\beta \neq \pm\pi/2$. In particular, for a domain wall, across which β varies from $\pi/2$ to $-\pi/2$, the balancing, in equilibrium, of this potential term against contributions to the free energy that result from gradients in β would produce a spatial configuration in which β changes from $\pi/2$ to $-\pi/2$ over a lengthscale (i.e., the domain-wall width) proportional to L. Thus, in the limit $L \to 0$, the widths of domain walls are controlled to be arbitrarily small, compared with the penetration depth (which, we remind the reader, we have chosen to set the unit for lengths).

This extension of the London limit results in useful simplifications. First, as the domain walls are arbitrarily thin, regions in which β is uniform and equal to $\pm\pi/2$ dominate, areally. Thus, terms proportional to $\cos\beta$ or $\sin\beta$ become 0 or $\mathrm{sgn}\beta$ respectively. [Note that $\mathrm{sgn}\beta$ is a step function, taking the values 1 (or -1) for regions of positive (negative) chirality i.e., $\beta > 0$ (or $\beta < 0$)]. As an explicit example, the term in the superfluid density tensor $\boldsymbol{g}$ proportional to $\cos\beta$ can be neglected in the extended London limit, and thus we may make the replacement $\boldsymbol{g} \to \boldsymbol{I}$. Physically, this means that, even in the presence of domain walls, the in-plane Meissner response is isotropic.

A second useful simplification that arises in the extended London limit is that it enables us to express contributions to the free energy and supercurrent involving gradients of β in terms the domain-wall density $\boldsymbol{\rho}_{\mathrm{dw}}$, defined in Eq. (3.10). Using Eq. (4.2) we can thus, e.g., write

$$\boldsymbol{J} \quad = \boldsymbol{\nabla}\theta - \boldsymbol{A} + \boldsymbol{\mathcal{J}}, \tag{4.6}$$

$$\boldsymbol{\mathcal{J}} \quad := -\mathrm{sgn}\beta\, \boldsymbol{\nabla}\gamma + \left(\mu \boldsymbol{E} + \frac{\pi}{4}\tau \boldsymbol{\mathcal{M}}^{\Gamma(s)}\right) \cdot \boldsymbol{\rho}_{\mathrm{dw}}\,. \tag{4.7}$$

For the sake of compactness, here and elsewhere we use the notation $\boldsymbol{\mathcal{M}}^{\Gamma(s)} \cdot \boldsymbol{\rho}_{\mathrm{dw}}$ as shorthand for $\int ds\, \mathcal{M}^{\Gamma(s)} \cdot \boldsymbol{n}(s)\, \delta(\boldsymbol{r} - \boldsymbol{R}(s))$.

Having discussed how, in the extended London limit, the spatial variation of β is fully incorporated via the locations of the domain walls $\{\boldsymbol{R}_n(s)\}$, we continue with our goal of

constructing an effective free energy by eliminating all degrees of freedom associated with excitations of the order parameter around the state of minimum free energy within a fixed topological sector. With this in mind, our next step is to eliminate the non-topological variations in the θ field.

As the superconducting order may possess vortices, θ is not, in general, a single-valued function of position, and therefore it may exhibit singular behavior (i.e., at the cores of vortices). Our initial strategy for eliminating the non-topological variations of θ is to decompose it into two components: $\theta = \theta_{\rm sm} + \theta_{\rm v}$, where $\theta_{\rm sm}$ is a smooth, single-valued part, and $\theta_{\rm v}$ is the part that accounts for any vortex singularities. This separation is not unique, but we shall see, after eliminating $\theta_{\rm sm}$ from the free energy by setting it equal to its stationary value $\bar{\theta}_{\rm sm}$, that the resulting free energy is—for any fixed choice of topological variables, such as vortex positions and strengths—independent of any particular choice of decomposition. To implement this elimination of $\theta_{\rm sm}$ we need only consider the terms in the free-energy density associated with the kinetic energy of the supercurrents (i.e., associated with J^2), as other terms do not depend on θ; in the extended London limit the free energy F_J constructed from these terms is given by

$$F_J = \int d^2r \, \frac{1}{2} \left| \boldsymbol{\nabla}\theta_{\rm sm} + \boldsymbol{\nabla}\theta_{\rm v} - \boldsymbol{A} + \boldsymbol{\mathcal{J}} \right|^2 . \tag{4.8}$$

Stationarity of this expression with respect to $\theta_{\rm sm}$ reads

$$-\nabla^2 \theta_{\rm sm} = \boldsymbol{\nabla} \cdot (\boldsymbol{\nabla}\theta_{\rm v} - \boldsymbol{A} + \boldsymbol{\mathcal{J}}), \tag{4.9}$$

and, by using the Green function for the Laplace operator in two dimensions [i.e., $G(\boldsymbol{r}) = -\frac{1}{2\pi} \ln |\boldsymbol{r}|$, obeying $-\nabla^2 G(\boldsymbol{r}) = \delta(\boldsymbol{r})$], the stationary solution $\bar{\theta}_{\rm sm}$ can be expressed as

$$\bar{\theta}_{\rm sm}(\boldsymbol{r}') = \int d^2r \, G(\boldsymbol{r}' - \boldsymbol{r}) \boldsymbol{\nabla} \cdot \big(\boldsymbol{\nabla}\theta_{\rm v} - \boldsymbol{A} + \boldsymbol{\mathcal{J}} \big)(\boldsymbol{r}). \tag{4.10}$$

By inserting $\bar{\theta}_{\rm sm}$ into Eq. (4.8), we arrive at the following form for the free energy:

$$F_J = \frac{1}{2}\int d^2r\,\left|\boldsymbol{J}^{\rm T}\right|^2, \tag{4.11}$$

$$\begin{aligned} J_a^{\rm T}(\boldsymbol{r}) :=& \int d^2r'\,\Big(I_{ab}\,\delta(\boldsymbol{r}-\boldsymbol{r}') - \nabla_a G(\boldsymbol{r}-\boldsymbol{r}')\,\nabla'_b\Big)\times\Big(\nabla_b\theta_{\rm v} - A_b + \mathcal{J}_b\Big) \\ =& \int d^2r'\,E_{ab}\nabla_b\,G(\boldsymbol{r}-\boldsymbol{r}')\,E_{cd}\nabla'_c\Big(\nabla'_d\,\theta_{\rm v} - A_d + \mathcal{J}_d\Big), \end{aligned} \tag{4.12}$$

where we have used the elementary result $E_{ab}E_{cd} = I_{ac}I_{bd} - I_{ad}I_{bc}$ and the defining equation obeyed by G. The procedure of minimizing F_J with respect to $\theta_{\rm sm}$ can be described, physically, as compensating for any source of longitudinal currents (i.e., current-flows that build up at some location) or, equivalently, as a projection on to the subspace of transverse currents. This construction brings to the fore the vorticial content of the transverse supercurrent, which arises both from vortices and domain walls. Specifically, one can identify the vorticity W via

$$W = E_{ab}\nabla_a\big(J_b + A_b\big) = E_{ab}\nabla_a\big(\nabla_b\theta_{\rm v} + \mathcal{J}_b\big). \tag{4.13}$$

Owing to the unconventional contribution to the supercurrent $\boldsymbol{\mathcal{J}}$, the vorticity W in unconventional superconductivity in the extended London limit comprises both a vortex term $W_{\rm v}$, which is common also to conventional superconductivity and is proportional to the total vortex density $\rho_{\rm v}$, and a domain-wall term $W_{\rm dw}$, which is proportional to the domain-wall density $\boldsymbol{\rho}_{\rm dw}$:

$$W = W_{\rm v} + W_{\rm dw}, \tag{4.14}$$

$$W_{\rm v} := 2\pi\left(\frac{1}{2}\,(1+{\rm sgn}\beta)\,\rho_{\rm v}^{+}(\boldsymbol{r}) + \frac{1}{2}\,(1-{\rm sgn}\beta)\,\rho_{\rm v}^{-}(\boldsymbol{r})\right), \tag{4.15}$$

$$W_{\rm dw} := \big(f(s)\,\boldsymbol{n}(s) + \boldsymbol{d}(s)\cdot\boldsymbol{\nabla}\big)\cdot\boldsymbol{\rho}_{\rm dw}, \tag{4.16}$$

where

$$f(s) := -2\,\partial_s \Gamma(s), \tag{4.17}$$

$$\boldsymbol{d}(s) := -\mu\,\boldsymbol{I} + \frac{\pi}{4}\tau\,\boldsymbol{R}^{2(\phi(s)-\Gamma(s))}. \tag{4.18}$$

Several points are worth noting here. First, $W_{\rm v}$ is a weighted sum of the vortex densities in the chiral domains, which makes evident the fact that only those singularities of θ^+ (θ^-) that are located in the positive-chirality (negative-chirality) domain are associated with local vorticity. Second, via Eq. (4.16), we see that the domain wall vorticity $W_{\rm dw}$ can be expressed as a sum of two contributions: a "monopole" contribution of strength f, which determines the net magnetic flux penetrating the superconductor; and a "dipole" contribution of strength $\boldsymbol{d}$, which is generated by currents that flow along domain wall cores but do not create net flux through the superconductor. Third, within this extended London limit, the monopole and dipole contributions are expressible in terms of the topological degrees of freedom $\Gamma(s)$ and $\phi(s)$. We remind the reader that $\phi(s)$ is determined from the trajectory of a domain wall $\boldsymbol{R}(s)$ via Eq. (3.9).

The final step in deriving the reduced free energy is to eliminate the vector potential $\boldsymbol{A}$. Although it is possible to proceed directly, using Eq. (4.11) (see Appendix), the fact that the current $\boldsymbol{J}^{\rm T}$ in Eq. (4.11) is determined via a nonlocal expression makes it more efficient to apply an alternative, 'dual' approach, which uses a Hubbard-Stratonovich transformation of the nonlocal kernel via an auxiliary field Λ; see, e.g., Ref. [59, 84]. The resulting, dual expression for the free energy F_J is thus given by

$$F_J[\Lambda] = \int d^2r\,\left\{-\frac{1}{2}|\boldsymbol{\nabla}\Lambda|^2 + \Lambda(W-B)\right\}. \tag{4.19}$$

Under the constraint that it be evaluated at the stationary value of Λ, this form for F_J has the same value as the one given in Eq. (4.11). We note, in passing, that the dual free

energy $F_J[\Lambda]$ depends explicitly on the local value of the perpendicular magnetic field B ($= E_{ab}\nabla_a A_b$). Thus, the full expression for the free energy in the extended London limit, which also includes the magnetic field energy $\int d^2r\, \frac{1}{2}(B-H)^2$, depends on B locally. This locality renders simple the task of identifying the stationary value of B. Eliminating B by setting it equal to its stationary value we arrive at the following form for the extended London limit of the free energy:

$$F_{\rm EL} = \int d^2r \left\{ -\frac{1}{2}\Lambda(-\nabla^2+1)\Lambda + \Lambda(W-H) + f_{\rm core} \right\}. \tag{4.20}$$

In this form, the first two terms, which together account for the kinetic energy of the supercurrent and the magnetic field energy, have the virtue of being local and determined via W (i.e., the vorticity of the supercurrent). The remaining contributions to the free energy given by Eq. (4.1) are accounted for via $f_{\rm core}$, which is associated with the core energy of the domain walls and are negligibly small in regions lying beyond a distance of a few wall widths L from a domain wall. An explicit expression for $f_{\rm core}$ in terms of the fields γ and β is given in the Appendix.[1] Thus, in the neighborhood of the extended London limit, in which L becomes small (but remains non-zero), the domain-wall energy $\int d^2r\, f_{\rm core}$ can be expressed in terms of an energy per unit domain-wall length $E_{\rm core}$, which depends locally upon on $\Gamma(s)$ (i.e., γ evaluated on the domain wall) together with the shape of the domain wall [(e.g., via $\phi(s)$)], along with their arclength derivatives:

$$\int d^2r\, f_{\rm core} = \sum_n \int_{-s_n}^{s_n} ds\, E_{\rm core}\left(\Gamma_n(s), \ldots; \phi_n(s), \ldots\right). \tag{4.21}$$

We are now in the position to complete our derivation of the reduced free energy $F_{\rm EL}$ in the extended London limit, reduced in the sense that it depends only on the external applied

[1] Here and elsewhere in this thesis, we take into account the core energies of domain walls but not the core energies of vortices. Our justification for doing this is that, in the standard London limit, the energy cost of a vortex core is negligibly small, compared with the kinetic energy of the supercurrents and magnetic fields, whereas the core energy of a domain wall is not.

magnetic field and the topological variables via the vorticity W and domain-wall core energy density $f_{\rm core}$. Upon eliminating Λ from Eq. (4.20), $F_{\rm EL}$ becomes

$$F_{\rm EL} = \int \frac{d^2r\, d^2r'}{4\pi}\big(W(\boldsymbol{r})-H(\boldsymbol{r})\big)K_0(|\boldsymbol{r}-\boldsymbol{r}'|)\big(W(\boldsymbol{r}')-H(\boldsymbol{r}')\big) + \int d^2r\, f_{\rm core} \tag{4.22}$$

where K_0 is a modified Bessel function of the second kind. A virtue of the formulation that we have employed is that it enables the efficient calculation of the magnetic response of the superconductor in the extended London limit, via the thermodynamic relation

$$M_{\rm EL}(\boldsymbol{r}) = -\frac{\delta F_{\rm EL}}{\delta H(\boldsymbol{r})} = \int \frac{d^2r'}{2\pi} K_0(|\boldsymbol{r}-\boldsymbol{r}'|)\big(W(\boldsymbol{r}') - H(\boldsymbol{r}')\big). \tag{4.23}$$

One can also use the Ampère-Maxwell law to determine the spatial distribution of equilibrium supercurrents in the this limit, which gives $\boldsymbol{J}_{\rm EL} = \boldsymbol{E}\cdot\boldsymbol{\nabla} M_{\rm EL}$. We see that, in this limit, the magnetic response of the superconductor resulting from domain walls can be grouped into a dipole term $M_{\rm dw,d}$ and a monopole term $M_{\rm dw,m}$ that result from the dipole and monopole contributions to the domain wall vorticity, and which respectively can be expressed as

$$M_{\rm dw,m}(\boldsymbol{r}) = \int \frac{d^2r'}{2\pi} K_0(|\boldsymbol{r}-\boldsymbol{r}'|)\, f\, \boldsymbol{n}\cdot\boldsymbol{\rho}_{\rm dw}(\boldsymbol{r}') \tag{4.24}$$

$$M_{\rm dw,d}(\boldsymbol{r}) = \int \frac{d^2r'}{2\pi} K_0(|\boldsymbol{r}-\boldsymbol{r}'|)\, (\boldsymbol{d}\cdot\boldsymbol{\nabla}')\cdot\boldsymbol{\rho}_{\rm dw}(\boldsymbol{r}'). \tag{4.25}$$

Expressions for f and $\boldsymbol{d}$ are given in Eq. (4.17). The dipole contribution results from currents that flow along the domain wall core and, in particular, is directly proportional to the magnitude of such currents. One way to understand the dipole contribution is to make the following analogy to a conventional superconductor: If it were possible to embed within a conventional superconductor an external sheet current, the magnetic response of the conventional superconductor would then have the form given by $M_{\rm dw,d}$. In contrast to the dipole contribution, the magnitude of the monopole contribution is independent of the magnitude of the currents that flow along the domain wall core and instead is determined

by the arc length derivative $\partial_s \Gamma(s)$.

As an initial illustration of this approach, we consider a straight domain wall, lying along the y-axis in an infinite, three-dimensional superconductor. We assume that there is no applied magnetic field, i.e., $H = 0$. We further assume that the superconducting state is of positive (negative) chirality for $x < 0$ ($x > 0$), so that by the convention defined by Eq. (3.9) we have $\boldsymbol{R}(s) = s\hat{\boldsymbol{y}}$. As we show in the Appendix , a variational analysis, based on an assumed form for the behavior of β transverse to a translationally invariant domain wall, suggests that the equilibrium value of Γ is ϕ. Assuming this to be case, we then find, from Eq. (4.17), that the domain-wall vorticity has no monopole part [i.e., $f(s) = 0$] but does have a dipole part, which is given by $\boldsymbol{d} = \big((\pi\tau/4) - \mu\big)\boldsymbol{I}$.[2] Then, from Eq. (4.23), we find that magnetization and current densities vary with the spatial distance x from the domain wall as follows:

$$M_{\rm EL}(x) = -\frac{1}{2}\big((\mu - (\pi\tau/4)\big)\,\mathrm{sgn}(x)\,e^{-|x|}, \tag{4.26}$$

$$\boldsymbol{J}_{\rm EL}(x) = \big(\mu - (\pi\tau/4)\big)\big(\delta(x) - e^{-|x|}/2\big)\,\hat{\mathrm{y}}. \tag{4.27}$$

As, for this domain-wall configuration, the monopole contribution $f(s)$ to the domain-wall vorticity is zero, the net magnetic flux (per unit length of domain wall) [e.g. the magnetic flux (per unit length of domain wall) integrated transversally] vanishes. The jump discontinuity in $M(x)$ at $x = 0$ results from a supercurrent that flows along the domain-wall core. For the case of Sr_2RuO_4, we can use Eq. (4.27) to estimate the magnitude of this current. In SI units the dimensionful current density $\boldsymbol{J}'$ is given in terms of its dimensionless counterpart $\boldsymbol{J}$ via $\boldsymbol{J}' = (2\pi\lambda f_0/\Phi_0)\boldsymbol{J}$. Then, using $\boldsymbol{J}$ to compute the current passing through a narrow window bracketing the domain wall, we arrive at the following expression for the dimensionful

[2] In the case that the equilibrium value of $\Gamma - \phi$ is $\pi/2$, the dipole part of the vorticity is given by $\boldsymbol{d} = \big(-(\pi\tau/4) - \mu\big)\boldsymbol{I}$. Thus, as is shown in the referring paragraph, the part of the domain-wall current proportional to τ can flow in either direction, for a given pattern of chirality, depending on the value of $\Gamma - \phi$.

domain-wall current I' per Ru-O layer:

$$I' = \frac{2\pi\lambda^2 f_0}{\Phi_0}\Delta z \int_{0^-}^{0^+} dx\ (\mu - (\pi\tau/4))\,\delta(x) \tag{4.28}$$

$$= \frac{2\pi\lambda^2 f_0}{\Phi_0}\Delta z\ (\mu - (\pi\tau/4))\,, \tag{4.29}$$

where Δz is the thickness of an Ru-O layer. To find the numerical value of this current in Amps, we note that in SI units f_0 can be expressed in terms of the thermodynamic critical field H_c as $2\kappa^{-2}\mu_0 H_c^2$. Using the parameter values appropriate for Sr_2RuO_4 [49], i.e., $\mu_0 H_c = 0.023\,\mathrm{T}$, $\lambda(0) = 0.15\,\mu\mathrm{m}$, $\kappa = 2.3$, and $\Delta z = 1.2\,\mathrm{nm}$, we arrive at the following estimate for the current: $\big(\mu - (\pi\tau/4)\big) \times 1.3 \times 10^{-5}\,\mathrm{A}$ per Ru-O layer flowing along a domain-wall core. For this result to match previously made theoretical estimates (see Ref. [52, 38]), one would need to have the material perameters obey $\big(\mu - (\pi\tau/4)\big) \approx 1$.

In the next chapter, we extend our discussion to cope with situations lying beyond straight domain walls, thus allowing the domain walls to have bends. As part of this discussion, we employ the reduced description of the superconductor in the extended London limit derived in the present chapter to show that: (i) a net magnetic flux penetrates the superconductor near bends; and (ii) this flux is generically a *nonintegral multiple* of the superconducting flux quantum Φ_0.

Chapter 5

Magnetic flux in the vicinity of a bend in a domain wall

In this chapter we derive the central result of this part of this thesis, viz., that an individual bend in a domain wall is accompanied by a nonintegral amount of magnetic flux that penetrates the superconductor near the bend; the amount—which we term the *bend flux*—depends on the geometry of the bend. In the limit in which the in-plane crystalline anisotropy is negligible (i.e., the isotropic limit), the bend flux is proportional to the angle through which the domain wall bends.

We derive the bend flux via two approaches. In the first, we analyze a bending domain wall via the effective theory of the topological variables, developed in Sec. 4. We then consider an alternative derivation, which, in the isotropic limit, yields the bend flux quite generally, without reliance on the assumption of either the standard or the extended London limit, or even on the validity of the Ginzburg-Landau expansion of the free energy. We end this chapter by considering modifications of the isotropic-limit bend flux result that would arise in settings of other pairing symmetries and/or tetragonal or hexagonal departures from the limit of crystalline isotropy.

5.1 Comparison with a spatially extended Josephson junction

Before establishing the existence of bend flux, we give a discussion of the essential differences between, on the one hand, a system comprising a domain wall and the superconducting

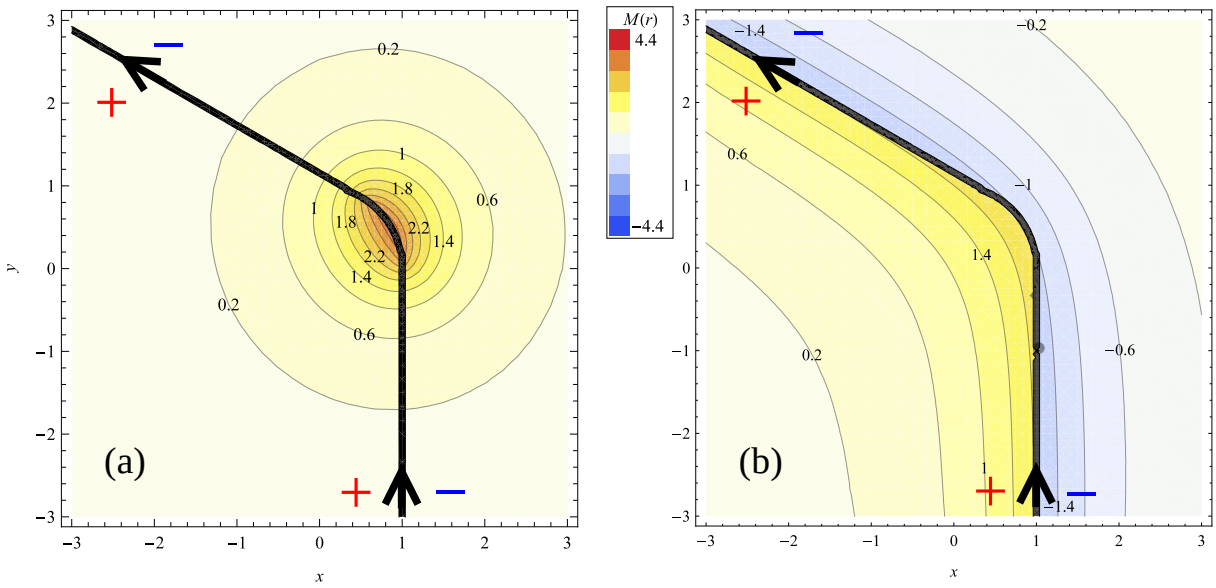

Figure 5.1: (a) "Monopole" and (b) "dipole" contributions to the magnetic field associated with a bending domain wall (oriented black line) for a bend angle of $\pi/3$, considered in the extended London limit [see Eq. (4.24)]. The z-axis magnetic field $M(\boldsymbol{r})$ is plotted as a function of position (color scale and contour lines). For this example, the Ginzburg-Landau parameters are taken to have the values $\mu = 0.2$ and $\tau = 1$. The penetration depth defines the unit lengthscale. The chirality is positive to the left of the domain wall and negative to the right of it, so that, via Eq. (3.9), we see that the domain wall has the indicated orientation. The dipole contribution produces no net magnetic flux through contours that surround the bend many penetration depths away, and cross the domain wall along locally identical paths. The monopole contribution produces a net flux $2\Phi_0/3$ through such contours, independent of the G-L parameters μ and τ that control the magnitude of the chiral currents that flow along the domain wall core.

regions of opposing chirality separated by it, and, on the other hand, a system of a spatially extended Josephson junction and two regions of conventional superconductivity coupled by it. For the extended Josephson-junction system it is possible to define a variable analogous to the domain wall variable $\Gamma(s)$, i.e., the local value $\Gamma_{\rm J}(s) := [-\theta_1(s) + \theta_2(s)]/2$ of (half of the) the difference between the phases $\theta_1(s)$ and $\theta_2(s)$ of the superconducting regions that lie on either side of the junction. The important distinction between Γ and $\Gamma_{\rm J}$ is that whereas $\Gamma_{\rm J}$ transforms trivially under in-plane rotations, Γ transforms nontrivially.

This observation has important implications, if we compare the local energy of a domain

wall $E_{\rm dw}$ with the Josephson energy $E_{\rm J}$ of a extended Josephson junction. In particular, for the extended Josephson junction, $E_{\rm J}$ is a periodic function of $\Gamma_{\rm J}$ alone. For the domain wall system, on the other hand, in order to preserve the $\mathrm{SO}(2)_z$ invariance of the free energy, the local energy-density of the domain wall must be a periodic function of the difference $\Gamma - \phi$ [in which ϕ is determined by the local direction of the domain wall normal; see Eq. (3.9)]. Thus, because they have distinct values of ϕ, two segments of straight domain wall separated by a bend will generically have distinct equilibrium values of Γ. This stands in contrast with the case of the spatially extended Josephson junction with a bend, the equilibrium value of $\Gamma_{\rm J}$ being independent of position along the junction. As we shall now see, the bend flux originates in this variation of the equilibrium value of Γ on either side of a bend.

5.2 Bend flux in terms of topological variables

We now turn to the derivation of the bend flux within the special context of the effective theory for topological variables, developed in the previous chapter. Part of the utility of this effective theory is that it allows for an efficient calculation of the magnetic response of the superconductor, given a configuration of the topological variables, viz., the position and strength of the vortices, the positions of the domain-wall lines, and the value of $\Gamma(s)$ along each such line. Thus, our approach will be to consider a specified configuration of topological variables *without* vortices but with a single, fixed domain wall having a bend and a specified form for $\Gamma(s)$ along it, and then to employ Eq. (4.23) in order to determine the corresponding magnetization density.

We define the position of the domain wall using three line-segments: an arc of Θ radians and unit radius of curvature, and two straight segments that continue tangentially from each of the end-points of the arc (see Fig. 5.1). Given this particular geometry, we say that the resulting domain wall has a bend angle of Θ in it. Our next assumption concerns the form of $\Gamma(s)$. In Appendix we give a variational analysis that suggests that, for a straight domain

wall, the equilibrium value of Γ is ϕ. To generalize to the situation in which the domain wall bends, we assume that Γ follows the local direction of the domain wall 'adiabatically', i.e., $\Gamma(s) = \phi(s)$. In this case, because $\partial_s \Gamma(s)$ is not everywhere zero a monopole contribution to the domain-wall vorticity arises [see Eqs. (4.16) and (4.17)], in addition to the dipole contribution. Figure 5.1 shows both the monopole and dipole contributions to the magnetic field, evaluated using Eq. (4.23).

Next, we determine the total flux $\Phi_{\text{var,bend}}$ associated with the bent domain wall furnished by this variational calculation. To do this, we integrate the total magnetic field through a large circular disc Ω centered at the vertex formed by the extrapolation of the straight-line segments, so that the straight-line segments lie radial to the disc. In the limit that the disc radius is much larger than the penetration depth, we find that the dipole contribution to $\Phi_{\text{var,bend}}$ tends to zero, whereas the monopole contribution is nonzero, tending to the following total flux:

$$\Phi_{\text{var,bend}} = \int_{\Omega} d^2 r \, M(\boldsymbol{x}) = 2 \int d\Gamma(s) = 2\Theta, \tag{5.1}$$

i.e., the net flux is simply given by twice the bend angle, regardless of how $\Gamma(s)$ interpolates between its limiting values far from the bend. In particular, for case shown in Fig. 5.1 (i.e., for $\Theta = \pi/3$) the bend flux is $2\pi/3$, i.e., the dimensionful value is $\Phi_0/3$, which is a nonintegral multiple of the flux quantum.

5.3 General analysis for the bend flux

In the remainder of this section we consider a more general context in which the existence of bend flux can be demonstrated. In particular, we need not employ the extended London limit, nor assume that the superconductor is in the Ginzburg-Landau regime. Rather, the central assumption is that the superconducting order has the following essential feature: in regions in which the chirality is maximal, local $\mathrm{SO}(2)_z$ rotations of the superconducting order can equally well be accomplished via U(1) gauge transformations, so that the local

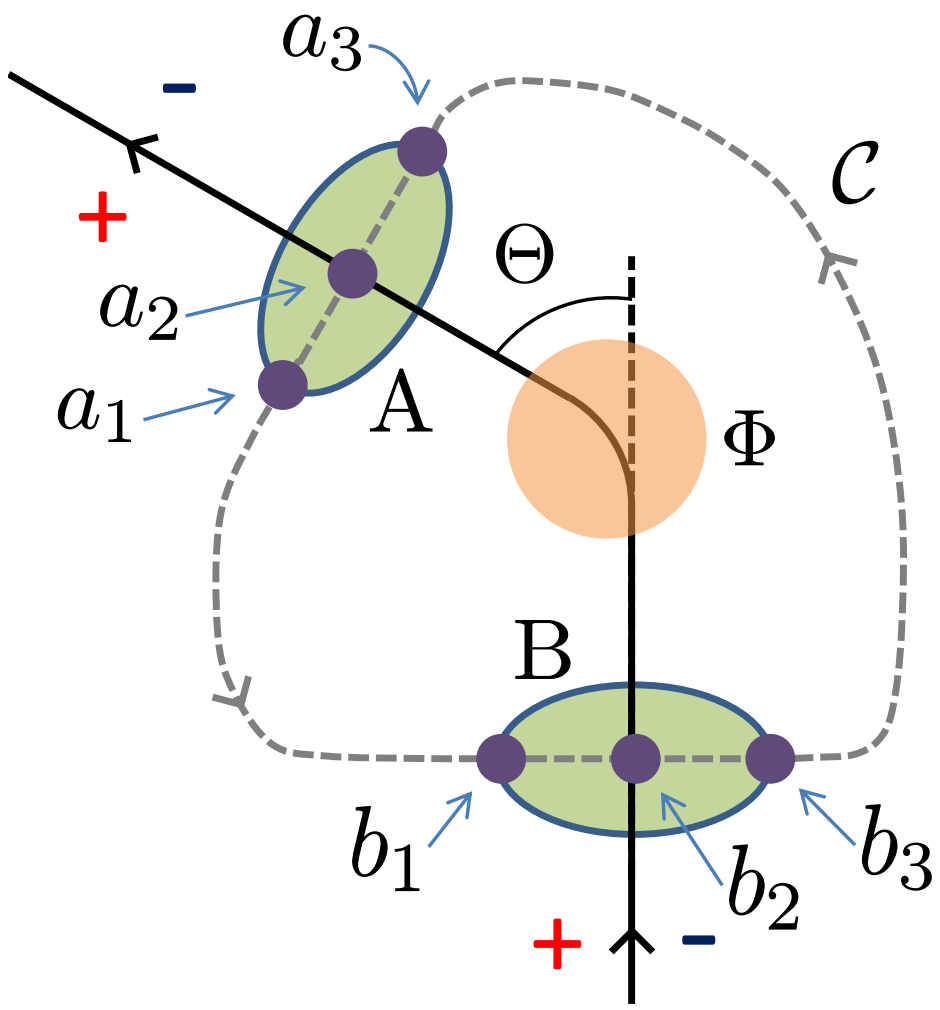

Figure 5.2: A bent domain wall (oriented black line) separating two domains of opposite chirality. En route to deriving Eq. (5.7), which expresses the flux Φ through the area bounded by the contour $\mathcal{C}$ in terms of the bend angle Θ, the circulation of the unconventional superfluid velocity $\boldsymbol{V}$ [see Eq. (5.2)] around $\mathcal{C}$ is shown to be zero. The contour $\mathcal{C}$ is assumed to be many penetration depths away from the region where the domain wall bends.

transformation $(\alpha, -\mathrm{sgn}(\beta)\,\alpha) \in \mathrm{U}(1) \times \mathrm{SO}(2)_z$ acts *trivially* on the superconducting order parameter. If this assumption holds then, provided the *amplitude* of the superconducting order is spatially homogeneous away from the domain wall, the unconventional superfluid velocity $\boldsymbol{V}$, defined via

$$\boldsymbol{V} := \boldsymbol{\nabla}\theta - \mathrm{sgn}(\beta)\,\boldsymbol{\nabla}\gamma - \boldsymbol{A}, \tag{5.2}$$

tends to zero within a maximally chiral region, as a result of the Meissner effect.

In deriving the bend flux we use the following construction to define the geometry of the domain wall. We consider a single domain wall that is fixed to pass through three points: the origin O, and two other points P and Q; then, we fix the angle $\angle POQ = \pi + \Theta$ where Θ is bend angle of the domain wall. We take the orientation of the domain wall, as defined by Eq. (3.9), to run from P to Q, and we let the points P and Q tend to infinity. The goal of the calculation is then to determine the net magnetic flux penetrating the superconductor in the vicinity of the domain wall bend. The key quantity that we use is the circulation of $\boldsymbol{V}$ around a closed contour $\mathcal{C}$ encircling the domain wall bend at a distance of many penetration depths (see Fig. 5.2). Care is needed in selecting the contour $\mathcal{C}$ because, in equilibrium, even for zero applied magnetic field, a domain wall may not be translationally invariant.[1] However, as the underlying free energy is local [as is manifest in Eq. (4.20)] and translationally and rotationally invariant; it is always possible to choose two geometrically congruent regions, A and B, each straddling the domain wall but located on opposite sides of the domain-wall bend, in which the equilibrium spatial configurations of the superconducting order in the regions (A and B) are related to one another via a rigid rotation and translation (see Fig. 5.2). Once a pair of such regions has been identified, we choose the contour $\mathcal{C}$ to

[1] For example, as noted in Ref. [76], in the limit of large domain-wall currents, vortices may be stabilized along the domain wall. Such vortices would then spoil the translational invariance of the domain wall. Although we know of no experimental evidence for such an effect, one interpretation of Josephson-junction tunneling experiments on Sr_2RuO_4 [32] is the absence of translational invariance (i.e., for the presence of multiple domains) along sample boundaries, which can be regarded in certain respects as analogous to domain walls. However, alternate explanations exist which are based on assumed line nodes in the superconducting order parameter [66].

cross the regions (and hence the domain wall) on locally identical paths $b_1 \to b_3$ and $a_1 \to a_3$ (i.e., on paths that are related by the same rotation and translation as the regions are). As a result, the following equality between line integrals holds:

$$\int_{a_1 \to a_3} d\boldsymbol{r} \cdot \boldsymbol{V} = \int_{b_1 \to b_3} d\boldsymbol{r} \cdot \boldsymbol{V}. \tag{5.3}$$

By using this result, and observing that $\boldsymbol{V} = \boldsymbol{0}$ away from the domain wall, we see that the circulation of $\boldsymbol{V}$ around the closed contour $\mathcal{C}$ is zero, i.e.,

$$\oint_{\mathcal{C}} d\boldsymbol{r} \cdot \boldsymbol{V} = 0. \tag{5.4}$$

The next step in the derivation is to consider the contour $\mathcal{C}^+$ ($\mathcal{C}^-$), which begins at the point a_2 (b_2) and follows $\mathcal{C}$ through the positive- (negative-)chirality domain to the point b_2 (a_2). The line-integrals of $(\boldsymbol{V} + \boldsymbol{A})$ along $\mathcal{C}^+$ and $\mathcal{C}^-$ respectively measure the change in the phase of the order parameter in the positive (negative) region from a_2 to b_2 (and from b_2 to a_2). Thus, again using the linear relation $\gamma = (-\theta^+ + \theta^-)/2$ [i.e., Eq. (3.7)], we see that the change in Γ from the point b_2 to the point a_2 [i.e., $\Delta\Gamma := \Gamma(a_2) - \Gamma(b_2)$], is given by the following formula:

$$\Delta\Gamma = \frac{1}{2}\int_{\mathcal{C}^+} d\theta^+ + \frac{1}{2}\int_{\mathcal{C}^-} d\theta^- = \frac{1}{2}\oint_{\mathcal{C}} d\boldsymbol{r} \cdot (\boldsymbol{V} + \boldsymbol{A}). \tag{5.5}$$

We now examine in more detail the equilibrium value of $\Delta\Gamma$. As discussed in Sec. 5.1, as a consequence of the rotational invariance of the underlying free energy, the energy (per unit arclength) $E_{\rm dw}$ of the domain wall must be a periodic function of the combination $\Gamma(s) - \phi(s)$, in which $\phi(s)$ continues to characterize the local direction normal to the domain wall. Furthermore, as—up to a global phase—the configurations having Γ and $\Gamma + \pi$ are equivalent, the dependence of $E_{\rm dw}$ on $\Gamma(s) - \phi(s)$ has period π. Importantly, we make the following additional assumption, viz., that the dependence of $E_{\rm dw}$ on $\Gamma(s) - \phi(s)$ has a *single*

minimum per period.

We now observe that, by construction, region A is rotated by an angle Θ relative to B (using the convention that positive rotations are measured counter-clockwise, relative to the domain-wall orientation) as a result $\Delta\phi := \phi(a_1) - \phi(a_2) = \Theta$. Thus, with these assumptions the equilibrium value of $\Delta\Gamma$ is equal to the bend angle Θ, up to an integer multiple of π, i.e.,

$$\Delta\Gamma = \Theta + n\pi. \tag{5.6}$$

Combining Eqs. (5.4,5.5, 5.6), and defining $\Phi_{\rm bend}$ to be the bend flux (i.e., net flux through the surface defined by the contour $\mathcal{C}$) we arrive at the result that

$$\Phi_{\rm bend} = \big((\Theta/\pi) + n\big)\,\Phi_0. \tag{5.7}$$

Because the bend flux, in the rotationally invariant limit, can evidently be an arbitrary fraction of the flux quantum, this result is a manifestation of the general result that broken time-reversal invariance allows for nonquantized amounts of flux to penetrate a superconductor, as predicted on general grounds in Refs. [78, 18, 69, 68, 67, 77]. Moreover, because $\Gamma(s)$ need not stay locked, relative to the local domain wall orientation (e.g, at the bend), or owing to the presence of vortices in either or both of the chiral domains, it makes sense that $\Phi_{\rm bend}$ be determined only modulo Φ_0.[2]

To emphasize the role of the unconventional nature of the superconducting order in deriving Eq. (5.7) we make the following comparison with a conventional superconductor. For a conventional superconductor, the fluxoid [46] through a contour is defined as $\Phi + \oint dr_a g^{-1}_{ab} J_b$ (where $\boldsymbol{g}$ is the superfluid density tensor, $\boldsymbol{J}$ is the current density, and $\Phi = \oint dr_a A_a$ is the

[2]As a particular case of Eq. (5.7), one can consider a straight domain wall. Then, Eqs. (5.6) and (5.7) imply that the topologically stable, localized solitons in $\Gamma(s)$ along a domain wall would obey $\Delta\Gamma = \pi$, and that each is associated with a flux Φ_0. However, if the dependence of $E_{\rm dw}$ on $\Gamma(s) - \phi(s)$ should have multiple minima per π period, then there could be topologically stable solitons in $\Gamma(s)$ along a straight domain wall, each having $\Delta\Gamma \neq \pi$ and connected with nonquantized amounts of flux (see Refs. [69, 67, 10]). In this case, in addition to the bend flux of Eq. (5.7), the flux associated with a bent domain wall may have a further contribution.

flux through the contour). For a conventional superconductor, any contour for which $\boldsymbol{g}$ remains everywhere positive definite (i.e. for paths that are interior to the superconductor) the fluxoid is equal to $n\Phi_0$ for an integer n. In deriving Eq. (5.7) we choose a contour $\mathcal{C}$ that crosses the two regions where $\boldsymbol{J}$ is non-zero along locally identical paths (these two regions are labeled A and B in Fig. 5.2). We therefore have that $\oint_{\mathcal{C}} dr_a g^{-1}_{ab} J_b = 0$. Thus, if the superconductivity were conventional, then the flux through the contour $\mathcal{C}$ would be integral and would not depend upon the bend angle Θ in contrast to Eq. (5.7). Thus, we see that the existence of bend flux depends in an essential way on the unconventional nature of the superconducting order. In the next section we expand upon this analysis, examining bend flux in the context of various other pairing and crystalline symmetries.

5.4 Bend fluxes for other pairing and crystalline symmetries

In this thesis, we have assumed that the superconducting order transforms as one particular representation of $\mathrm{SO}(2)_z$. We now obtain the generalization of the formula for the bend flux, Eq. (5.7), that remains valid for arbitrary irreducible representations, which can be indexed in terms of an integer m (see, e.g., Ref. [39]). For brevity's sake, we refer to the $m = 1$ case as p-wave (which is the case focused on in this thesis), and the $m = 2$ case as d-wave. En route to generalizing Eq. (5.7) to arbitrary m, we assume that transformations of the form $(m\,\alpha, -\mathrm{sgn}(\beta)\,\alpha) \in \mathrm{U}(1) \times \mathrm{SO}(2)_z$ act trivially on a uniform, maximally chiral phase. Under this assumption, and repeating the line of argument given in Sec. 5.3, *mutatis mutandis*, the bend flux formula becomes

$$\Phi_{\mathrm{bend,m}} = \big((m\Theta/\pi) + n\big)\,\Phi_0. \tag{5.8}$$

Another version of Eq. (5.7) results when we address the setting of tetragonal D_{4h} symmetry (which is, of course, discrete). In this case, the argument given in Sec. 5.3 leading

to Eq. (5.7) holds only for $\Theta = \pm\pi/2$, for which the minimum magnitude net flux through the domain wall bend in the p-wave case is $\Phi_0/2$; this is distinct from a conventional vortex, for which the net flux is always Φ_0 in magnitude. In contrast, for the d-wave case and $\Theta = \pm\pi/2$, a net flux of $n\Phi_0$ (with n integral) penetrates the bend. As a last observation, we note that for "p-wave pairing" and D_{6h} symmetry and a domain-wall bend angle of $\pi/3$, the smallest *positive* net flux accompanying the bend is $\Phi_0/3$, whereas the smallest *negative* net flux accompanying it is $-2\Phi_0/3$.

Now that we have established that in, various settings, one anticipates that a bent domain wall is accompanied by nonintegral net magnetic flux, we shall, in the next chapter, explore a range of experimental situations in which such effects might be observable.

Chapter 6

Experimental implications

We now describe three experimental scenarios in which it may prove possible to observe, via scanning magnetic microscopy, the phenomenon of sample penetration by nonintegral net magnetic flux associated with bends in walls separating regions of opposing chiral superconducting order. These scenarios are depicted schematically in Figs. 6.1, 6.2, and 6.3. Augmenting the bend flux phenomenon, which is the primary focus of the present work, it is known that domain walls are expected to produce Ampère magnetic fields, resulting from chiral currents that flow along the cores of domain walls; see Refs. [76, 52]. Such Ampère magnetic fields, and the magnetic fields that result from the associated screening currents, constitute the dipole contribution to the magnetic field shown in Fig. 5.1(b). We emphasize that, even if there were a specific, microscopic reason for the magnitude of such currents to be reduced (cf., e.g., Refs. [43, 4, 60]), e.g., below currently detectable levels [23], such a reduction would not affect the existence or magnitude of the bend fluxes discussed here which are fixed by symmetry. Thus, it is perhaps useful to regard bend fluxes as providing a robust magnetic signature of domain walls, alternate to the magnetic signature of the chiral currents themselves.

As a first scenario, consider a domain wall that intersects a physical surface of the superconducting system, the surface being oriented perpendicular to the z-axis. In this thesis we are neglecting effects resulting from the finite height above the sample surface at which magnetic fields would typically be detected. (For a discussion of such effects see, e.g., Ref. [9].) In addition, we envision domain walls to be pinned at generically located sites, e.g., by impurities. In the limit in which the bulk terms in the free energy that break $\mathrm{SO}(2)_z$ sym-

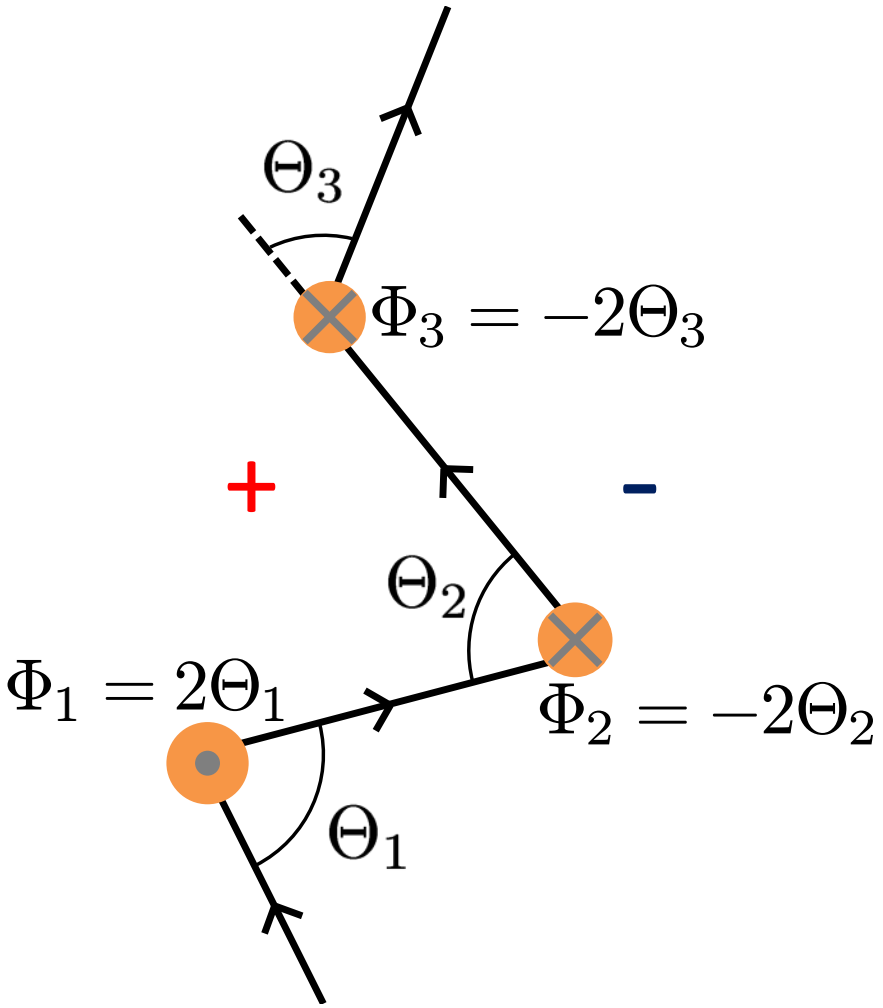

Figure 6.1: Schematic depiction of a chiral domain wall running along an ab-face of a superconductor and pinned to various locations. The wall is indicated by the oriented black line [the orientation is defined by Eq. (3.9)]. We assume that deviations from $SO(2)_z$ symmetry are sufficiently small that the arrangement of the pinning sites determines the path of the domain wall. Orange dots denote pinning sites. Near them, the domain wall bends and flux penetrates the superconductor. The specified positive angles $\{\Theta_i\}$ express the geometry of the bends, as indicated. The bend fluxes are then determined via Eq. (5.7). For each bend, we have chosen the value of n in Eq. (5.7) to give the corresponding bend fluxes $\{\Phi_i\}$ the smallest possible magnitudes. The orientation of the flux accompanying each bend is indicated via a dot (up) or a cross (down).

metry are small (as can hold occur near T_c), the spatial arrangement of these pinning sites predominates in determining the bend angles that characterize a domain wall as it traverses the sample. Assuming that these pinning sites are spaced further apart than the penetration depth, Eq. (5.7) indicates that these pinning locations would show up in scanning magnetometry as local regions of nonintegral flux penetrating the superconductor (see Fig. 6.1).

We now outline a scenario specific to Sr_2RuO_4. In both zero and nonzero in-plane magnetic fields, scanning magnetic imaging of Sr_2RuO_4 shows that vortices arrange themselves in line-like structures [8, 16, 15, 23]. One of the possible scenarios put forth to explain these structures is that the line-like structures are due to the binding of vortices to a parallel array of chiral domain walls [67]. However, to date, the line-like structures have not exhibited characteristics that would uniquely identify them as domain walls because, to within experimental uncertainty, the vortices (i.e., the local regions of penetrating magnetic field) were observed to have total fluxes that were integer multiples of Φ_0, and Ampère magnetic fields along the line-like features were not observed. The phenomenon of bend flux provides an additional route for determining whether the observed line-like structures are indeed associated with domain walls. If it proves possible to prepare a sample (e.g., via a field-sweep procedure) so that the line-like features are bent then, if the line-like structures do indeed correspond to domain walls, bends would be accompanied by a nonintegral flux penetrating the superconductor (see Fig. 6.2). The observation of nonintegral bend flux at a $\pi/2$ bend would provide further confirmation of p-wave pairing in Sr_2RuO_4 because, as noted in Sec. 5.4, d-wave pairing would produce integer bend flux. However, the fact that Refs. [8, 16, 15] do not report regions of nonintegral localized flux suggests that, in these experiments, if there are domain walls then they are aligned in parallel arrays, and thus are not bent.

A further consequence of domain walls should be evident in annular rings of broken time-reversal symmetry superconductors. As the analysis leading to Eq. (5.7) is local only to the contour $\mathcal{C}$, and does not require inspection of the superconductivity near the domain-wall

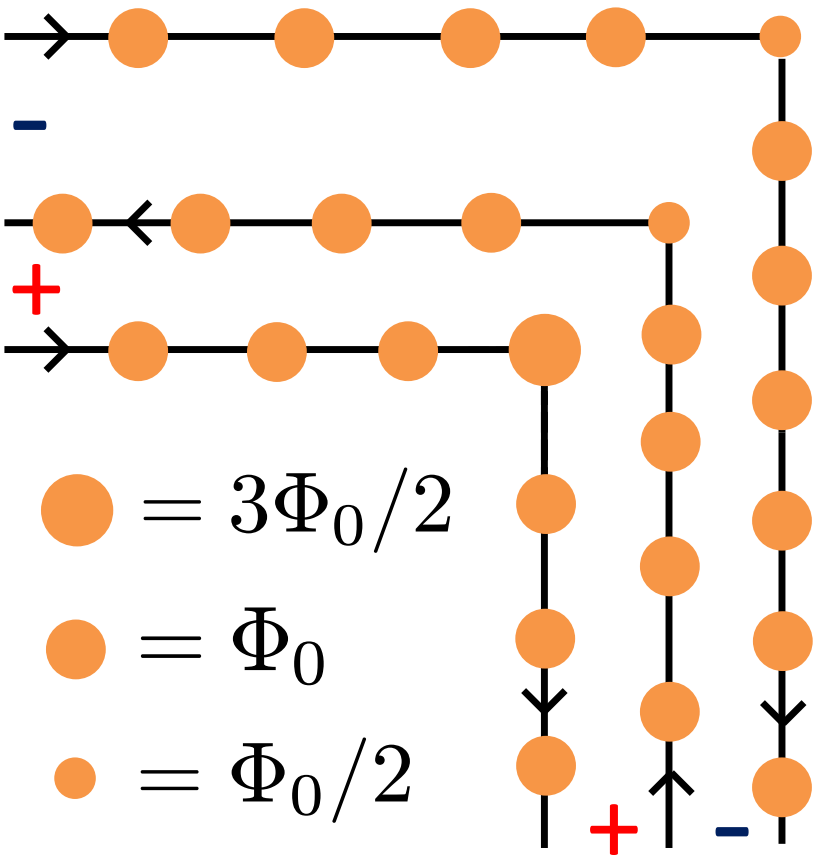

Figure 6.2: Schematic depiction of an array of domain walls (oriented black lines), each intersecting an ab-face of a superconductor. D_{4h} deviations from $\mathrm{SO}(2)_z$ symmetry are assumed to be large enough to pin domain walls to lie along specific crystallographic directions, and each domain wall is assumed to have a $\pi/2$ bend. Integral-flux vortices (intermediate size orange dots) penetrate the superconductor along the straight sections of the domain walls. At each bend, a bend flux penetrates the superconductor (large and small orange dots) and is fixed, via Eq. (5.7), to be a half integer multiple of the flux quantum. All regions of localized flux are shown as if they had the same sign, as would be energetically favorable in the presence of a magnetic field applied along the z-axis.

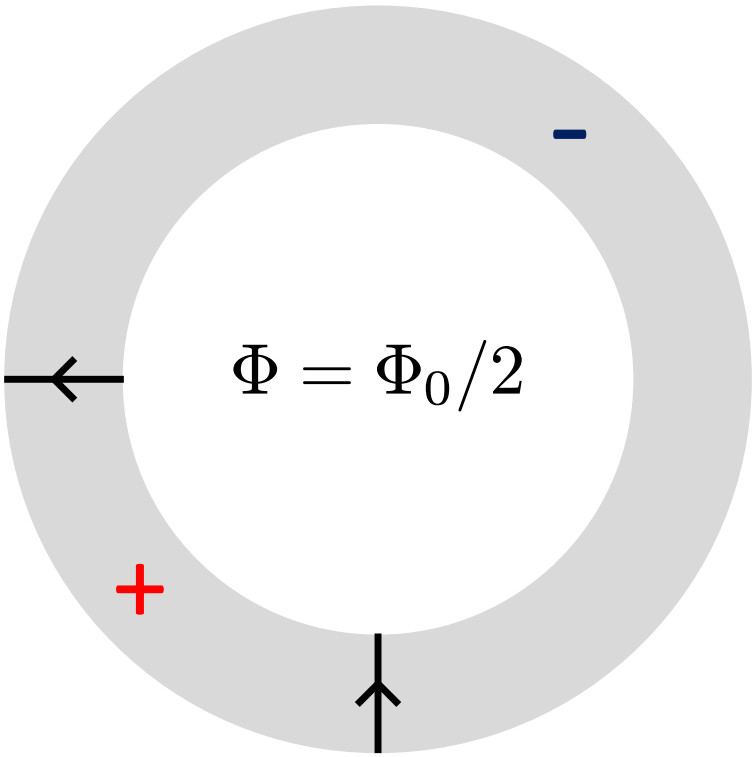

Figure 6.3: Schematic depiction of an annular sample (shaded gray) the thickness and hieght of which is larger that the penetration depth. The annulus is crossed radially by a pair of domain walls oriented at $\pi/2$ relative to one another. Tetragonal D_{4h} terms in the free energy are assumed to be large enough to pin the direction of the domain walls to crystallographically to lie along the specified directions. The minimum magnitude of the total flux through the hole would then be $\Phi_0/2$.

bend itself, it can be generalized to the case in which the bend is replaced by a hole in the superconductivity (see Fig. 6.3). Recently, evidence for half integer fluxoid behavior has been obtained in experiments on mesoscopic rings of Sr_2RuO_4 using cantilever torque magnetometry [30]. However, in those experiments the half integer fluxoid behavior was found to be accompanied by a small, rotationally invariant, in-plane component of the magnetization, and we are not aware of any reason why such a magnetization component would arise in the context of domain walls.

Part II

Half Quantum Vortices

As discussed in Chapter 1 of Part I of this thesis, the superconductivity of Sr_2RuO_4 has been proposed to be unconventional [49], having Cooper pairs of the triplet type [63, 25, 58]. There and in the remaining chapters of Part I we analyzed the magnetic properties of domain walls. Domain walls are topologically stable when the space of degenerate homogeneous equilibrium states $\mathcal{R}$ is *disconnected*, being comprised of subspaces that are related only by a discrete symmetry such as time reversal (see Fig. 3.1). In the present part of the thesis we shall study topological structures that result from a *connected* component of $\mathcal{R}$, namely line-like (i.e., vortex) and point-like topological defects.

Sr_2RuO_4 and other proposed spin-triplet superconductors and superfluids can potentially support, in additional to domain walls, other exotic topological defects, such as half quantum vortices (HQVs), characterized by the nontrivial winding of the spin structure [79, 12]. Recently, evidence for half quantum vortices has been obtained by the Budakian group at the University of Illinois, in experiments on mesoscopic rings of Sr_2RuO_4, using cantilever torque magnetometry [30]. Besides providing further support for the triplet-pairing hypothesis, this development is particularly exciting as HQVs are expected to support zero-energy Majorana modes [36, 62] and suggests that Sr_2RuO_4 could be an example of a non-abelian phase of matter, and therefore be of potential use as a host medium for topological quantum computing [34, 57].

In this part of the thesis, we study experimental and theoretical issues related to HQVs in layered, equal-spin-pairing (ESP) triplet superconductors and is organized as follows. In Chapter 7 we give a basic introduction to spin-triplet superconductivity. We discuss how spin-triplet superconductivity is naturally characterized in terms of a complex d-vector, and describe the necessary conditions for the superconductivity to be of the ESP type. ESP superconductors can be effectively described as two interpenetrating condensates, one of up-spin electrons and one of down-spin electrons. We describe how equal spin pairing raises the possibility that the superconducting order is capable of hosting half quantum vortices, which would be characterized by the relative winding of the phase of the up-spin and

down-spin components of the superconducting order parameter. Previously in Chapter 2 of Part I, we considered the general phenomenological theory of superconductors with broken time-reversal symmetry in crystalline materials of tetragonal point group symmetry, and classified the stable topological defects in Chapter 3. This analysis did not include HQVs. Thus, for the longest lengthscales HQVs are not generically stable. However, as we explain in Chapter 9, for lengthscales shorter than a characteristic "spin-orbit" length $L_{\rm SO}$, the collection of states reached by spin rotations of the superconducting order defines a subspace of homogenous states that are effectively degenerate. Even though this collection of states are not exactly degenerate, it is conventional to use the same notation as was introduced in Chapter 3, denoting this space of states as $\mathcal{R}$. As the $\mathcal{R}$ that arise in Chapter 8 are not as simple to understand intuitively as the case considered in Chapter 3, in Chapter 8 we shall classify the stable topological structures derived from $\mathcal{R}$ using the general group theoretical techniques [53]. The primary results of such an analysis are as follows: Similarly to the case of superfluid ^{3}He-A [79, 12], in addition to conventional line defects of integer vorticity, line defects of half integer vorticity (HQVs) are topologically stable excitations. However, our findings are in contrast with the case of bulk superfluid ^{3}He, in that HQVs can occur in phases which preserve time-reversal symmetry, as well as for phases which spontaneously break time-reversal symmetry. Our results also differ from those for bulk ^{3}He-A, in that the fundamental group $\pi_1(\mathcal{R})$ is now infinite, rather than finite and isomorphic to $\mathbf{Z}_4$ [79, 12]. In the next chapter, Chapter 9, we introduce the appropriate London free energy that describes layered ESP superconductors, and discuss estimates for the various coefficients in the free energy density. Building on this in Chapter 10, we study this free energy for various sample geometries, determining the conditions for equilibrium HQV stability. In contrast to previous studies [11, 74], we do not assume the sample geometry to be translationally invariant along a particular axis and thus effectively infinite in height, rather we consider sample geometries of finite height. Here, our main result is that HQVs are expected to be the equilibrium ground state for a greater range of parameters than previously estimated

on the basis of calculations for infinite height samples. An "annular," ring-shaped, geometry is particularly useful in the study of topological line defects such as half quantum vortices because such a geometry is expected to yield a discrete family of low energy "fluxoid" states in which the superconducting order parameter winds around the annulus as it would around the line defect and thus, like vortices, are indexed by the fundamental group $\pi_1(\mathcal{R})$. Recently, evidence for half integer fluxoids (the generalization of a HQV to an anuular, ring-shaped geometry) has been obtained by the Budakian group at the University of Illinois in experiments on mesoscopic rings of Sr_2RuO_4 [30] using cantilever torque magnetometry [30, 29]. In Chapter 11 we briefly describe the cantilever torque magnetometry technique and review the key experimental results of Ref. [30]. We then discuss two possible scenarios for the theoretical interpretation of the observations of Ref. [30]: a half quantum vortex scenario, and a wall vortex scenario. We argue that the HQV scenario is more consistent with observations of Ref [30]. Finally, we suggest an extension of the cantilever torque magnetometry technique that could help further determine whether the observed behavior is indeed due to HQVs. We then conclude with Chapter 12, in which we summarize our key results from Parts I and II of the thesis.

Chapter 7

Introduction to half quantum vortices

In Chapter 2 we argued on physical grounds that if the superconductivity of Sr_2RuO_4 breaks time-reversal symmetry then the superconducting order parameter would transform according to the Γ_5 representation of the tetragonal symmetry group D_{4h}. The assumption that the superconducting order transforms as Γ_5 allowed us to develop a phenomenological description of the superconducting order without having to consider the microscopic electron degrees of freedom that give rise to such order. However, in this second part of the thesis, it will be helpful to develop a more microscopic model of the superconducting order based on Yang's notion of off-diagonal long-range order [81, 44], as it will enable a discussion of how the superconducting order transforms when a spin rotation is applied to the underlying electronic degrees of freedom. Within this framework, the description of the superconducting order starts from the general quantum-mechanical state of a many-electron system plus environment, and then proceeds to the two-electron density matrix. The two-electron density matrix can be compactly expressed in terms of electron field-operators $\hat{\psi}^\dagger_a(\boldsymbol{r})$ and $\hat{\psi}_a(\boldsymbol{r})$, which respectively create and annihilate an election at position $\boldsymbol{r}$ and with spin projection a:

$$\rho^{(2)}_{a'_1 a'_2; a_1 a_2}(\boldsymbol{r}'_1 \boldsymbol{r}'_2; \boldsymbol{r}_1 \boldsymbol{r}_2) := \langle \hat{\psi}^\dagger_{a'_1}(\boldsymbol{r}'_1) \hat{\psi}^\dagger_{a'_2}(\boldsymbol{r}'_2) \hat{\psi}_{a_1}(\boldsymbol{r}_1) \hat{\psi}_{a_2}(\boldsymbol{r}_2) \rangle, \tag{7.1}$$

where the angle brackets represent both a quantum-mechanical and a statistical-mechanical average.[1] As $\boldsymbol{\rho}^{(2)}$ is a Hermitian kernal in the exchange of coordinate and spin indices, it can

[1] In general, due to spin-orbit coupling, quasiparticle states are not eigenstates of spin. However, when the crystal point group possesses an inversion symmetry (as is the case for D_{4h}) then, due to Kramers' theorem, for each value of $\boldsymbol{k}$ there still exist two degenerate states. These degenerate states are referred to as psudo-spin states. It is still possible to apply SU(2) rotation matrices to the psudo-spin indices to generate

be diagonalized and expressed in terms of its eigenvalues n_i and eigenfunctions $\Psi^i_{a_1a_2}(\boldsymbol{r}_1\boldsymbol{r}_2)$ as

$$\rho^{(2)}_{a_1'a_2';a_1a_2}(\boldsymbol{r}_1'\boldsymbol{r}_2';\boldsymbol{r}_1\mathbf{r}_2) = \sum_i n_i\, \Psi^{i*}_{a_1'a_2'}(\boldsymbol{r}_1'\boldsymbol{r}_2')\, \Psi^i_{a_1a_2}(\boldsymbol{r}_1\boldsymbol{r}_2). \tag{7.2}$$

Superconducting order is then associated with the largest eigenvalue, n_0, being of order $N/2$, where N is the number of electrons in the system. The corresponding eigenfunction $\Psi^0_{a_1a_2}(\boldsymbol{r}_1\mathbf{r}_2)$ then plays the role of an order parameter for the superconducting transition. It is useful to implement a change of basis, and express Ψ^0 in terms of the relative and center-of-mass coordinates of $\boldsymbol{r}_1$ and $\boldsymbol{r}_2$, viz., $\boldsymbol{R} \equiv (\boldsymbol{r}_1 + \mathbf{r}_2)/2$ and $\boldsymbol{r} \equiv \boldsymbol{r}_1 - \boldsymbol{r}_2$ and then to perform a Fourier transform on the relative variables, thus defining an equivalent order parameter $\psi_{ab}(\mathbf{R}, \boldsymbol{k})$, via

$$\Psi^0_{ab}(\boldsymbol{R} + \boldsymbol{r}/2, \boldsymbol{R} - \boldsymbol{r}/2) = \int \frac{d^3k}{(2\pi)^3}\, e^{i\,\boldsymbol{k}\cdot\boldsymbol{r}}\, \psi_{ab}(\boldsymbol{R}, \boldsymbol{k}). \tag{7.3}$$

We shall refer to $\boldsymbol{\psi}$ as the pairing matrix or, equivalently, the superconducting order parameter. As $\boldsymbol{\psi}$ transforms under the full symmetry group of the physical system, it provides a representation of this group. For simplicity, we assume that $\boldsymbol{\psi}$ transforms trivially under lattice translations. Thus, at the lengthscales relevant for a phenomenological description that we consider in this thesis, the equilibrium ground state of the superconducting order can be considered to be independent of $\boldsymbol{R}$. In this section we make the additional assumption that the order parameter is *odd* under the application of inversion symmetry, i.e., $\psi_{ab}(\boldsymbol{k}) = -\psi_{ab}(-\boldsymbol{k})$. This is justified in the case of superconductors such as Sr_2RuO_4, for which Josephson tunneling experiments suggest that the superconductivity has odd parity [58]. If $\boldsymbol{\psi}$ is indeed odd under inversion symmetry then, due to fermion anti-symmetry, it must be *symmetric* under exchange of its two spin-1/2 indices, so that $\boldsymbol{\psi}$ would transform as

transformations of the superconducting order. In the rest of this thesis, when we refer to the presence or absence of spin-rotational symmetry we mean, in principle, the presence or absence of degeneracy with respect to transformations of the psudo-spin indices of this type. For simplicity, however, we shall continue to use the language of spin.

a spin-1 'triplet'. Then, in terms of the conventional notion, for each value of $\boldsymbol{k}$ the pairing matrix $\boldsymbol{\psi}(\boldsymbol{k})$ can be expressed in terms of a complex d-vector $\boldsymbol{d}(\boldsymbol{k})$ via

$$\psi_{ab} = d_i(\boldsymbol{k})\sigma^i_{ac}\epsilon_{cb}. \tag{7.4}$$

Here, σ^i are Pauli spin matrices and $\boldsymbol{\epsilon}$ is the antisymmetric tensor in two indices. Traditionally, the notation $i\sigma^y$ is used for $\boldsymbol{\epsilon}$ but as there is nothing 'y' about this procedure, the ϵ notation seems favorable. The d-vector is particularly useful, intuitively, since it transforms as a vector under SO(3) spin rotations, and since, for so-called "unitary" states, it can, up to a $\boldsymbol{k}$-dependent phase, be taken to be real. All states considered in this thesis will be taken to be unitary.

One particular class of spin-triplet superconducting pairing states, which may be applicable to the superconductivity of Sr_2RuO_4 [49], is the equal spin pairing (ESP) class of states. A state is defined to be in the ESP class if $\boldsymbol{d}(\boldsymbol{k})$ is co-planer for all $\boldsymbol{k}$. An axis perpendicular to this plane is referred to as the ESP axis. If $\boldsymbol{d}(\boldsymbol{k})$ is collinear then the ESP axis can be chosen to lie anywhere within the plane perpendicular to the direction of collinearity. If the ESP axis is used to define the spin quantization axis (for the rest of this section we identity the ESP axis with the z-axis) the pairing matrix takes the form

$$\begin{pmatrix} -(d_x - id_y) & 0 \\ 0 & (d_x + id_y) \end{pmatrix} =: \begin{pmatrix} \psi_{\uparrow\uparrow} & 0 \\ 0 & \psi_{\downarrow\downarrow} \end{pmatrix}. \tag{7.5}$$

The second of these expressions makes it clear that an ESP state can be conceptualized as two interpenetrating condensates: a condensate of up-spin pairs, and a condensate of down-spin pairs. Applying a spin rotation of an angle α around the ESP axis generates the usual vector rotation transformation of the d-vector:

$$\boldsymbol{d} \to R^{\alpha\hat{z}} \circ \boldsymbol{d} = (\cos(\alpha)d_x - \sin(\alpha)d_y, \sin(\alpha)d_x + \cos(\alpha)d_y, 0). \tag{7.6}$$

Thus, a spin rotation of an angle α around the ESP axis transforms the pairing matrix as follows:

$$\boldsymbol{\psi} \to R^{\alpha\hat{z}} \circ \boldsymbol{\psi} = \begin{pmatrix} \psi_{\uparrow\uparrow} e^{-i\alpha} & 0 \\ 0 & \psi_{\downarrow\downarrow} e^{i\alpha} \end{pmatrix}, \tag{7.7}$$

i.e., it changes the relative phase between the two condensates. If a spin rotation about the ESP axis of the superconductor order does not change the free energy of the superconductor, then the phase, $\theta_\uparrow$, of the up spin condensate and the phase, $\theta_\downarrow$, of the down spin condensate is not fixed energetically to have a preferred relative value. Thus, in this case, the phases of each condensate would be treatable—not just kinematically but energetically—as independent degrees of freedom. Importantly, each condensate could potentially have an independent winding number around a given spatial contour. Vortices for which one of the two condensates has unit vorticity, while the other has no vorticity, are called half quantum vortices (HQVs). Another way to characterized such HQVs is to say both the relative phase $\alpha = (-\theta_\uparrow + \theta_\downarrow)/2$ and the overall phase $\theta = (\theta_\uparrow + \theta_\downarrow)/2$ rotate by π around a contour that encircles a vortex. As the overall phase θ is gauge-coupled to the vector potential, a isolated HQV in a bulk superconductor results in a net flux of $\Phi_0/2$ penetrating the superconductor, which is half of the net flux of a conventional vortex. In the next section we will consider the topological stability of such HQVs.

Chapter 8

Analysis of the topological stability of half quantum vortices

In this chapter we consider the general topological stability of line and point defects for layered ESP superconductors with weak spin-orbit coupling. Starting with reference ESP superconducting states of Γ_5^- and Γ_1^- symmetry (which we refer to throughout the rest of this thesis as the A and B phases respectively), we construct the space of states $\mathcal{R}$ as the coset space G/H. Here, G is the appropriate symmetry group that includes either $\mathrm{SO}(2)_z$ or SO(3) spin rotations of the superconducting order parameter, and H is the isotropy subgroup of G, i.e., H is the subgroup of G that acts trivially on the reference state [53]. In this part of the thesis we will only consider line and point topological defects. As explained in Ref. [53], we thus only need to consider a *connected* component of $\mathcal{R}$.

A primary distinction between the analysis of topological defects in the case of superfluid ^{3}He and in the case of layered ESP superconductors is that for layered ESP superconductors is that, due to the significant physical differences between in-plane directions and the z-axis direction, the orbital angular momentum of Cooper pairs is likely to be confined to be either aligned or anti-aligned with the z-axis. Thus, in contrast to the case of *bulk* superfluid ^{3}He, in the case of layered spin triplet superconductors, arbitrary SO(3) rotations of the orbital degrees of freedom are disfavored energetically. As remarked in Chapter 2 of Part I, a residual $\mathrm{SO}(2)_z$ orbital symmetry may remain. However, in the cases that we consider in Part II, it is not necessary to include such a symmetry in G, as it is degenerate with $U(1)$ gauge transformations (in the case of the A phase), or degenerate with $\mathrm{SO}(2)_z$ spin symmetry (in the case of the B phase).

For a cylindrical Fermi-surface, with the symmetry axis of the cylinder defining the z-

axis, the usual representative ESP superconducting states of Γ_5^- and Γ_1^- symmetry [49] are, respectively,

$$\boldsymbol{d}_A(\boldsymbol{k}) = (0, 0, k_x + ik_y), \tag{8.1}$$

$$\boldsymbol{d}_B(\boldsymbol{k}) = (k_x, k_y, 0). \tag{8.2}$$

The B state *preserves* time-reversal symmetry, whereas the A state *breaks* time-reversal symmetry and transforms to the state $(0, 0, k_x - ik_y)$ under time reversal. For electrons moving through periodic crystals, $\boldsymbol{d}$ and $\boldsymbol{\psi}$ are periodic functions of $\boldsymbol{k}$. Thus, on the right hand side of Eq. (8.1), k_x and k_y should be replaced by periodic functions of $\boldsymbol{k}$, which transform like k_x and k_y under the operations of the crystal point group; e.g., for tetragonal symmetry, k_x could be replaced by $\sin(ak_x)$, where a is the in-plane lattice spacing of the unit cell.[1]

As we are interested in how these reference states transform under the action of the simply connected SU(2) spin symmetry group, and not just SO(3), it will be useful to consider the form of the order parameter matrix for these reference states:

$$\boldsymbol{\psi}_A(\boldsymbol{k}) = \begin{pmatrix} 0 & k_x + ik_y \\ k_x + ik_y & 0 \end{pmatrix}, \tag{8.3}$$

$$\boldsymbol{\psi}_B(\boldsymbol{k}) = \begin{pmatrix} -(k_x + ik_y) & 0 \\ 0 & k_x - ik_y \end{pmatrix}. \tag{8.4}$$

[1]It should be noted that pairing with Γ_5^- and Γ_1^- symmetry need not, in general, be ESP. For example, pairing of the form $(K_x, K_y, \epsilon K_z)$ (where $K_i(\boldsymbol{k})$ are periodic functions of $\boldsymbol{k}$) also has Γ_1^- symmetry. In this thesis, we shall not analyze non-ESP pairing in detail. However, we note that if the ESP axis is allowed to change directions as a function of $\boldsymbol{k}$ then a state having pairing of the form $(K_x, K_y, \epsilon K_z)$ may still be "effectively" ESP, whereby we mean that the superconductivity can still be effectively described as two interpenetrating condensates and that the analysis developed in this thesis may still, with minor modifications, be largely applicable. An important question, which helps to determine if a state is effectively ESP is whether, given a representative pairing matrix, a smooth choice of ESP axis is possible for all $\boldsymbol{k}$ where $\boldsymbol{\psi}$ is non-zero. For for a spherical Fermi surface and B-phase pairing, a smooth choice of ESP axis is not possible.

For both of the above pairing matrices, Eqs. (8.3) and (8.4), we have chosen the crystal z-axis to be the spin-quantization direction. As the ESP axes are in-plane for the A phase, this form of $\boldsymbol{\psi}_A$ is not diagonal. The action of an element of $\boldsymbol{U} \in \mathrm{SU}(2)$ on $\boldsymbol{\psi}$ is given by $U \circ \boldsymbol{\psi} = \boldsymbol{U} \cdot \boldsymbol{\psi} \cdot \boldsymbol{U}^{\mathrm{t}}$, where $^{\mathrm{t}}$ indicates a transpose, and the operation $\cdot$ represents usual matrix multiplication.[2]

In the sections that follow, namely Secs. 8.1, 8.2, and 8.3, we classify the topologically stable defects for the following three cases :

(I) B phase with $\mathrm{SO}(2)_z$ spin symmetry;

(II) B phase with SO(3) spin symmetry;

(III) A phase with SO(3) spin symmetry.

As explained in Ref. [53], this classification can be accomplished via the following steps:

(i) Extend G to its simply connected universal covering group.

(ii) Generate an (over) complete covering of the order parameter space $\mathcal{R}$ by considering all states generated by the action of the elements of G on a reference order parameter state $\boldsymbol{\psi}_{\mathrm{R}}$. (The particular choice of $\boldsymbol{\psi}_{\mathrm{R}}$ does not effect the classification.)

(iii) Determine the isotropy subgroup H of G. The isotropy subgroup consists of the elements $g \in G$ such that $g \circ \boldsymbol{\psi}_{\mathrm{R}} = \boldsymbol{\psi}_{\mathrm{R}}$.

(iv) Determine the (normal) subgroup H_0 of H that is connected to the identity.

(v) Then, line defects are classified by the discrete group H/H_0, i.e., $\pi_1(\mathcal{R}) \cong H/H_0$,

(vi) And point defects are classified by $\pi_1(H_0)$, i.e., $\pi_2(\mathcal{R}) \cong \pi_1(H_0)$.

[2]The transpose operation is necessary, rather than the usual adjoint †, because $\boldsymbol{\psi}$ is a type $(2,0)$ tensor rather than a type $(1,1)$ tensor.

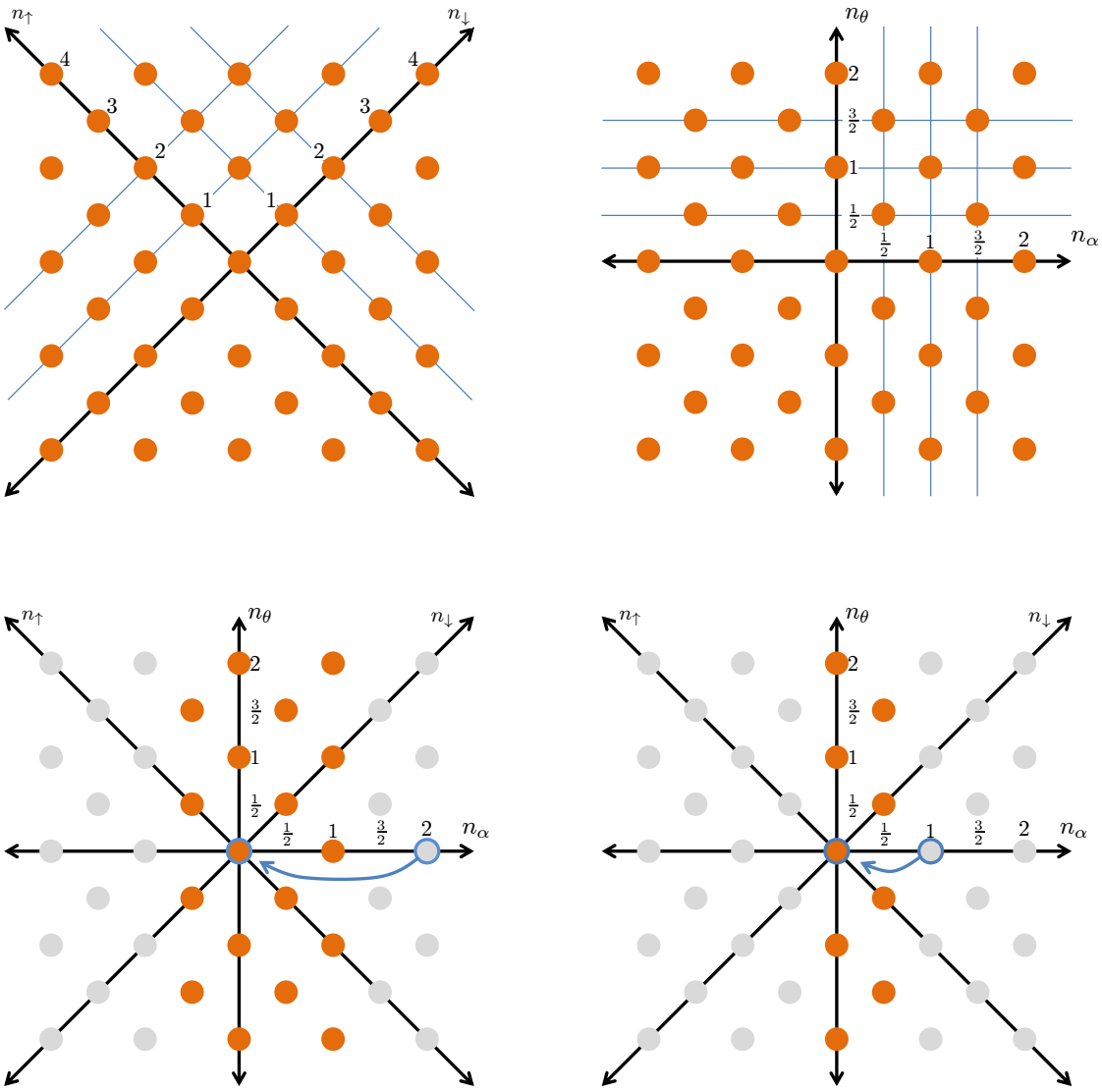

Figure 8.1: Visual representation of the groups $\pi_1(\mathcal{R})$. Each dark orange point represents a distinct group element. The top two panels represent the B phase with $\mathrm{SO}(2)_z$ spin symmetry. In this case, $\pi_1(\mathcal{R}_{B,I}) \cong \mathbf{Z} \oplus \mathbf{Z}$. The bottom left panel represents the case of B phase pairing with SO(3) spin symmetry, for which $\pi_1(\mathcal{R}_{B,II}) \cong \mathbf{Z} \oplus \mathbf{Z}_2$. The bottom right panel represents the case of A phase pairing with SO(3) spin symmetry, for which $\pi_1(\mathcal{R}_A) \cong \mathbf{Z}$. The top two panels illustrate two different ways π_1 (and thus the stable topological defects) can be indexed. Any element with $|n_\theta| = 1/2$ indexes a half quantum vortex topological defect. In the bottom two panels the trivial [i.e., (0,0)] state is equivalent to states of either 2π or 4π spin winding. Such an equivalence indicates that, e.g., in these two cases a vortex in which the up-spin condensate winds by 2π and the down spin condensate winds by -2π can be continuously deformed to a state with no spin winding. In all pictured cases, the state with $(n_\theta, n_\alpha) = (1/2, 1/2)$ is topologically non-trivial. Thus, in these three cases HQVs are topologically stable and distinct from conventional vortices.

The results of this classification are summarized in Fig. 8.1. As the reference A phase is invariant under $\mathrm{SO}(2)_z$ spin symmetry, HQVs do not exist in this case, and we shall thus not consider it in any detail in the the following sections.[3]

8.1 Vortex topological defects of the B phase with $\mathrm{SO}(2)_z$ spin symmetry

In this section we begin our analysis of the topologically stable line and point defects with the most elementary situation: the B phase with $\mathrm{SO}(2)_z$ spin symmetry. As the physical properties of Sr_2RuO_4 (such as its electrical resistivity) are typically more similar for two in-plane directions than they are for an in-plane direction and the z-axis, $\mathrm{SO}(2)_z$ spin symmetry is likely to be an intermediate between the fully spin-orbit locked and complete SO(3) spin symmetry. We now execute the steps required to determine the stable topological defects listed in the previous section. Step (i) is to extend $U(1) \times \mathrm{SO}(2)_z$ to its simply connected universal covering group. This is done by extending both the $U(1)$ gauge group and the $\mathrm{SO}(2)_z$ spin group to the group $\mathbf{R}$ of real numbers under addition. To implement step (ii) we act on the reference order parameter $\boldsymbol{\psi}_B$ of Eq. (8.1) with an arbitrary element of $\mathbf{R} \times \mathbf{R}$.

As the ESP axis coincides with the z-axis, $\mathrm{SO}(2)_z$ spin rotations transform the order parameter as Eq. (7.7). Thus, the action of $(\theta, \alpha) \in \mathbf{R} \times \mathbf{R}$ on $\boldsymbol{\psi}_B$ results in the general element of $\mathcal{R}_{B,I}$:

$$(\theta, \alpha) \circ \boldsymbol{\psi}_B = e^{i\theta} \begin{pmatrix} -(k_x - ik_y)e^{-i\alpha} & 0 \\ 0 & (k_x + ik_y)e^{i\alpha} \end{pmatrix}. \tag{8.5}$$

The space of states $\mathcal{R}_{B,I}$ can be visualized as the product of two circles, $S^1 \times S^1$, i.e. a torus,

[3] It is sometimes suggested that a large z-axis magnetic field may induce a state with A phase pairing to simply rotate the d-vector to an arbitrary in-plane direction. However, the work of Ref. [2] suggests that a transition to a phase of B-like symmetry is energetically favored instead.

with the points (θ, α) and $(\theta + \pi, \alpha + \pi)$ being identified. We now consider the isotropy subgroup H. By inspection, we see that for

$$(\theta, \alpha) = \left(\frac{1}{2}(n_\uparrow + n_\downarrow), \frac{1}{2}(-n_\uparrow + n_\downarrow) \right), \qquad (n_\uparrow, n_\downarrow) \in \mathbf{Z} \oplus \mathbf{Z} \tag{8.6}$$

the order parameter matrix is invariant. As the group H is discrete, H_0 (i.e., the subgroup of H connected to the identity) is simply the identity itself. Thus, for the B phase with $\mathrm{SO}(2)_z$ spin symmetry, the vortices have the structure that we anticipated in Sec. 7, i.e., $\pi_1(\mathcal{R}_{B,I}) \cong \mathbf{Z} \oplus \mathbf{Z}$, and half quantum vortices are allowed (see Fig. 8.1). As H_0 is trivial, there are no stable point defects.

8.2 Vortex topological defects of the B phase with SO(3) spin symmetry

We now consider the topological defects of the B phase assuming SO(3) (rather than $\mathrm{SO}(2)_z$) spin symmetry. The first step is to extend $U(1) \times \mathrm{SO}(3)_{\mathrm{spin}}$ to its simply connected universal covering group $\mathbf{R} \times \mathrm{SU}(2)_{\mathrm{spin}}$. We choose $\boldsymbol{\psi}_B$ of Eq. (8.4) as the reference state. To generate an arbitrary element of $\mathcal{R}_{B,II}$ we apply a general element $(\theta, \boldsymbol{U}) \in \mathbf{R} \times \mathrm{SU}(2)_{\mathrm{spin}}$ to $\boldsymbol{\psi}_B$:

$$\begin{aligned} (\theta, U) \circ \boldsymbol{\psi}_B &= e^{i\theta}\, U\, \boldsymbol{\psi}_B\, U^{\mathrm{t}} \\ \boldsymbol{U} &= e^{i\alpha\hat{\alpha}\cdot\sigma/2}. \end{aligned} \tag{8.7}$$

We now consider the corresponding isotropy subgroup H. The elements of G that leave $\boldsymbol{\psi}_B$ invariant come in four sets:

$$H = (\mathbf{Z}, \boldsymbol{I}) \cup (\mathbf{Z}, -\boldsymbol{I}) \cup (\mathbf{Z} + \frac{1}{2}, +i\sigma_z) \cup (\mathbf{Z} + \frac{1}{2}, -i\sigma_z), \tag{8.8}$$

where the elements of the last two sets are rotations of $\pm\pi$ around the z-axis, combined with half integer translations of the gauge degree of freedom. That H cannot be larger is due to the fact that, around any axis other than the z-axis, the reference state first returns to itself after a 2π rotation. However, a rotation by 2π about an arbitrary axis corresponds to the group element $-\boldsymbol{I}$, and such a group element is already part of the second of the four sets in the previous equation.

As can be checked by explicit evaluation, H is abelian. One can also check that each element $h \in H$ can be written (in a non-unique way) as

$$\begin{aligned} h &= \left(\frac{1}{2}, -i\sigma_z\right)^{n_\downarrow} \circ \left(\frac{1}{2}, i\sigma_z\right)^{n_\uparrow} \\ &= \left(\frac{1}{2}(n_\uparrow + n_\downarrow), (-i\sigma_z)^{(-n_\uparrow + n_\downarrow)}\right), \end{aligned} \tag{8.9}$$

where $n_\uparrow$ and $n_\downarrow$ are both integers. Thus, there exists a surjective homomorphism of abelian groups $\mathbf{Z}\oplus\mathbf{Z} \to H$. Under this homomorphism, elements of the form $(\frac{1}{2}, -i\sigma_z)^{2n} \circ (\frac{1}{2}, i\sigma_z)^{-2n}$ are mapped to the identity $(0, \boldsymbol{I})$. Therefore, the kernel subgroup of the homomorphism is $\mathbf{Z}(2, -2)$. By the first isomorphism theorem of abelian groups [17], we then have

$$H \cong \mathbf{Z} \oplus \mathbf{Z}/\mathbf{Z}(2, -2) \cong \mathbf{Z} \oplus \mathbf{Z}_2. \tag{8.10}$$

Again, as in the previous section, H_0 is trivial, so $\pi_1(\mathcal{R}_{B,II}) \cong \mathbf{Z} \oplus \mathbf{Z}_2$, and there are no topologically stable point defects. Using the homomorphism $\mathbf{Z} \oplus \mathbf{Z} \to \pi_1(\mathcal{R}_{B,II})$, the elements of $\pi_1(\mathcal{R}_{B,II})$ can be indexed by the conjugacy classes $\overline{(n_\uparrow, n_\downarrow)} \cong (n_\uparrow, n_\downarrow) + \mathbf{Z}(2, -2)$ where $n_\uparrow$ and $n_\downarrow$ are both integers. In Fig. 8.1 a unique value of $(n_\uparrow, n_\downarrow)$ is indicated for each conjugacy class. Another way to index $\pi_1(\mathcal{R}_{B,II})$ is by the following conjugacy classes: $(n_\theta, n_\alpha)+\mathbf{Z}(0, 2)$, where n_θ and n_α are equal to $(n_\uparrow+n_\downarrow)/2$ and $(-n_\uparrow+n_\downarrow)/2$ respectively and are either both integral or both half integral. Due to the conjugacy relation n_α is defined only modulo 2. Thus, for the B phase with SO(3) spin symmetry, vortices are indexed

in same way as in Sec. 8.1, with the additional proviso that a 4π winding of the α field is topologically trivial and can be smoothly deformed to the trivial configuration (see Fig. 8.1).

8.3 Vortex and point topological defects of the A phase with SO(3) spin symmetry

Lastly, we consider the topological defects of the A phase, assuming SO(3) spin symmetry. In this case we choose $\boldsymbol{\psi}_A$ of Eq. (8.1) as the reference state. To generate an arbitrary element of $\mathcal{R}_A$ we again apply a general element $(\theta, \boldsymbol{U}) \in \mathbf{R} \times \mathrm{SU}(2)_{\mathrm{spin}}$, in this case to $\boldsymbol{\psi}_A$:

$$\begin{aligned} (\theta, U) \circ \boldsymbol{\psi}_A &= e^{i\theta}\, U\, \boldsymbol{\psi}_A\, U^{\mathrm{t}} \\ \boldsymbol{U} &= e^{i\alpha\hat{\alpha}\cdot\sigma/2}. \end{aligned} \tag{8.11}$$

To determine the isotropy subgroup H, we first consider H_0, i.e., the connected subgroup of H. As $\boldsymbol{d}$ points along the z-axis, the subgroup H_0 is the set of group elements of the form $(0, \exp(i\alpha\sigma_z/2))$ such that $\alpha \in [0, 4\pi)$ i.e. are rotations about the z-axis. We now consider the full structure of H. In addition to group elements in H_0, the other elements of H are rotations by $\pm\pi$ about any axis in the x-y plane combined with $\pi + 2\pi n$ gauge translations, where n is an integer. These group elements can be expressed as $(\pi + 2\pi n, i\sigma_y) \circ (0, \exp(i\alpha\sigma_z/2))$. The ability to express such group elements in this way is related to the fact that the elements $h \in H$ can be partitioned into conjugacy classes of the subgroup H_0. Each conjugacy class $\overline{h}_n$ can be indexed by a unique representative element $h_n \in H$ as

$$h_n = (\pi, i\sigma_y)^n, \qquad n \in \mathbf{Z}, \tag{8.12}$$

$$\overline{h}_n = \left\{(\pi, i\sigma_y)^n \circ (0, e^{i\alpha\sigma_z/2})\right\}_{\alpha\in[0,4\pi)}. \tag{8.13}$$

This choice of representative elements makes it clear that the conjugacy classes form a group[4] isomorphic to the integers, so that $H/H_0 \cong \mathbf{Z}$. As $\pi_1(\mathcal{R}_A) \cong H/H_0$, the topologically stable line defects of the A phase are indexed by $\mathbf{Z}$. Equivalently, we can describe the elements of $\pi_1(\mathcal{R}_A)$ via the conjugacy classes $\overline{(n_\theta, n_\alpha)}_n = (n/2, n/2) + \mathbf{Z}(0,1)$ where n_θ and n_α are both integers or both half integers. Importantly, in the present case, an application of a 2π spin rotation to the superconducting order is topologically trivial. Thus, the numbers n_α are defined only modulo 1 and are not independent of n_θ. Even though the structure of the fundamental group is isomorphic to $\mathbf{Z}$, in contrast to conventional superconductors HQV's are now topologically *stable*, and correspond, in bulk systems, to vortices which generate a net flux of $n_\theta \Phi_0$. Interestingly, the merging of any two half integer vortices results in a vortex that is topologically equivalent to a conventional integer vortex, i.e., results in a vortex that can be transformed, via local continuous deformations of the superconducting order, into a vortex with trivial spin structure. Also, as $H_0 \cong S^1$, stable point-defects exist, that are also indexed by the group $\pi_2(\mathcal{R}_A) \cong \mathbf{Z}$. An example for $n = 1$ is the "hedgehog" configuration, for which $\hat{d} = \hat{r}$, where $\hat{r}$ is the radial unit vector.

[4] As H_0 is generically a normal subgroup of H, the conjugacy classes of H/H_0 form a group (see Ref. [53]).

Chapter 9

Role of spin-orbit symmetry breaking

In the previous chapter we established that for layered ESP superconductors, half quantum vortices are topologically stable in either the A or the B phase, assuming SO(3) spin rotation symmetry, as well as in the case of the B phase, assuming $\mathrm{SO}(2)_z$ spin rotation symmetry. We now study the form of the "spin-orbit" coupling that breaks the spin rotation symmetry. Such symmetry breaking in superfluid ^{3}He arises from the dipole interaction between ^{3}He atoms, whereas in Sr_2RuO_4 and other triplet superconductors such symmetry breaking can arise from both single-particle effects and from electron-electron interactions.

We first consider the case of $\mathrm{SO}(2)_z$ symmetry breaking. In the case of D_{4h} tetragonal symmetry, $\mathrm{SO}(2)_z$ spin transformations mix states of Γ_1^- and Γ_2^- symmetry as well as mixing states of Γ_3^- and Γ_4^- symmetry. As such states are generically not degenerate, there can exist a symmetry-allowed potential term in the free-energy density of the form

$$f_{\mathrm{pot,SO}} = \frac{1}{2} E_{\mathrm{SO}} \sin^2 \alpha. \tag{9.1}$$

As, up to a global gauge transformation, a spin rotation through π degrees returns a state to its original configuration, the spin orbit potential term $f_{\mathrm{pot,SO}}$ must be π periodic in α. In this thesis we consider only the fundamental harmonic.

We now study how such a term is related to a "spin-orbit" length L_{SO}, which has the feature that on lengthscales shorter than L_{SO}, effective spin symmetry is restored, whereas for lengthscales larger than L_{SO}, the spin degrees of freedom become "locked" to the orbital degrees of freedom which are themselves locked to the crystal lattice. If we also assume that

variations in the superconducting order only occur along in-plane directions, the gradient terms of the London-limit free-energy density take an especially simple form [11, 14]:

$$F[\theta, \alpha, \boldsymbol{A}, \boldsymbol{H}] = \frac{1}{2}\int_{\mathrm{SC}} d^3r \left\{|\boldsymbol{\nabla}\theta - \boldsymbol{A}|^2 + \rho|\boldsymbol{\nabla}\alpha|^2 + E_{\mathrm{SO}}\sin^2\alpha\right\} + \frac{1}{2}\int d^3r|\boldsymbol{\nabla}\times\boldsymbol{A} - \boldsymbol{H}|^2, \tag{9.2}$$

where we have employed the unit conventions defined in Chapter 2. The parameter ρ is the ratio of the spin superfluid density to the charge superfluid density (i.e., $\rho_{\mathrm{sp}}/\rho_{\mathrm{s}}$), and quantifies the ratio of the kinetic energy of spin and charge currents of the same velocity [42]. A variational argument indicates that generically, ρ is less than unity [41]. However, the experimentally realized value for Sr_2RuO_4 is not yet known.

By comparing the coefficients of the $|\boldsymbol{\nabla}\alpha|^2$ and $\sin^2\alpha$ terms, we see that $L_{\mathrm{SO}} = (\rho/E_{\mathrm{SO}})^{1/2}$ defines a characteristic lengthscale for variations in the α field. For volumes that have characteristic lengths short compared to L_{SO}, the gradient energies dominate the potential energy, and the free energy can be regarded as being effectively rotationally invariant. Conversely, for large volumes, the potential term dominates.

So far in this section we have been considering the case of $\mathrm{SO}(2)_z$ spin symmetry. We now consider the case of SO(3) spin symmetry. The construction of a potential term that breaks the spin symmetry can be treated similarly to the case of $\mathrm{SO}(2)_z$ symmetry. We first note that a generic SO(3) rotation $R^{\boldsymbol{\theta}}$ can be decomposed, in terms of Euler angles, into a sequence of three rotations: $R^{\phi\hat{z}}R^{\alpha\hat{y}}R^{\zeta\hat{z}}$. If we assume that there is a residual $\mathrm{SO}(2)_z$ spin symmetry, the free energy potential term cannot depend upon ϕ or ζ. This term then reduces to that of Eq. (9.2); however in the case of SO(3) spin symmetry the energy scale E_{SO} is expected to be larger, and the corrsponding lengthscales are expected to be shorter than the case of $\mathrm{SO}(2)_z$ spin symmetry. In the following section we describe an experimental estimate of the energy scale for SO(3) spin symmetry breaking.

9.1 Experimental estimate of the strength of SO(3) symmetry breaking

An estimate of the energy scale for the SO(3) symmetry breaking in unitary ESP superconductors can be made from experiments that measure the spin susceptibility in the superconducting state. This is because, in unitary ESP superconductors, the spin susceptibility along the ESP axis is essentially equal to the normal-state spin susceptibility, whereas it is reduced in the direction(s) in which the d-vector points. Thus, if a magnetic field can be made to penetrate the bulk of the sample (e.g., if the field is above the first critical field for a given sample geometry or if a probe is sensitive to volumes within a penetration depth of the surface), and if the magnetic field points along the d-vector, then the superconducting order has an energetic choice: It can either remain in the same state, or it can have the d-vector rotated away from its preferred direction, costing spin-orbit energy but saving energy by allowing the spins to polarize. Thus, the spin-orbit energy can be estimated by the magnetic field $H_{\rm unlock}$ at which the d vector would unlock from the direction preferred by the spin-orbit energy, which allows the spins to more fully polarize, i.e.,

$$E_{\rm SO} \sim \chi_S H_{\rm unlock}^2. \tag{9.3}$$

Here, χ_S is the normal state spin susceptibility. For Sr_2RuO_4, χ_S is of order 10^{-3} emu/mole and is isotropic to within 5% at low temperatures [50].

Below the unlocking field, the z-axis spin susceptibility is expected to be reduced for the A phase, whereas for the B phase the in-plane spin susceptibility is expected to be reduced. Knight-shift measurements of the spin-susceptibility show no reduction of this susceptibility in the superconducting state, for either in-plane *or* z-axis directions. Thus, the pairing symmetry cannot be simply determined from such spin-susceptibility measurements. To date, the lowest magnetic fields at which Knight shift experiments have been reported are

550 Oe for in-plane field directions [55] and 200 Oe for the z-axis field direction [56]. Using the estimate

$$\frac{L_{\mathrm{SO}}}{\xi_0} \sim \left(\frac{H_c^2}{\chi_S H_{\mathrm{unlock}}^2} \right)^{1/2}, \tag{9.4}$$

along with the experimentally determined coherence length ξ_0 and thermodynamic critical field H_c appropriate for Sr_2RuO_4[49], the SO(3) spin-orbit length L_{SO} for Sr_2RuO_4 at low temperatures can be estimated to be greater than approximately $30\,\xi_0 = 2\,\mu m$.

Chapter 10

Stability of half quantum vortices: Effects of sample geometry

For ESP superconductors, in which the current carriers are electrically charged, individual HQVs have a prohibitive energy cost, relative to conventional vortices, even if the spin-orbit coupling were neglected. This energy cost is due to the fact that charge currents, which are features of both HQVs and conventional vortices, decay in strength exponentially, away from the vortex core, on a lengthscale set by the penetration depth λ. In contrast, spin currents, which are featured by HQVs, go unscreened and decay in strength only algebraically as $1/r$, where r is the distance away from the vortex core. Because of this, relative to conventional integer vortices, HQVs have an energy cost that grows logarithmically with the system size.[1] Although isolated HQV have a prohibitive energy cost in bulk systems, it is possible that they would be stable in "mesoscopic" samples, i.e., samples with linear size comparable to λ [11].

We now consider the effects a mesoscopic sample having a multiply connected geometry. A multiply connected geometry (such as an annular geometry) is useful, both theoretically and experimentally, in the study of topological line defects because such a geometry yields a discrete family of states, in which the order parameter winds around the annulus as it would around a vortex core. (When we seek to distinguish this discrete family of low energy states from bulk vortex states we will use the term "fluxoid state," however for simplicity we will often refer to them as vortices or as vortex states.) Thus, these fluxoid states are

[1] As the contribution from the spin-orbit energy is positive-definite for HQVs, whereas it is zero for conventional integer vortices, the inclusion of the spin-orbit potential energy can only make HQVs more unstable. In fact, if one *does* include the spin-orbit potential energy, for lengthscales larger than $L_{\rm SO}$ the energy cost of an HQV relative to an integer vortex would grow linearly with the system size.

indexed by the elements of the first homotopy group $\pi_1(\mathcal{R})$ of the order parameter coset space $\mathcal{R}$, just as vortices are, but have a number of advantages over conventional vortices. One such advantage is that fluxoid states are often lower in energy and are stabilized at lower applied fields compared to vortices that pass through the bulk of the sample. Thus, they can potentially be studied independently of bulk vortices, i.e., they can be studied in a parameter regime where bulk vortices are thermodynamically unstable. Another advantage of fluxoid states it that they evades complications that would arise from additional degrees of freedom associated with the core of a vortex passing through the bulk of the superconductor.

In the next section we consider the energetics of fluxoid states in the following two geometries: (i) An infinitely long, hollow cylinder of radius R and wall thickness d, as considered in Ref. [11]. The wall thickness d is assumed to be small compared to R and λ, where λ is the penetration depth.[2] (ii) An annulus of radius R and cross sectional diameter d. Again, d is assumed to be small compared to R and λ.

The free energy that we shall employ in our analysis is that of Eq. (9.2), with the spin-orbit potential term neglected. This free energy only *directly* applies to the case of B-phase pairing with $\mathrm{SO}(2)_z$ spin symmetry. However, it also applies in the form of a variational estimate to the cases of SO(3) spin symmetry and either A or B pairing; the variational assumption being the requirement that the ESP axis points in a single, in-plane direction throughout the superconducting sample. Relaxing this variational assumption can only *decrease* the energy of the HQVs and integer vortices, and since HQVs feature spin currents while integer vortices do not, it is natural to assume that this decrease would be larger for HQVs than for integer vortices.

[2]The generalization to arbitrary values of the ratios d/λ and R/λ, and also for the case of a constriction is studied in [74].

10.1 Energetic stability of an half quantum vortex: Hollow, thin-walled, infinitely long cylinder sample geometry

We begin our analysis of the energetical stability of HQVs with the case, considered in Ref. [11], of a hollow cylinder of radius R and wall thickness d, where the height of the cylinder is assumed to be infinite and $d \ll R, \lambda$. The free energy is constructed using Eq. (9.2), and we neglect the spin-orbit potential term. For clarity, we restore the parameter λ, which is unity in our system of units. The free energy depends on the parameters $(\phi_H, \phi_M, n_\theta, n_\alpha)$ which are defined as follows:

$$\phi_H = \frac{\pi R^2 H}{\Phi_0}, \tag{10.1}$$

$$\phi_M = \frac{2\pi R A_\phi(R)}{\Phi_0} - \phi_H, \tag{10.2}$$

$$n_\theta = \frac{1}{2\pi} \oint d\theta, \tag{10.3}$$

$$n_\alpha = \frac{1}{2\pi} \oint d\alpha. \tag{10.4}$$

Here, $A_\phi(R)$ is the $\hat{\phi}$ component of A, evaluated at radial distace R. The fluxes ϕ_H and ϕ_M respectively characterize the external and induced magnetic flux through the cylinder. The vortex parameters n_θ and n_α are defined for contours that once circle the central hole of the cylinder and, as they index the elements of $\pi_1(\mathcal{R})$, characterize the fluxoid state of the superconducting order (see Fig. 10.1). Expressed in terms of these parameters, the free energy of Eq. (9.2) takes the form

$$\frac{2\pi d}{R}\left[\frac{1}{2}(n_\theta - \phi_H - \phi_M)^2 + \frac{1}{2}\,\rho\, n_\alpha + \frac{1}{2}\,\beta_{\rm cyl}^{-1}\,\phi_M^2\right]. \tag{10.5}$$

The parameter $\beta_{\rm cly}$ is expressed in terms of the geometrical factors as

$$\beta_{\rm cyl} = Rd/2\lambda^2. \tag{10.6}$$

The value of ϕ_M is determined by the stationary condition $\delta F/\delta\phi_M = 0$, which yields the value

$$\phi_M = \frac{1}{1+\beta^{-1}}(n_\theta - \phi_H). \tag{10.7}$$

Substituting this value for ϕ_M back into the free energy, the free energy (up to a constant term) reduces to

$$F[n_\theta, n_\alpha, \phi_H] = \frac{2\pi d}{R}\left[\frac{1}{2(1+\beta)}(n_\theta - \phi_H)^2 + \frac{1}{2}\,\rho\; n_\alpha^2\right]. \tag{10.8}$$

For $\phi_H = 1/2$, the integer vortex states $(n_\theta, n_\alpha) = (0,0)$ and $(1,0)$ are energy-degenerate, whereas the half quantum vortex states $(n_\theta, n_\alpha) = (1/2, 1/2)$ can be either metastable or the globally stable equilibrium state. The condition for an HQV at $\phi_H = 1/2$ to be the globally stable equilibrium state (i.e., the state with the lowest free energy) is given by

$$\rho < (1+\beta)^{-1}. \tag{10.9}$$

Thus HQV stability occurs for smaller values of β. This requires that *both* R and d be small, or at most comparable to λ. We note that although λ increases with increasing temperature, ρ is also temperature dependent, tending to unity as $T \to T_c$ [42].

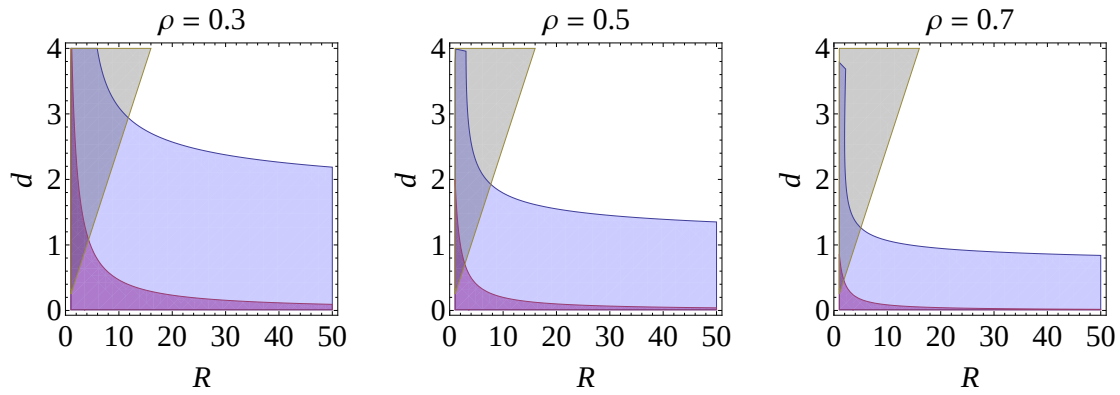

Figure 10.1: HQV stability for various choices of radius R, sample thickness d, and ratio ρ of the spin superfluid density to charge superfluid density. The penetration depth λ sets the unit length scale. The darker purple regions indicate parameter ranges for which HQVs are stable for the case of an hollow, infinitely long cylinder. The lighter blue regions corresponds to the case of an annulus. In the regions for which R is comparable to d, the approximations break down; and are shaded gray.

10.2 Energetic stability of an half quantum vortex: Annular sample geometry

We now consider the case of an annular sample of radius R and cross-sectional diameter d. This case is similar to the cylindrical one, but allows for finite height effects; as such, the annular case is expected to match more closely the geometry of the experiments reported in Ref. [30]. The essential difference with the cylindrical case involves the modification of the expression for the self inductance. Defining $\boldsymbol{A}_M = \boldsymbol{A} - (\boldsymbol{H} \times \boldsymbol{r}/2)$, the self inductance term of Eq. (9.2) can be expressed as

$$\frac{1}{2}\int d^3r \lambda^2 |\boldsymbol{\nabla} \times \boldsymbol{A}_M|^2 = \frac{1}{2}\int d^3r\, \boldsymbol{A}_M\, \boldsymbol{J}, \tag{10.10}$$

where the above equality can be demonstrated by an integration by parts and the use of the following relation:

$$\boldsymbol{J}(\boldsymbol{r}) = -\lambda^2 \boldsymbol{\nabla} \times \boldsymbol{\nabla} \times \boldsymbol{A}_M(\boldsymbol{r}). \tag{10.11}$$

In the thin ring limit (i.e., $d \ll R, \lambda$) one may approximate $\boldsymbol{A}_M(\boldsymbol{r})$ interior to the superconducting annulus as constant and equal to its value evaluated at a radius R, $A_\phi^M(R)\hat{\phi}$, which allows the self inductance to be approximated as

$$\frac{1}{2}\int d^3r\, \boldsymbol{A}_M\, \boldsymbol{J} \approx \pi R\, A_\phi^M(R)\, I. \tag{10.12}$$

Here, $A_\phi^M(R)$ is the $\hat{\phi}$ component of $\boldsymbol{A}_M$, evaluated inside the annulus, and I is the supercurrent in the ring. $A_\phi^M(R)$ can be expressed in terms of I by inverting Eq. (10.11), and has a simple form in the limit $d \ll R$ as derived in Ref. [40], Sec. 34:

$$A_\phi^M(R) \approx \frac{I}{2\pi\lambda^2} \ln\frac{16R}{e^2 d}. \tag{10.13}$$

By using this result, the free energy in the annular case can be put into a form identical to Eq. (10.8), except that $\beta_{\rm cyl}$ is replaced by its annulus counterpart $\beta_{\rm ann}$, which is given by

$$\beta_{\rm ann} = \frac{d^2}{8\lambda^2} \ln\frac{16R}{e^2 d}. \tag{10.14}$$

We thus see that for a finite height annulus, $\beta_{\rm ann}$ grows only logarithmically with R. Thus, for fixed ρ and d/λ, the range of R/λ over which HQVs are energetically stable is significantly larger in the case of an annulus than for the case of an hollow, thin-walled, infinitely long cylinder (see Fig. 10.1).

In this and the previous chapter we have studied the existence and stability of HQVs theoretically. In the following chapter we review experiments that suggest HQVs can be stabilized in mesoscopic annular rings of Sr_2RuO_4.

Chapter 11

Half-height magnetization steps in Sr_2RuO_4: Evidence for half quantum vortices?

In the previous sections we have studied the general structure, existence, and stability of HQVs for various pairing symmetries and sample geometries. We now describe recent cantilever magnetometry measurements of mesoscopic samples of Sr_2RuO_4. The central results are as follows: For micrometer sized annulus-shaped samples, transitions between integer fluxoid states were observed, as was a regime of half integer transitions. Such half integer transitions are characterized by a change in the magnetization of the superconducting samples that is half the change in magnetization that occurred for transitions between integer fluxoid states.

In the following sections we first review, in Sec. 11.1, the cantilever torque magnetometry technique, which was used to make these measurements. Next, we present the theoretical expectations of the London-limit free energy of Eq. (9.2), appropriate for the ring shaped sample geometries of the experiments of the Budakian group [30], allowing for conventional integer fluxoid states as well as half integer fluxoid states. Then, in Sec. 11.2, and subsections thereof, we highlight the key experimental observations and describe a Gibbs free energy that captures the main features of the observations. Next, in Sec. 11.3, we compare the main features of the observations with the HQV scenario and a wall vortex scenario. We argue that the HQV scenario is more consistent with the experimental observations than the wall vortex scenario. Finally, in Sec. 11.4, we propose an extension of the cantilever magnetometry technique that can more stringently distinguish between these two scenarios.

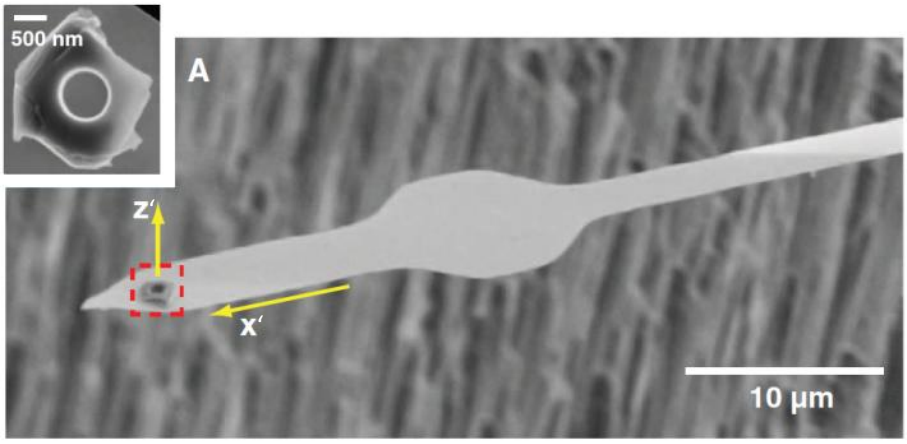

Figure 11.1: Image of a cantilever with attached annular Sr_2RuO_4 particle. Yellow arrow indicate directions parallel to the x' and z' axes (see Fig. 11.2). The inset shows a magnified image of the superconducting particle. From Jang et al. [30].

11.1 Cantilever torque magnetometry

In this section we will briefly review the cantilever torque magnetometry technique. The basic goal of the cantilever torque magnetometry is to measure the magnetic moment of a sample, such as a superconductor, by attaching it to the end of a cantilever (see Fig. 11.1). As the cantilever bends, the attached superconducting particle undergoes a rigid rotation of angle θ around an axis that points in the $\hat{\theta}$ direction (see Fig. 11.2). The angle θ is used to characterize the amplitude of the lowest-frequency mode of elastic vibration of the cantilever. All other modes of the cantilever are neglected. It is useful to employ two coordinate systems in description of the cantilever torque magnetometry technique: a "stationary" coordinate system that is fixed in the frame of the laboratory for which we shall employ "primed" notation, and an unprimed "rotating" coordinate system that is fixed relative to the superconductor's crystal axes and thus rigidly rotates with the sample (see Fig. 11.2). In the present section we assume a spatially uniform magnetic field is applied to the sample. In the rotating coordinate system the spatially uniform applied magnetic field has compo-

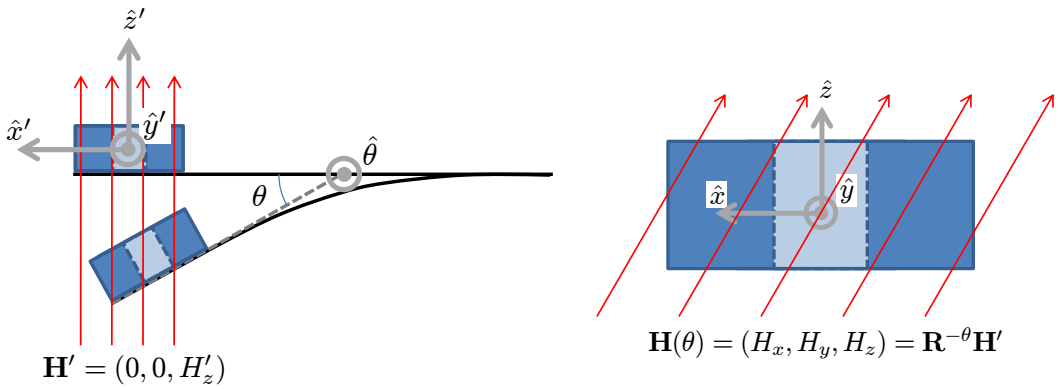

Figure 11.2: Schematic depiction of a cantilever and attached annular Sr_2RuO_4 particle (see Fig. 11.1), along with and related coordinate systems. As the cantilever undergoes elastic deformation, the superconducting sample rigidly rotates by an angle θ about an axis that points in the $\hat{\theta}$ direction. In this schematic depiction, the magnitude of θ is greatly exaggerated. The primed coordinate system is defined to be fixed in the frame of the laboratory. The unit directions $(\hat{x}', \hat{y}', \hat{z}')$] are indicated. The x' axis is defined to be parallel to the direction of the undeformed cantilever, and the z' axis is defined to be perpendicular to both the axis of rotation and the x' axis. The origin of the primed coordinate system is defined to be coincident with the centroid of the annular sample when $\theta = 0$, i.e., when the cantilever is undeformed. The unprimed coordinate system is fixed relative to the superconductor's crystal axes and rigidly rotates with the sample. For $\theta = 0$ the primed and unprimed coordinates systems coincide. A spatially uniform magnetic field (indicated by red field lines) is depicted as being applied to the sample along the $\hat{z}$' axis and thus has the components $(0, 0, H'_z)$ in the stationary coordinate system. In the rotating coordinate system the applied magnetic field has components (H_x, H_y, H_z). These components are related via $H_i = R^{-\boldsymbol{\theta}}_{ij} H'_j$ where $\boldsymbol{R}^{\boldsymbol{\theta}}$ is a rotation matrix.

nents (H_x, H_y, H_z), while in the stationary coordinate system the applied magnetic field has components (H'_x, H'_y, H'_z). These components are related via $H_i = R^{-\boldsymbol{\theta}}_{ij} H'_j$ where $\boldsymbol{R}^{\boldsymbol{\theta}}$ is a rotation matrix, which acts to reorient the applied magnetic field (see Fig. 11.2).

We assume that the dynamics of the superconductor are sufficiently fast compared to the frequency of the cantilever ($\sim$ 10 kHz in Refs. [30, 29]) that the superconducting degrees of freedom adjust adiabatically to the value of the spatially uniform applied magnetic field in the rotating reference frame of the superconductor. Thus, the free energy of the superconductor $F_{\rm SC}(\boldsymbol{H}) = F_{\rm SC}(\boldsymbol{R}^{-\boldsymbol{\theta}}\boldsymbol{H}')$ depends upon the angle θ via the dependence of $\boldsymbol{H}$ on θ. Accordingly, the cantilever will be subject to a y-axis torque, $\tau_{\rm SC}$, arising from the superconductor, given by

$$\tau_{\rm SC} = -\frac{\partial F_{\rm SC}}{\partial \theta} = \mu_i(\boldsymbol{H})\frac{\partial H_i}{\partial \theta} = \hat{y}\cdot(\boldsymbol{\mu}\times\boldsymbol{H}), \tag{11.1}$$

where the repeated index i is summed over, and $\boldsymbol{\mu}$, the magnetic moment of the superconductor, is defined via

$$\mu_i(\boldsymbol{H}) := -\frac{\partial F}{\partial H_i}(\boldsymbol{H}), \tag{11.2}$$

and for later convenience we also introduce the magnetic susceptibility tensor, given by

$$\chi_{ij}(\boldsymbol{H}) := -\frac{\partial^2 F}{\partial H_i \partial H_j}(\boldsymbol{H}). \tag{11.3}$$

In addition to the temporally static and spatially uniform applied magnetic field, a temporally oscillating and spatially uniform magnetic field is also applied to the sample. This oscillatory field is frequency-locked to the cantilever motion. Thus, in the rotating frame of the superconductor the applied applied magnetic is of the form $\boldsymbol{H} = \bar{\boldsymbol{H}} + \delta\boldsymbol{H}$, where $\bar{\boldsymbol{H}}$ is static in time, and the contribution $\delta\boldsymbol{H}$ is oscillatory in time. (In subsequent sections the overbar notation will often be suppressed). The components of the temporally static applied magnetic field are equal in the stationary and rotating frames. The oscillatory field $\delta\boldsymbol{H}$ in

the rotating frame has two contributions: one that originates from rotations of the superconducting sample, and one that originates from the applied temporally oscillating field. If the temporally static and temporally oscillating magnetic fields have roughly equal magnitude in the stationary frame, then in the rotating frame the contribution to $\delta \boldsymbol{H}$ from applied temporally oscillating field is roughly a factor of $1/\theta^{\max}$ larger than the contribution from the effect of rotations, where $\theta^{\max}$ characterizes the maximum amplitude of the rotations. In the experiments reported in Ref. [30, 29] $\theta^{\max}$ is typically $10^{-}3$. Expanding in the small parameter $\delta \boldsymbol{H}$ the torque on the cantilever due to the superconductor is of the form

$$\tau_{SC} = \hat{y}_i \left(\epsilon_{ijk} \mu_j(\bar{\boldsymbol{H}}) \bar{H}_k + \left(\epsilon_{ijk} \mu_j(\bar{\boldsymbol{H}}) + \epsilon_{ij\ell} \chi_{jk}(\bar{\boldsymbol{H}}) \bar{H}_\ell \right) \delta H_k + \cdots \right) \tag{11.4}$$

where repeated indices $i, j, k, \ldots$ are summed over. As, in the experiments, $\delta \boldsymbol{H}$ is frequency-locked to the cantilever, the time Fourier transform of $\delta \boldsymbol{H}$ is given by

$$\delta \boldsymbol{H}(\omega) = \delta \boldsymbol{H}^{\max} e^{i\phi} \frac{\theta(\omega)}{\theta^{\max}}, \tag{11.5}$$

where ϕ is the relative phase shift between the motion of the cantilever and the oscillating fields (for simplicity we have assume each components of the applied field has the same relative phase shift). By altering experimentally the relative phase shift ϕ, the torque due to the superconductor can shift either the resonance frequency or dissipation at resonance of the cantilever motion. If we assume for definiteness that the relative phase shift ϕ is experimentally fixed to be zero, then the torque due to the cantilever shifts the *resonance* frequency of the cantilever with the change in this frequency (in the low dissipation limit) being given by

$$\delta\omega = \frac{1}{2I\omega_0 \theta^{\max}} \hat{y}_i \epsilon_{ijk} \left(\mu_j(\bar{\boldsymbol{H}}) + \epsilon_{ij\ell} \chi_{jk}(\bar{\boldsymbol{H}}) \bar{H}_\ell \right) \delta H_k^{\max} \tag{11.6}$$

where I is the effective moment of inertia and ω_0 is the resonance frequency of the cantilever in the absence of the torque due to the superconductor. The parameters $\theta^{\max}$, $\delta H^{\max}$, and

ω_0 in the experiment of Ref. [30, 29] are typically of order 10^{-3}, 1 Oe, and 10 kHz. This magnetometry scheme allows for the detection of magnetic moments with a sensitivity of $7 \times 10^{-16}\,\mathrm{emu} = 8 \times 10^4\,\mu_B$ for a 1 s signal integration time [29]. (Note: μ_B is the magnetic moment of a single electron.)

11.2 Experiments of the Budakian group: Theoretical expectations and experimental results

In the previous section of this chapter we reviewed the cantilever torque magnetometry technique that allows for the detection of the magnetic moment of a magnetically active sample attached to the end of a cantilever. In the experiments of Ref. [30, 29], this technique was applied to micron-sized superconducting samples of Sr_2RuO_4 that were shaped by a gallium focused ion beam into annuli. In the present section we present the theoretical expectations for the magnetic response of the superconducting particle based upon the London-limit free energy of Eq. (9.2), allowing for conventional integer as well as half integer fluxoid states of the annular ring.

As discussed in Chapter 10, an annular, ring-shaped, sample geometry yields a discrete family of "fluxoid" states in which the superconducting order parameter winds around the annulus as it would around a vortex core, and as such this family of fluxoid states are thus indexed by the elements of the first homotopy group $\pi_1(\mathcal{R})$ of the order parameter coset space $\mathcal{R}$. In the case of *conventional* superconductivity, $\pi_1(\mathcal{R})$ (i.e. fluxoid states) are indexed by integers. As discussed in Sec. 8, in cases where HQVs can exist, fluxoid states are indexed by *two* numbers (n_θ, n_α), which are either both integer or both half integer (see Fig. 8.1). When the superconducting order is in the London regime, the magnitude of the superconuducting order parameter is not strongly influenced by either the applied magnetic field or the fluxoid state of the ring. In this regime, Eq. (9.2) becomes a good approximation for the free energy of the sample. Because of the linearity of Eq. (9.2) in θ and $\boldsymbol{A}$, the free

energy is generically of the form

$$F(n_\theta, n_\alpha, \boldsymbol{H}) = \frac{1}{2}\Delta\mu_z\,\Delta H_z\,n_\theta^2 - \Delta\mu_z\,n_\theta\,H_z + E_{\rm spin}(n_\alpha) - \frac{1}{2}H_i\chi_{ij}H_j \tag{11.7}$$

(with summation implied over the indices $i, j = 1, 2, 3$). The magnetic moment of the annular superconductor can be derived from F via

$$\boldsymbol{\mu} = -\frac{\partial F}{\partial H_i} = \Delta\mu_z\hat{z}n_\theta + \boldsymbol{\chi}\boldsymbol{H}. \tag{11.8}$$

In these equations $\Delta\mu_z$, ΔH_z and $\boldsymbol{\chi}$ are parameters that are determined, in part, by the geometry of the sample. When the state of the superconductivity changes its value of n_θ by unity, the magnetic moment of the ring shaped superconductor changes by $\Delta\mu_z\,\hat{z}$; for simplicity we assume that this change in moment is along the z-axis. In the limit that $L_{\rm SO} \gg R$ (where R is the radius of the sample and $L_{\rm SO}$ is the spin orbit length, see Chapter 9), the free energy is also linear in α, and $E_{\rm spin}(n_\alpha)$ is equal to $\frac{1}{2}\Delta\mu_z\Delta H_z(1+\beta)\rho\,n_\alpha^2$; more generally $E_{\rm SO}$ is zero for $n_\alpha = 0$ and positive definite for $|n_\alpha| > 0$.

Considering only the conventional integer fluxoid states for which n_α is zero, the free energy of Eq. (11.7) has the form $F(n_\theta, H_z) = E_0(n_\theta - H_z/\Delta H_z)^2$, where we have neglected a term independent of n_θ. Thus, considering only the integer fluxoid states, Eq. (11.7) predicts the equilibrium value of n_θ will grow in a stepwise manor with increasing applied field H_z, with the steps in n_θ occurring with the period ΔH_z. We assume for simplicity that the susceptibility tensor $\boldsymbol{\chi}$ is diagonal in the frame of the particle. Then, with these assumptions, and assuming the applied magnetic field is temporally modulated in the in-plane x direction, the change in resonant frequency $\delta\omega$ of the cantilever [Eq. (11.6)], is predicted to be proportionally

$$\delta\omega \propto \Delta\mu_z n_\theta + (\chi_{zz} - \chi_{xx})H_x. \tag{11.9}$$

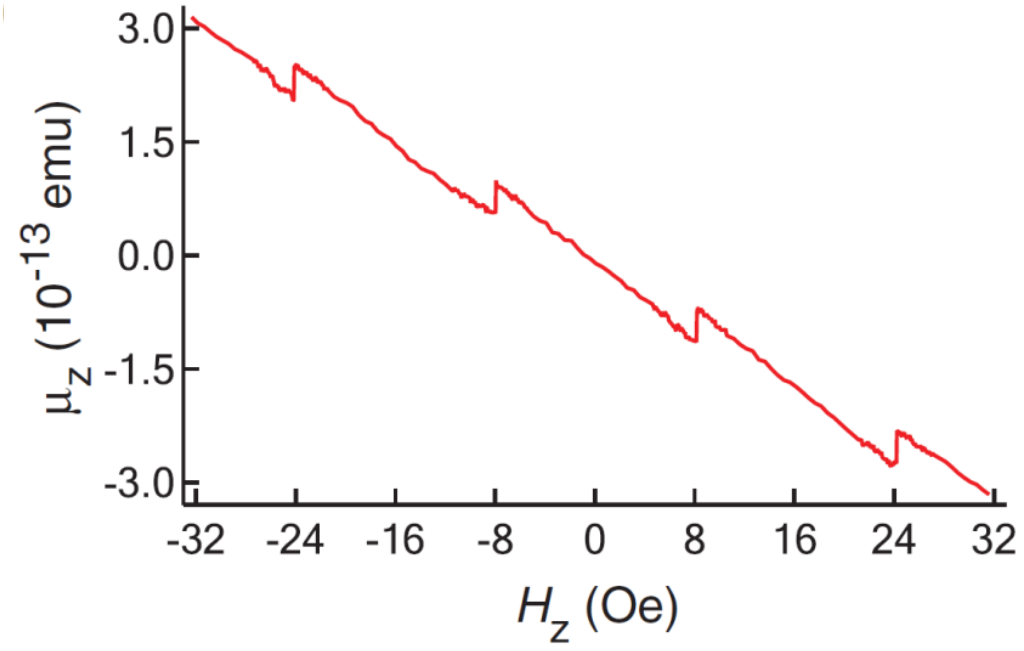

Figure 11.3: Measured z-axis component of the equilibrium magnetic moment μ_z of the Sr_2RuO_4 sample shown in Fig. 11.1, plotted as a function of the static applied z-axis magnetic field H_z at $T = 0.45$ K. The in-plane applied magnetic field H_x is fixed to be zero. From Jang et al. [30].

Due to the large anisotropy factor of the magnetic response of the superconductor Sr_2RuO_4, the quantity $\chi := (\chi_{zz} - \chi_{xx})$ can be approximated as χ_{zz}. Thus, when the applied field is modulated in the in-plane x direction, the change in frequency $\delta\omega$ effectively measures the essential physical quantity $\mu_z(\boldsymbol{H})$. In the next three subsections we highlight the key experimental observations and describe a Gibbs free energy that captures the main features of these observations.

11.2.1 Integer fluxoid states

In this subsection we discuss the initial observations of the Budakian group reported in Ref. [30]. For a static applied magnetic field with zero in-plane component and varying

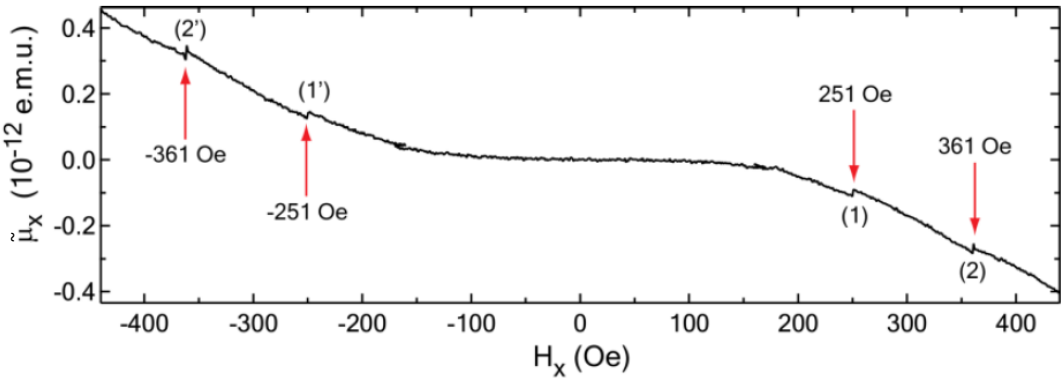

Figure 11.4: Measured in-plane magnetic moment $\tilde{\mu}_x$ (with the linear low-field Meissner response subtracted) as a function of static applied in-plane field H_x, obtained for the sample shown in Fig. 11.1. The Meissner response has been subtracted to more clearly reveal the steps in the in-plane moment indicated by red arrows. The data was obtained for zero z-axis static applied field and for $T = 0.5$ K. From Jang et al. [30] Supplemental Online Material.

z-axis component H_z, the equilibrium magnetic moment μ_z of annular rings of Sr_2RuO_4 exhibits periodic steps of nearly constant magnitude $\Delta\mu_z$ and period ΔH_z, together with a component of the magnetization that varies linearly with H_z (see Fig. 11.3 and Ref. [30]). Theoretical estimates for ΔH_z and $\Delta\mu_z$, obtained from the case of a hollow superconducting cylinder [3, 74], are in reasonable agreement with the observed values [30]. Thus, the observed periodic events can reasonably be ascribed to equilibrium transitions between distinct integer fluxoid states of the annular particle. However, importantly, the pre sence of an in-plane magnetic field H_x brings two new features. We discuss these features in turn in the next two subsections.

11.2.2 In-plane wall vortex

For an static applied magnetic field with zero z-axis component ($H_z = 0$), and varying in-plane component H_x, the in-plane magnetic response of the sample μ_x (which can be probed by oscillating the z-axis component of the applied magnetic field) varies continuously

for $H_x < 250\,\mathrm{Oe}$. At $250\,\mathrm{Oe}$, a step in the in-plane magnetic moment, of magnitude $\approx 2 \times 10^{-14}\,\mathrm{emu}$ is observed (see Fig. 11.4 and Ref. [30] Supplemental Online Material). As is discussed in the subsequent paragraphs, both the magnitude of the step and the value of H_x at which it occurs are consistent with those expected for the critical field $H_{c1||ab}$, and change in moment $\Delta\mu_{ab}$ of an in-plane wall vortex for the micron-sized sample shown in Fig. 11.1.

The energetics of equilibrium vortex penetration into the bulk of a superconductor is dependent on the geometry of the sample. In particular, if the magnetic field is applied parallel to the surface of a thin superconducting film, H_{c1} (i.e., the field at which vortices first penetrate) is increased above its bulk value [1]. This enhancement in H_{c1} increases as the penetration depth increases relative to the thickness of the film. Roughly speaking, this is due to the fact that while the energy cost of the vortex core is nearly the same as in the bulk case, in thinner films a vortex saves a smaller amount of magnetic energy when the thickness of the film decreases. We now present a theoretical estimate for $H_{c1||ab}$ and $\Delta\mu_{ab}$ for the geometry similar to that of the particle shown in Fig. 11.1, namely a superconducting box of height L_z, width L_y, and volume Ω. The applied magnetic field is assumed to be directed along the x-axis.

For the Sr_2RuO_4 sample shown in Fig. 11.1, the longest dimension of the sample is approximately $1.8\,\mu\mathrm{m}$, which is nearly a factor of two smaller than the z-axis zero temperature limit of the penetration depth $\lambda_z(0)$ [49]; thus, we expect very little screening of H_x. For an in-plane applied field it is therefore reasonable to adopt the Laplace limit of the London free energy, i.e.,

$$F = \int_{\mathrm{SC}} d^3r \frac{1}{2}\Gamma_{ij}(\nabla_j\theta - A_i^H)(\nabla_i\theta - A_j^H), \tag{11.10}$$

where $\boldsymbol{A}^H$ is the vector potential of the external magnetic field only and does not include a contribution from the magnetic field due to the superconductor, i.e., $\boldsymbol{A}^H$ obeys $\boldsymbol{\nabla} \times \boldsymbol{A}^H = \boldsymbol{H}$. To account for the anisotropy of Sr_2RuO_4, the tensor $\boldsymbol{\Gamma}$ is assumed to have the form $\mathrm{diag}(1, 1, \gamma^{-2})$ with $\gamma = 20$ [49]. As discussed in Chapter 4, the phase field θ

can be decomposed into a smooth, single-valued part and a vortex part $\theta_{\rm v}$. The vortex part satisfies $\boldsymbol{\nabla}\times\boldsymbol{\nabla}\theta_{\rm v} = 2\pi n_{\rm v}\hat{z}\delta(y)\delta(z)$, where $n_{\rm v}\in\{1,0\}$ indicates whether the vortex is present or absent. Making F stationary with respect the smooth part of θ amounts to solving for the London gauge version of $\boldsymbol{A}^H$ and $\boldsymbol{\nabla}\theta_{\rm v}$, i.e., solving the bulk equations

$$\begin{aligned}
\Gamma_{ij}\nabla_i A_j^H &= 0, && (11.11)\\
\boldsymbol{\nabla}\times\boldsymbol{A}^H &= \boldsymbol{H}, && (11.12)\\
\Gamma_{ij}\nabla_i\nabla_j\theta_{\rm v} &= 0, && (11.13)\\
\boldsymbol{\nabla}\times\boldsymbol{\nabla}\theta_{\rm v} &= 2\pi n_{\rm v}\hat{z}\delta(y)\delta(z), && (11.14)\\
& && (11.15)
\end{aligned}$$

for $\boldsymbol{A}^H$ and $\theta_{\rm v}$, subject to the boundary conditions

$$\begin{aligned}
n_i\Gamma_{ij}A_j &= 0, && (11.16)\\
n_i\Gamma_{ij}\nabla_j\theta_{\rm v} &= 0, && (11.17)
\end{aligned}$$

where the unit vector $\hat{\boldsymbol{n}}$ characterizes the boundary normal. The solutions to these equations for the assumed rectangular box geometry are

$$\begin{aligned}
\boldsymbol{A}^H &= (0,0,yH_x) + \sum_{n=1}^{\infty}\frac{4(-1)^n L_y H_x}{\pi^2\gamma(2n-1)^2\cosh\left(\pi(2n-1)\gamma L_z/2L_y\right)} && (11.18)\\
&\times\left(0,\cos\left(\frac{\pi(2n-1)y}{L_y}\right)\sinh\left(\frac{\pi(2n-1)\gamma z}{L_y}\right),\gamma\sin\left(\frac{\pi(2n-1)y}{L_y}\right)\cosh\left(\frac{\pi(2n-1)\gamma z}{L_y}\right)\right),\\
\theta_{\rm v} &= \sum_{n=-\infty}^{\infty}(-1)^n\arg\left(\sin\left(\frac{\pi y}{L_y}\right)+i\sinh\left(\frac{\pi\gamma(z-nL_z)}{L_y}\right)\right). && (11.19)
\end{aligned}$$

Using these solutions for $\boldsymbol{A}^H$ and $\theta_{\rm v}$, together with the assumption $L_y \ll \gamma L_z$, the free

energy of Eq. (11.10) takes the form

$$F[n_{\rm v}, H_x] = \frac{L_x}{8\pi\lambda_z^2}\left(\frac{\Phi_0}{2\pi}\right)^2\left(2\pi\gamma\ln\left(\frac{L_y}{\pi\xi_{ab}}\right)n_{\rm v}^2 - n_{\rm v}\frac{\pi^2 L_y^2}{\Phi_0}H_x\right) + O(H_x^2), \tag{11.20}$$

in which, for convenience, we have restored Gaussian units. We have also omitted the $O(H_x^2)$ term that does not influence the value of $H_{c1||ab}$ or $\Delta\mu_x$. The value of $H_{c1||ab}$ is determined by the condition that the $n_{\rm v} = 0$ and $n_{\rm v} = 1$ be energy-degenerate, i.e., $F(0, H_{c1||ab}) = F(1, H_{c1||ab})$. The jump in the x-axis moment at the transition is given by $\Delta\mu_x = -\partial^2 F/(\partial n_{\rm v}\partial H_x)$. Using this we arrive at the following expressions:

$$H_{c1||ab} = \frac{2\gamma\Phi_0}{\pi L_y^2}\ln\left(\frac{L_y}{\pi\xi_{ab}}\right), \tag{11.21}$$

$$\Delta\mu_x = \frac{\Phi_0 L_y \Omega}{32\pi L_z \lambda_z}. \tag{11.22}$$

Thus, for a sample having a box geometry and parameter values

$$(L_y, L_z, \Omega, \lambda_c, \xi_{ab}) = (1.8\,\mu{\rm m}, 0.35\,\mu{\rm m}, 0.45\,\mu{\rm m}^3, 4.3\,\mu{\rm m}, 90\,{\rm nm}) \tag{11.23}$$

which approximate the geometry of the superconducting particle shown in Fig. 11.1, these calculations yield $H_{c1||ab} \approx 150\,{\rm Oe}$ and $\Delta\mu_x \approx 4\times10^{-14}\,{\rm emu}$, which is in reasonable agreement with the observed values of $H_{c1||ab} = 250\,{\rm Oe}$ and $\Delta\mu_x = 2\times10^{-14}\,{\rm emu}$. We note that, as expected for such mesoscopic geometries, the observed value of $H_{c1||ab}$ for the sample shown in Fig. 11.1 is much higher than the bulk value of $H_{c1||ab} \approx 8\,{\rm Oe}$ for Sr_2RuO_4 [82].

11.2.3 Half integer states

In this subsection we discuss the measurement of μ_z for an temporally static and spatially uniform applied magnetic field having both non-zero in-plane, H_x, and z-axis, H_z, components (see Fig. 11.5 and Ref. [30]). The experimental results focused on in the present section

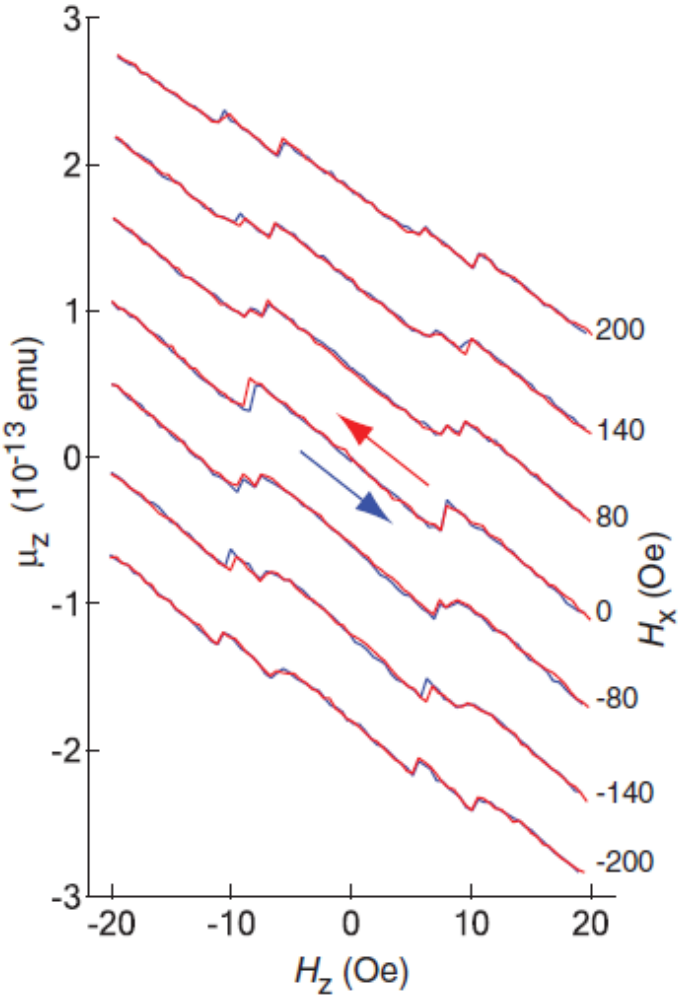

Figure 11.5: Evolution of $\mu_z(H_z)$ as a function of the static in-plane magnetic field H_x at $T = 0.6$ K obtained for the sample shown in Fig. 11.1. The curves have been offset for clarity by an amount proportional to H_x. The data was obtained by cooling the sample through T_c with $H_z = 0$ and performing a cyclic H_z field sweep starting at $\bar{H}_z = 0$. At this temperature, the zero-field cooled and field cooled data are nearly identical, indicating that the equilibrium response is well-described by the zero-field cooled data. From Jang et al. [30].

are those that satisfy $H_x < H_{c1||ab}$, so that no in-plane vortices are expected to penetrate the sample. Remarkably, for sufficiently large in-plane field, the step in the equilibrium magnetic moment $\Delta\mu_z$ corresponding to the transition between the $n_\theta = 0$ and $n_\theta = 1$ states, is observed to split into two half-height steps. Thus, in the range of fields between the two half-height steps, the equilibrium state of the annulus has an observed z-axis moment of the form $\Delta\mu_z n_\theta + \chi H_z$, where n_θ is equal to 0.50 to within the statistical significance of the experiment [30]. The statistical significance of the measured n_θ varies with temperature and across the varrious annuli for which the $n_\theta = 0.50$ state is observed, but is typically of order 0.02 (see Ref. [30] and Supplemental Online Material). We shall refer to the state of the superconductivity as being in the "half integer" (HI) state when the experimentally determined value of $|n_\theta|$ is consistent with 0.50. It was found that such HI states can be stabilized for in-plane magnetic fields applied in directions rotated by $0, 35, 180$ and 225 degrees with respect to the in-plane x'-axis. (Other in-plane directions were not studied). Further, the growth in stability of the HI state did not change appreciably for any of these in-plane directions.

Based on these measurements it seems reasonable to construct the following total Gibbs free energy, which captures the main features of the observed magnetic response:

$$F(\boldsymbol{H}, n_\theta) = \frac{1}{2}\Delta\mu_z \Delta H_z n_\theta^2 - \Delta\mu_z n_\theta H_z - \frac{1}{2}\boldsymbol{H}\cdot\boldsymbol{\chi}\cdot\boldsymbol{H} + E_{\rm HI} - \boldsymbol{\mu}_{\rm HI}\cdot\boldsymbol{H}, \tag{11.24}$$

where n_θ can be integral or half integral (i.e., half integral n_θ correspond to HI states). To account for the growth of the stability region of the HI states with in-plane field we have included two terms that are only nonzero in HI states: one is $-\boldsymbol{\mu}_{\rm HI}\cdot \mathrm{H}$, where $\boldsymbol{\mu}_{\rm HI}$ is a magnetic moment that exists only in the HI state and points in the direction of the in-plane field; the other is a field independent constant contribution $E_{\rm HI}$. We note that the value of $\mu_{\rm HI}$ that explains the growth in stability of the HI states is roughly 200 times smaller than the magnitude of the in-plane magnetic moment $\Delta\mu_x$ measured for the in-plane vortex

discussed in the previous subsection. In the next section we discuss two scenarios which potentially explain the observed HI states.

11.3 Scenarios for the half integer states

In this section we further compare the observed half integer (HI) states of mesoscopic rings of Sr_2RuO_4 reported in Ref. [30], with the expectations of two scenarios: (i) a half quantum vortex scenario; and (ii) a wall vortex scenario.[1]

We first discuss the HQV scenario. In the previous section, Sec. 11.2.3, we summarized the observed fluxoid behavior of mesoscopic rings of Sr_2RuO_4 [30] in terms of the free energy of Eq. (11.24). As expressed in Eq. (11.7), HQVs are expected to yield an free energy of form similar to Eq. (11.24), differing only by the term $-\boldsymbol{\mu}_{\rm HI}\cdot {\rm H}$. Although the origin of this in-plane moment in the half integer (HI) states is as yet unknown, recent work by Vakaryuk and Leggett [75] finds that a kinematic spin polarization $\boldsymbol{\mu}_{\rm kin}$ can develop in the HQV state, as a result of the velocity mismatch between the two superfluid spin components. Although the theoretical expectation is that the magnitude of the kinematic spin polarization would depend upon the distribution of both charge and spin currents, an estimate of the order of magnitude of $\mu_{\rm kin}$ agrees with the observed value of $\mu_{\rm HI}$ [30]. Thus, the observed behavior of the HI states can be understood qualitatively on the basis of existing theoretical models of HQVs.

A final important point to make about the HQV interpretation of the HI state is that $\boldsymbol{\mu}_{\rm HI}$ cannot depend solely on n_α because it couples linearly to an applied field, and must therefore be odd under time reversal, whereas n_α is even under time reversal.[2] Thus, it is

[1] In Chapter 6 we noted that two perpendicular domain walls crossing the annulus can also result in half fluxoid behavior. However there are a number of reasons why the HI state, discussed in Sec. 11.2.3, is unlikely to correspond to such a domain wall configuration. For example, domain walls are expected to be energetically costly and would thus be unlikely to be the equilibrium state of the annulus as the HI state is observed to be. Also, we know of no reason why such a configuration of domain walls would have an in-plane moment with properties consistent with $\mu_{\rm HI}$. For these reasons we do not consider it likely that such a domain wall scenario explains the observed properties of the HI state, and will not consider it further.

[2] Ref. [74] also discusses these considerations

natural to propose that $\boldsymbol{\mu}_{\rm HI}$ might, in addition to n_α, depend on n_θ and/or H_z. However, $\boldsymbol{\mu}_{\rm HI}$ cannot depend solely only upon n_θ and n_α because n_θ grows stepwise with the applied magnetic field whereas $\mu_{\rm HI}$ remains roughly constant (see Ref. [30] Supplemental Online Material). For the same reason, $\boldsymbol{\mu}_{\rm HI}$ cannot depend solely only upon H_z and n_α. $\boldsymbol{\mu}_{\rm HI}$ cannot even depend linearly on the difference $(n_\theta - H_z/\Delta H_z)$ (which is both odd under time reversal and, on average, independent of H_z) because $\boldsymbol{\mu}_{\rm HI}$ would then be zero when $n_\theta = H_z/\Delta H_z$, and the stability of the HI state increases when this condition is satisfied. Thus, if the HQV scenario is correct, it is likely that $\boldsymbol{\mu}_{\rm HI}$, in addition to n_α, also depends on an additional parameter that breaks time reversal symmetry that is distinct from n_θ and H_z.[3]

We now turn to the wall vortex scenario. We define a wall vortex (WV) state to be any superconducting state in which a vortex penetrates through the volume of the sample (see, e.g., Fig. 11.6). In general, a transition between a WV state and the $n_\theta = 0$ integer fluxoid state corresponds to a change in the magnetic moment of the particle ${}^{\rm WV}\Delta\boldsymbol{\mu}$. Thus, to interpret the HI state as a WV state, ${}^{\rm WV}\Delta\boldsymbol{\mu}$ would have to be consistent with the observed value of $(\Delta\mu_z/2)\hat{z} + \boldsymbol{\mu}_{\rm HI}$. For the particles in which the HI state is observed experimentally, the local superconducting properties are not known in detail. Therefore, it is difficult to constrain the possible forms of WV states. However, one can make the following general observations:

(i) For the observed in-plane vortices that are stabilized for fields $H_x \geq 250$Oe (see Sec. 11.2.2), the magnitude of the in-plane component of ${}^{\rm WV}\Delta\boldsymbol{\mu}$ is approximately 200 times larger than $\mu_{\rm HI}$. Thus, the HI state is *not* a simple generalization of the observed in-plane WV state.

[3]It should be noted, of course, that there are many experimental probes that detect signatures of spontaneously broken time reversal symmetry that are coincident with the superconducting transition of Sr_2RuO_4 [48, 32, 80]. Perhaps, the observation that $\mu_{\rm HI}$ has the same order of magnitude as a spin polarization effect, indicates that $\mu_{\rm HI}$ results from a non-unitary spin polarization in the superconducting state that is enhanced by the HQV. Such ideas are difficult to test with the current experimental technique because the currently employed cantilever torque magnetometry technique only directly detects magnetic moments that rotate rigidly with the cantilever.

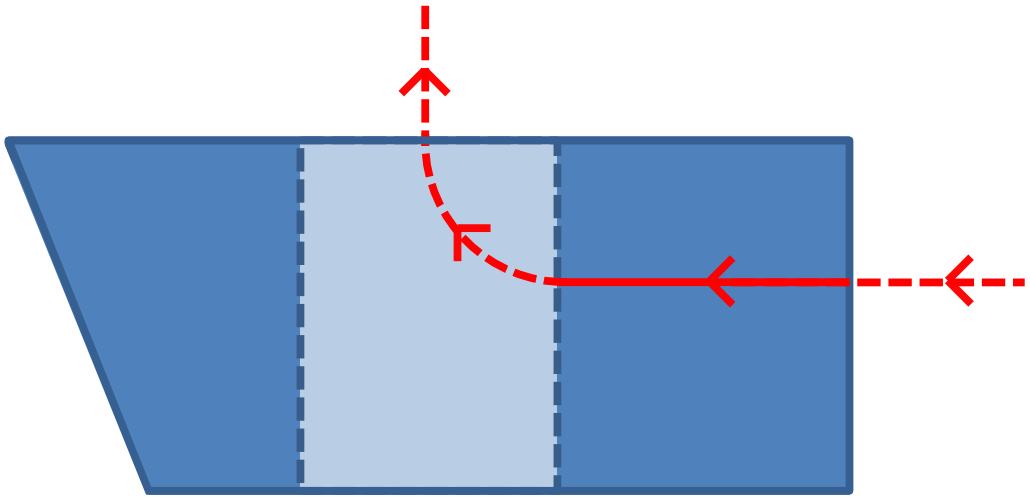

Figure 11.6: Schematic depiction of an integer wall-vortex penetrating the volume of an annular superconductor. A cross section through the annulus is shown. For emphasis the hollow central region is shaded in light blue and is outlined with dashed lines. The sample does not have perfect axial symmetry. The vortex line penetrates through one wall of the annulus and then "goes out through the hole." In regions where the vortex passes through the wall of the sample it is indicated in solid red. Where the vortex line intersects a surface of the superconductor it turns into a dashed red "fluxoid line," and continues outside the superconductor. Contours within the superconductor that surround the fluxoid/vortex line have nontrivial order parameter winding (e.g., $n_\theta = 1$). Contours that do not surround the fluxoid/vortex line have trivial winding $n_\theta = 0$. Thus, for the situation indicated, the top half of the annulus has winding $n_\theta = 1$ and the bottom half has winding $n_\theta = 0$. As the annulus is not completely symmetric and the vortex is not positioned symmetrically between the top and bottom surface, the z component of ${}^{\mathrm{WV}}\Delta\mu$ need not be $\Delta\mu_z/2$ (see Sec. 11.2.2 in text).

(ii) The z-axis component of ${}^{\mathrm{WV}}\Delta\boldsymbol{\mu}$ can be any fraction of $\Delta\mu_z$ and is not generically $\Delta\mu_z/2$ (see Fig. 11.6). Thus, the occurrence in multiple samples of wall vortices having robust half integer fluxoid behavior is unlikely (see Ref. [30] Supplemental Online Material).

(iii) In general, the location/orientation of wall vortices should vary with the magnitude and direction of the applied field. Hence, multiple fractional steps in the magnetic moment are expected; these steps corresponding to transitions involving various WV states/configurations (see Ref. [30]).

(iv) Given the geometric asymmetry of the samples of Ref. [30], the component ${}^{\mathrm{WV}}\Delta\boldsymbol{\mu}$ along the in-plane field is expected to vary strongly with the direction of the in-plane field. Consequently, the stability region of the WV state is expected to be strongly affected by the direction of the in-plane field. As previously noted in Sec. 11.2.3, however, the stability region of the HI state is *not* strongly influenced by the direction of the in-plane field (see also Ref. [30] Supplemental Online Material).

Given these considerations, we conclude that to formulate a wall vortex scenario that is consistent with the observed properties of the HI state would require a rather finely tuned set of assumptions, and thus seems unlikely.

11.4 Further test of half quantum vortex scenario

In the previous section we presented an analysis that suggested that the observations of the half integer fluxoid state in mesoscopic annular rings of Sr_2RuO_4 can be understood, at least at the qualitative level, on the basis of existing theoretical models of HQVs. We also considered alternative scenarios based on wall vortices, which we concluded were unlikely explanations of the experimental observations, but could not rule such scenarios out completely. Thus, further tests to establish that the HI states are due to HQVs are warranted.

One possibility is to probe characteristics that are particular to the HQV states, such as spin currents, or to design schemes that can detect [64, 20] the presence of nonabelian, zero-energy, Majorana quasi-particles [36, 62, 26] bound to the HQV core.

In the final section of this chapter we propose a more straightforward generalization of the current cantilever magnetometry technique, which would provide an independent test of the HQV scenario. The proposal relies on the simple relationship between the change in supercurrent density when the state of the superconductor makes a transition from the $n_\theta = 0$ fluxoid state to the $n_\theta = 1$ state ${}^{(n_\theta=1)}\Delta\boldsymbol{J}(\boldsymbol{r})$, and the change in supercurrent density when the state of the superconductor makes a transition from the $n_\theta = 0$ fluxoid state to the $n_\theta = 1/2$ state ${}^{(n_\theta=1)}\Delta\boldsymbol{J}(\boldsymbol{r})$. [In this section we will generically use the ${}^{(\cdot)}\Delta$ notation to denote the change in a quantity when the state of the superconductor changes from the $n_\theta = 0$ fluxoid state to the state "$(\cdot)$"]. In the linear London regime these changes in current densities satisfy the following *local* equality:

$$ {}^{(n_\theta=1/2)}\Delta\boldsymbol{J}(\boldsymbol{r}) = \frac{1}{2}\,{}^{(n_\theta=1)}\Delta\boldsymbol{J}(\boldsymbol{r}). \tag{11.25} $$

The cantilever torque magnetometry technique of Refs. [30, 29], described in Sec. 11.1, can be employed to measure the change in the z-axis magnetic moment $\Delta\mu_z$ that occurs when the superconductor changes its fluxoid state.[4] Neglecting effects due to spin polarization, $\Delta\mu_z$ can be expressed in terms of the change in supercurrent density $\Delta\boldsymbol{J}$ as

$$ \Delta\mu_z = \hat{z}_i \int d^3r \frac{1}{2}\,\epsilon_{ijk}\, r_j \Delta J_k(\boldsymbol{r}). \tag{11.26} $$

As $\Delta\mu_z$ is linear in $\Delta\boldsymbol{J}$ it follows from Eqs. (11.26) and (11.25) that ${}^{(n_\theta=1/2)}\Delta\mu_z = {}^{(n_\theta=1)}\Delta\mu_z/2$.

Importantly, all higher order spatial moments of the supercurrent density $\boldsymbol{J}$, i.e., $\mu^{(2)}_{ij}, \mu^{(3)}_{ijk}, \ldots$, are also linear in the current density. For example the next higher (second) order moment

[4] In using the notation of this section the $\Delta\mu_z$ introduced in Eq. (11.7) is expressed as ${}^{(n_\theta=1)}\Delta\mu_z$.

is of the form

$$\mu_{ij}^{(2)} = \int d^3r \frac{1}{3} \epsilon_{ik\ell}\, r_j\, r_k\, J_\ell(\boldsymbol{r}). \tag{11.27}$$

Thus, in the London regime, the spatial moments $\boldsymbol{\mu}^(n)$ of the supercurrent of every order n, are predicted to have the relationship that the change ${}^{(n_\theta=1/2)}\Delta\boldsymbol{\mu}^(n)$ that occurs for the transition between the $n_\theta = 0$ integer fluxoid state and the $n_\theta = 1/2$ state will be half the change ${}^{(n_\theta=1)}\Delta\boldsymbol{\mu}^(n)$ for the $n_\theta = 1$ integer fluxoid state

$${}^{(n_\theta=1/2)}\Delta\boldsymbol{\mu}^(n) = {}^{(n_\theta=1)}\ \Delta\boldsymbol{\mu}^(n)/2. \tag{11.28}$$

In contrast for wall vortex states, which have current vorticity within the walls of the sample, the change ${}^{\mathrm{WV}}\Delta\boldsymbol{J}(\boldsymbol{r})$ is *not* generically half of ${}^{(n_\theta=1)}\Delta\boldsymbol{J}(\boldsymbol{r})$. Thus even though ${}^{\mathrm{WV}}\Delta\mu_z$ may, by chance, be nearly half ${}^{(n_\theta=1)}\Delta\mu_z$, such a simple "half" relation *must* be violated for some higher orders moment. For example for a wall vortex state similar to the wall vortex state of Fig. 11.6, because of the different fluxoid windings in the top and bottom halves of the sample, the change ${}^{\mathrm{WV}}\Delta\mu_{zz}^{(2)}$ will certainly not be half of ${}^{(n_\theta=1)}\Delta\mu_{zz}^{(2)}$ and, in fact, will likely be many times larger.

We now describe an extension of the current cantilever torque magnetometry technique that brings the potential to enable measurement of the higher-order moments of the supercurrent density vector field $\boldsymbol{J}(\boldsymbol{r})$. The primary modification of the current technique is to apply a spatially varying magnetic field to the sample. Assuming that the applied magnetic field has spatial variations, in the stationary frame defined in Sec. 11.1 (see Fig. 11.2), such a magnetic field can be represented in the form

$$H_i'(\boldsymbol{r}') = H'^{(1)}_i + H'^{(2)}_{ij} r'_j + \cdots . \tag{11.29}$$

where $\boldsymbol{H}'^{(n)}$ are the coefficients of the Taylor expansion of $\boldsymbol{H}'$ around the point $\boldsymbol{r}' = 0$. Due to the divergence free property of $\boldsymbol{H}$ (i.e., the absence of magnetic monopoles) not

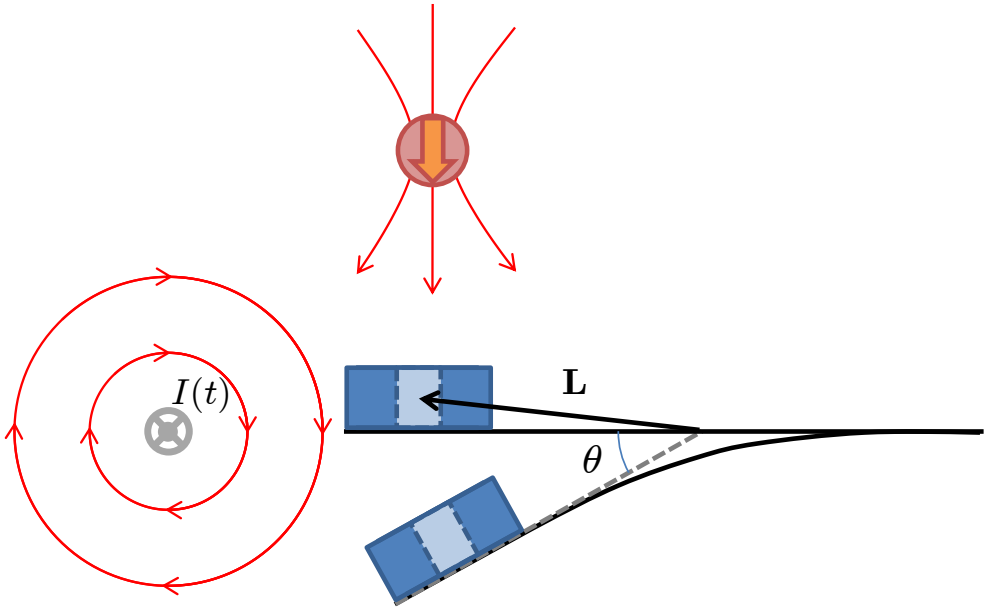

Figure 11.7: Schematic depiction of the proposed extension of the current version of the cantilever magnetometry technique. The extension is proposed to measure higher-order spatial moments of the supercurrent density pattern. In the schematic, a magnetic nanoparticle (red sphere with orange arrow) and line current $I(t)$ generates an applied magnetic field (red arrows) in the vicinity of the tip of a cantilever with large spatial gradients. The line current is depicted to be oscillatory in time, with the current directed into (indicated by a cross) and out of (indicated by a dot) the page. A cross section of the superconducting annulus is shown in dark blue. The vector $\boldsymbol{L}$ connects the point of intersection of the x'-axis and the axis of rotation with the origin of the stationary "primed" coordinates (See Fig. 11.2).

all components of the coefficient tensors $\boldsymbol{H}'^{(n)}$ are independent, e.g., the tensor $\boldsymbol{H}'^{(2)}$ is constrained to obey $H'^{(2)}_{ii} = 0$. As in Sec. 11.1, quantities defined in the stationary frame are given primes, while quantities defined in the rotating frame go unprimed (see Fig. 11.2). The applied magnetic field in the rotating frame, $\boldsymbol{H}(\boldsymbol{r})$, can be expressed in terms of the angle θ, the vector $\boldsymbol{L}$ (see Fig.11.7), and the applied field $\boldsymbol{H}'(\boldsymbol{r}')$ in the stationary frame, via

$$H_i(\boldsymbol{r}) = R^{-\boldsymbol{\theta}}_{ij} H'_j(\boldsymbol{R}^{\boldsymbol{\theta}}(\boldsymbol{L} + \boldsymbol{r}) - \boldsymbol{L}). \tag{11.30}$$

Similarly to the stationary frame, in the rotating frame we define $\boldsymbol{H}^{(n)}$ to be the coefficients of the Taylor expansion of $\boldsymbol{H}$ around the point $\boldsymbol{r} = 0$,

$$H_i(\boldsymbol{r}) \equiv H^{(1)}_i + H^{(2)}_{ij} r_j + \cdots . \tag{11.31}$$

If the spatial variation of the applied magnetic field has only a uniform and linearly varying term, then $\boldsymbol{H}^{(1)}$ and $\boldsymbol{H}^{(2)}$ are related to $\boldsymbol{H}'^{(1)}$ and $\boldsymbol{H}'^{(2)}$ via

$$H^{(1)}_i = R^{-\boldsymbol{\theta}}_{ij} H'^{(1)}_j + R^{-\boldsymbol{\theta}}_{ij} H'^{(2)}_{jk} (R^{\boldsymbol{\theta}}_{k\ell} - I_{k\ell}) L_\ell, \tag{11.32}$$

$$H^{(2)}_{ij} = R^{-\boldsymbol{\theta}}_{ik} H'^{(2)}_{k\ell} R^{\boldsymbol{\theta}}_{\ell j}. \tag{11.33}$$

We now derive an expression for the torque on the cantilever due to the superconducting particle. First, we note that the free energy of the superconductor depends upon the angle θ, via the dependence of $\boldsymbol{H}^{(n)}$ on θ.

$$F_{\rm SC}(\theta) = F_{\rm SC}(H^1_i(\theta), H^2_{ij}(\theta), \cdots). \tag{11.34}$$

The torque on the cantilever due to the superconductor is then of the form

$$\tau_{\rm SC} = -\frac{dF_{\rm SC}}{d\theta} = -\frac{\partial F_{\rm SC}}{\partial H^1_i}\frac{\partial}{\partial\theta} H^1_i(\theta) - \frac{\partial F_{\rm SC}}{\partial H^2_{ij}}\frac{\partial}{\partial\theta} H^2_{ij}(\theta) + \cdots , \tag{11.35}$$

which generalizes Eq. (11.4). Employing the thermodynamic relations,[5]

$$\begin{aligned} \frac{\partial F_{\rm SC}}{\partial H_i^{(1)}} &= \mu_i \\ \frac{\partial F_{\rm SC}}{\partial H_{ij}^{2}} &= \mu_{ij}^{(2)}, \\ &\vdots \quad , \end{aligned} \tag{11.36}$$

the torque can be expressed via the various orders of spatial moments of the supercurrent density via

$$\tau_{\rm SC} = -\mu_i \frac{\partial}{\partial\theta} H_i^1(\theta) - \mu_{ij}^2 \frac{\partial}{\partial\theta} H_{ij}^2(\theta) + \cdots . \tag{11.37}$$

Similarly to Sec. 11.1 we now express $\boldsymbol{H}^n$ and $\partial \boldsymbol{H}^{(n)}/\partial\theta$ as the sum of a temporally constant part and an oscillating part (in the rotating frame of the superconductor):

$$\boldsymbol{H}^{(n)} = \bar{\boldsymbol{H}}^{(n)} + \delta\boldsymbol{H}^{(n)}, \tag{11.38}$$

$$\frac{\partial}{\partial\theta}\boldsymbol{H}^{(n)}(\theta) = \boldsymbol{\zeta}^{(n)} + \delta\boldsymbol{\zeta}^{(n)}, \tag{11.39}$$

where the temporally oscillating parts $\delta\boldsymbol{H}^{(n)}$ and $\delta\boldsymbol{\zeta}^{(n)}$ can result from passive rotation effects or can be generated dynamically using oscillating applied fields and/or applied field gradients that are frequency locked to the oscillations of the cantilever. Using this notation the change in resonance frequency of the cantilever is then proportionally

$$\delta\omega \propto \sum_n \boldsymbol{\mu}^{(n)}\delta\boldsymbol{\zeta}^{(n)} + \sum_{nm} \frac{\partial\boldsymbol{\mu}^{(n)}}{\partial\boldsymbol{H}^{(m)}}\delta\boldsymbol{H}^{(m)}, \tag{11.40}$$

where for compactness we have suppressed the sum over tensor indices. We now derive an expression for the change in resonance frequency when the superconductor changes its

[5]These relations can be employed to express $\boldsymbol{\mu}^(n)$ in terms of spatial moments of $\boldsymbol{J}(\boldsymbol{r})$ using the following mnemonic: $\boldsymbol{\mu}^{(n)} = -\frac{\partial F}{\partial \boldsymbol{H}^{(n)}} = -\int d^3r \frac{\delta f}{\delta \boldsymbol{A}} \frac{\partial \boldsymbol{A}^H}{\partial \boldsymbol{H}^{(n)}}$, where $\delta f/\delta\boldsymbol{A} = \boldsymbol{J}$ and $A_i^H(\boldsymbol{r}) = -\epsilon_{ijk} r_j \left(\frac{1}{2}H_k^{(1)} + \frac{1}{3}r_\ell H_{k\ell}^{(2)} + \cdots\right)$ satisfies $\boldsymbol{\nabla}\times\boldsymbol{A}^H(\boldsymbol{r}) = \boldsymbol{H}(\boldsymbol{r})$.

fluxoid state. In the London regime, due to the free energy having only a linear coupling between n_θ and $\boldsymbol{H}$, a change in the fluxoid state of the superconductor affects a change in resonance frequency of the cantilever only via changes in the various moments $\boldsymbol{\mu}^{(n)}$ in the first summand of Eq. (3.11). In particular when the superconductor makes a transition between the $n_\theta = 0$ fluxoid state to either the $n_\theta = 1/2$ or $n_\theta = 1$ fluxoid state the change in resonance frequency of the cantilever is predicted to be in proportion to

$$\Delta\omega \propto \sum_n \Delta\boldsymbol{\mu}^{(n)} \delta\boldsymbol{\zeta}^{(n)}. \tag{11.41}$$

Here $\Delta\boldsymbol{\mu}^{(n)}$ are the changes in the n^{th} order spatial moment of the current distribution, which in the London regime, do not depend upon the applied field. Even though generating an arbitrary, well-controlled $\delta\boldsymbol{\zeta}^{(n)}$ represents quite an engineering challenge, it is important to emphasize that due to the "half" relationship between the changes in the spatial moments of the current distribution ${}^{(n_\theta=1/2)}\Delta\boldsymbol{\mu}^{(n)} =^{(n_\theta=1)} \Delta\boldsymbol{\mu}^{(n)}/2$ [Eq. (11.27)] for all orders n, for any constant configuration of $\delta\boldsymbol{\zeta}^(n)$, the prediction of the HQV scenario is that the "halving" relationship between the change in frequencies for the half integral (HI) and integer fluxoid (IF) states remains

$${}^{\text{HI}}\Delta\omega =^{\text{IF}} \Delta\omega/2. \tag{11.42}$$

Thus, by generating large temporally oscillating field gradients in the frame of the superconductor [e.g., by bringing the tip of the cantilever in close proximity to a magnetic nanoparticle or temporally oscillating line current (see Fig. 11.7)] it would be possible to test the HQV scenario in a stringent manner. This is because the relative ratios of the $\{\delta\boldsymbol{\zeta}^{(n)}\}$ would change as the position or orientation of cantilever tip is is translated or rotated relative to the source of applied magnetic field gradient. In contrast, if the HI state corresponds to a wall vortex of the type shown in Fig. 11.6 then ${}^{\text{HI}}\Delta\mu_{zz}$ would be predicted to be many times ${}^{\text{IF}}\Delta\mu_{zz}$. Then, as long as $\delta\zeta_{zz}$ has a sufficiently large component, the halving relationship between the frequency ${}^{\text{HI}}\Delta\omega$ and ${}^{\text{IF}}\Delta\omega$ would be violated, perhaps strongly.

Chapter 12

Concluding remarks

In Part I of this thesis we analyzed the properties of unconventional superconductors in which the superconducting state spontaneously breaks time-reversal symmetry and thus have the potential to exhibit domain walls that separate regions of opposing order-parameter chirality. By employing an extension of the well-known London limit of the superconducting state, we have formulated an effective theory in terms of the topological variables that describe vortices and domain walls of the order parameter. We have used this effective-theory formulation to show that localized near a bend in a domain wall through an angle Θ, there is an associated net magnetic flux $((\Theta/\pi) + n)\,\Phi_0$ (for some integer n)—provided the system can be taken to be rotationally invariant, crystallographically, about the z-axis. We have also shown that this result for the flux near a domain-wall bend holds more generally. Neither the London limit nor the regime of validity of the Ginzburg-Landau theory are required. Rather, it is sufficient for the following condition to hold: within regions of maximal chirality the two transformations, $\mathrm{SO}(2)_z$ rotations and U(1) gauge transformations of the superconducting order parameter, are degenerate transformations, in the sense that they have equivalent impacts on the state of the superconducting order.

We have addressed the issue of the relaxation of the assumption of crystallographic rotational invariance, and its replacement by discrete rotational invariance. In this situation we have found that the result for the bend flux continues to hold, but only for specific values of the bend angle, which are determined by the crystalline symmetry.

We have also sketched three candidate settings in which the interplay between chiral-domain-wall geometry and magnetic flux discussed might be observable, e.g., in experiments

using scanned probe magnetic imaging. We emphasize that the magnitude of the flux that is associated with a bend in a domain wall is fixed by symmetry, and is independent of the magnitude of the chiral-charge currents that are proposed to flow along the cores of domain walls. Thus, it is perhaps useful to regard such "bend flux" as providing a robust magnetic signature of domain walls, and hence the form of superconductivity that spontaneously breaks time-reversal symmetry. The analysis that we have presented may be of use in determining the existence and distribution of domain walls in various superconducting materials such as Sr_2RuO_4, and may thus be of use in resolving the question of whether superconductivity in Sr_2RuO_4 does indeed spontaneously break time-reversal symmetry.

In Part II of the thesis we have analyzed half quantum vortex (HQV) structures in the superconducting order parameter that can potentially exist in layered equal spin pairing superconductors. First, we studied the theoretical existence and stability of HQVs, finding that, in contrast to the case of bulk superfluid ^{3}He, HQVs can exist for "B" phases (which preserve time reversal symmetry) as well as for "A" phases (which break time reversal symmetry). As the local structure of an HQV can be described as a vortex of a spin-polarized p-wave superfluid (with electrons of the opposing spin being fully gapped), we expect HQVs for either the A or B phase to have bound quasi-particle states (numbering one per layer, but which may possibly hybridize) of the Majorana type. By analyzing the special case of an annular geometry, we have also established a more optimistic constraint on the geometries for which HQVs are potentially stabilized. Such analysis may be relevant for studies of the stability of HQVs in *networks* of superconducting Sr_2RuO_4 wires, which—due to recent advances in pulsed laser deposition growth of superconducting thin films of Sr_2RuO_4 [37]—may prove possible to fabricate.

We have also reviewed experiments that have recently been performed by the Budakian group on mesoscopic rings of Sr_2RuO_4 in which strong evidence for half integer fluxoid behavior was observed. Our theoretical analysis of such behavior focused on a comparison between the HQV and a wall vortex scenario. Whereas the wall vortex scenario is difficult

to constrain, we have argued that a fine-tuned set of assumptions is necessary to formulate a wall vortex scenario that is consistent with the observed properties of the half integer states, and thus a wall vortex scenario seems unlikely. In contrast, the robust halving of the magnetization steps, observed in multiple samples and for wide ranges of temperature and applied fields, follows naturally from the theoretical framework of HQVs. Although its origin remains unknown, we noted that the small in-plane moment $\mu_{\rm HI}$ that accompanies the half integer state was found to be of the same order of magnitude as that expected of the kinematic spin-polarization effect recently proposed by Vakaryuk [75]; alternatively we discussed in Sec. 11.2.2 that in-plane wall vortices are theoretically expected, and experimentally observed, to have in-plane moments 200 times as large as $\mu_{\rm HI}$.

In the final section of the thesis we have proposed an extension of the cantilever magnetometry technique that may enable the detection of higher-order spatial moments of the charge current density, which would provide further tests of the HQV and wall vortex scenarios. As in the experiments of the Budakian group an oscillating field of order 1 Oe generates a detectable change in resonance frequency when the fluxoid state makes a transition, a reasonable estimate is that a static field gradients of magnitude $(1\,{\rm Oe})/(1\,\mu{\rm m}\times\theta^{\rm max})\sim 10\,{\rm Oe/nm}$ (or an applied oscillating field gradient smaller by a factor of $\theta^{\rm max}$) would be necessary to detect higher order moments of the super current density.

Aside from their intrinsic interest, resolving the essential questions associated with the superconducting state of Sr_2RuO_4 and determining whether it is possible to stabilize HQVs in Sr_2RuO_4 would, *inter alia*, be valuable in assessing the utility of Sr_2RuO_4 for exhibiting Majorana modes, nonabelian physics and, potentially, the robustness with respect to decoherence that could prove useful for quantum information processing purposes.

Appendix

A: Free energy of a translationally invariant domain wall

In this appendix we use a variational approach to derive an estimate for the free energy per unit length $E_{\rm dw}$ of a translationally invariant domain wall, starting from the free energy $F_{\rm EL}$ (in the extended London limit), given in Eq. (4.22). (Similar calculations can be found throughout the literature; see, e.g., Refs. [76, 69, 70, 67, 45, 4, 10].) As we discussed in Sec. 4, $F_{\rm EL}$ contains two contributions: one, $f_{\rm core}$, due to the core energy of a domain wall, which we estimate variationally; and the other, the London term, that describes both the kinetic energy of supercurrents and the magnetic field energy. In order to express $f_{\rm core}$ compactly, we define $(\alpha_1, \alpha_2) = (\gamma, \beta)$, and thus $f_{\rm core}$ become

$$f_{\rm core} = \frac{1}{2}\nabla_a \alpha_i \Upsilon_{aibj} \nabla_b \alpha_j + \frac{1}{8L^2}\cos^2\beta, \tag{.1}$$

$$\begin{aligned}\Upsilon_{aicj} &:= \frac{1}{4} I_{ab} \begin{pmatrix} 4\cos^2\beta & 0 \\ 0 & 1-\mu^2\cos^2\beta - \frac{\tau^2}{4} \end{pmatrix}_{ij} \\ &- \frac{\tau\cos\beta}{8}\mathcal{M}^{\gamma-(\pi/4)}_{ab} \begin{pmatrix} 4 & 0 \\ 0 & 1-2\mu \end{pmatrix}_{ij} + \frac{\mu\sin 2\beta}{4} E_{ab}\, E_{ij},\end{aligned} \tag{.2}$$

where repeated indices $\{a, b, i, j\}$ are summed from 1 to 2. The approach taken in this appendix is to evaluate independently the two contributions to Eq. (4.22), expressing separately the variational estimate for the core energy per unit length $E_{\rm core}$ and the London energy per unit length $E_{\rm L}$, and then to add these contributions to determine $E_{\rm dw}$.

To derive the variational estimate, we make the following assumptions for the spatial dependence of the γ and β fields transverse to the domain wall: we take γ to be constant

and equal to Γ, and we take $\beta(x)$ to be equal to $\beta_\ell(x) := 2\tan^{-1}\tanh(x/2\ell)$, where ℓ is a variational parameter specifying the width of the domain wall. [To motivate the form β_ℓ, we note that for $(\mu,\tau) = (0,0)$ and γ constant, the term $f_{\rm core}$ reduces to $\frac{1}{8}|\boldsymbol{\nabla}\beta|^2 + \frac{L^{-2}}{8}\cos^2\beta$, and this form has the property of being stationary at $\beta_\ell(x)$, provided $\ell = L$.]

By using the variational assumptions for γ and β we obtain the following expressions for $E_{\rm core}$, which depends upon ℓ and Γ as well as the angle ϕ [which specifies the direction $\hat{\boldsymbol{n}} = (\cos\phi, \sin\phi)$ normal to the domain wall]:

$$E_{\rm core}(\Gamma,\phi,\ell) = \frac{1}{\ell}\left(\frac{\ell^2}{4L^2} + \frac{1}{4} - \frac{\mu^2}{6} - \frac{\tau^2}{16} + \left(\frac{\pi\,\mu\tau}{16} - \frac{\pi\,\tau}{32}\right)\cos(2(\Gamma-\phi))\right). \tag{.3}$$

By minimizing $E_{\rm core}$ with respect to ℓ, we see that, in the extended London limit (for which L tends to zero), the value of ℓ that makes $E_{\rm dw}$ stationary, would also tend to zero, provided the other energetic contribution, $E_{\rm L}$, does not force the stationary value of ℓ away from this result. To see that indeed $E_{\rm L}$ does not do this, using the same varriational assumptions for γ and β we examine $E_{\rm L}$ expressed as power series in ℓ to $\mathcal{O}(\ell^0)$:

$$E_{\rm L}(\Gamma,\phi,\ell) = \frac{1}{\ell}\left(\frac{\mu^2}{6} + \frac{\tau^2}{32} - \frac{\pi\,\mu\tau}{16}\cos 2(\Gamma-\phi) + \frac{\tau^2}{32}\cos 4(\Gamma-\phi) + \mathcal{O}(\ell)\right). \tag{.4}$$

Combining the two terms, $E_{\rm core}$ and $E_{\rm L}$, we arrive at the following variational expression for the free energy per unit length of a translationally invariant domain wall:

$$E_{\rm dw}(\Gamma,\phi,\ell) = \frac{1}{4\ell}\left(\frac{\ell^2}{L^2} + 1 - \frac{\tau^2}{8} - \frac{\pi\,\tau}{8}\cos 2(\Gamma-\phi) + \frac{\tau^2}{8}\cos 4(\Gamma-\phi) + \mathcal{O}(\ell)\right). \tag{.5}$$

By minimizing $E_{\rm dw}$ with respect to ℓ, and recalling that in the extended London limit L is small, we find the stationary value of ℓ to be proportional to L, consistent with the assumption, just made, that ℓ is also small in the extended London limit. Then, by replacing ℓ by its stationary value one obtains a value for $E_{\rm dw}$ having the following properties, some of which we make use in Sec. 5: (i) it depends on Γ and ϕ only through the combination

$\Gamma - \phi$ and is π periodic in this quantity; (ii) it is independent of μ (to leading order in L); and (iii) when $\tau \leq \pi/4$ the values of Γ that minimizes $\min_\ell E_{\rm dw}$ are $\phi + n\pi$ (for integer n).

Appendix

B: Free energy in terms of topological variables for the case of conventional superconductivity

To motivate the derivation of the effective free energy for the topological variables given in Sec. 4 of the main text, resulting in Eq. (4.22), we review in detail how it would proceed in the simpler setting of conventional superconductivity, and without employing the dual approach. For a conventional superconductor, the order parameter is the complex scalar field $\psi(\boldsymbol{r})$. We assume that, in the absence of a magnetic field, the system is translationally and rotationally invariant, and we consider magnetic fields that are oriented along the z direction and states of the superconductivity that are homogeneous in the z direction. In addition, we work with dependent and independent variables that have been rendered dimensionless via the rescalings given in Sec. 2.

With these assumptions we begin this derivation with the Ginzburg-Landau free energy per unit length of sample

$$F[\psi, \boldsymbol{A}, \boldsymbol{H}] := \frac{1}{2}\int d^2r \left(|(\boldsymbol{\nabla} - i\boldsymbol{A})\psi)|^2 + \frac{\kappa^2}{2}(|\psi|^2 - 1)^2 + |(\boldsymbol{\nabla}\times\boldsymbol{A}) - \boldsymbol{H}|^2 \right). \tag{.1}$$

In the London limit, in which $\kappa \to \infty$, the potential terms of this free energy fix the magnitude of ψ to be unity. Then, ψ can be parametrized via a U(1) phase field $\theta(\boldsymbol{r})$, so that $\psi(\boldsymbol{r}) \to \exp i\theta(\boldsymbol{r})$. Making this replacement in the free energy, we obtain the London form of the free energy, i.e.,

$$\frac{1}{2}\int d^2r \left(|\boldsymbol{\nabla}\theta - \boldsymbol{A}|^2 + |(\boldsymbol{\nabla}\times\boldsymbol{A}) - \boldsymbol{H}|^2 \right). \tag{.2}$$

The two terms in the London free energy can be regarded as frustrating one another, energetically, as they impose competing demands on the $\boldsymbol{A}$ field. The first term favors the transverse (i.e., divergence-free) part of $\boldsymbol{A}$ to be zero, the θ field can compensating for any longitudinal (i.e., curl-free) part; in contrast, the second term favors the transverse part of $\boldsymbol{A}$ to be nonzero.

For Type II superconductors at magnetic fields above the lower critical field, a partial resolution to this frustration comes from the introduction of vortices, which alter the structure of the θ field: θ becomes multi-valued, and is singular in the cores of the vortices. In particular, the expression $\boldsymbol{\nabla}\theta$ is not curl free and, correspondingly, has a transverse part.

To derive the effective free energy in terms of the appropriate topological variables (in this case, the density of vortices) one now decomposes the θ field into a smooth, single-valued part $\theta_{\rm sm}$ and a part $\theta_{\rm v}$ that contains the vortex singularities, so that $\theta = \theta_{\rm sm} + \theta_{\rm v}$. Next, one seeks to eliminate $\theta_{\rm sm}$ from the free energy by setting it to the value that makes the free energy stationary. As the only term in the free energy that depends on $\theta_{\rm sm}$ is the one corresponding to the kinetic energy of the supercurrents [i.e., the former term in Eq. (.2)], for the issue of stationarity one need only consider this term. Expanding it and integrating by parts, gives

$$\int d^2r \left(\frac{1}{2}\theta_{\rm sm}(-\nabla^2)\theta_{\rm sm} - \theta_{\rm sm}\boldsymbol{\nabla}\cdot(\boldsymbol{\nabla}\theta_{\rm v} - \boldsymbol{A}) + \frac{1}{2}|\boldsymbol{\nabla}\theta_{\rm v} - \boldsymbol{A}|^2 \right). \tag{.3}$$

Then, using the Green function for the Laplacian in two dimensions, which obeys $-\nabla^2 G(\boldsymbol{r}) = \delta(\boldsymbol{r})$ and reads $G(\boldsymbol{r}) = -(2\pi)^{-1}\ln|\boldsymbol{r}|$, one finds that at stationarity $\theta_{\rm sm}$ is given by

$$\bar{\theta}_{\rm sm}(\boldsymbol{r}') = -\int d^2r\, G(\boldsymbol{r}'-\boldsymbol{r})\boldsymbol{\nabla}\cdot\big(\boldsymbol{\nabla}\theta_{\rm v}(\boldsymbol{r}) - \boldsymbol{A}(\boldsymbol{r})\big). \tag{.4}$$

By inserting $\bar{\theta}_{\rm sm}$ into Eq. (.3) and using the defining equation for $G(\boldsymbol{r})$ to express the last

term of Eq. (.3) in terms of G, one obtains for the kinetic energy of the supercurrent

$$\frac{1}{2}\int d^2r\, d^2r' \Big(\; - \; \Big(\nabla_a(\nabla_a\theta_{\rm v} - A_a)(\boldsymbol{r})\Big)\, G(\boldsymbol{r}-\boldsymbol{r}')\Big(\nabla'_b(\nabla'_b\theta_{\rm v} - A_a)(\boldsymbol{r}')\Big) \\ + \; \Big((\nabla_a\theta_{\rm v} - A_a)(\boldsymbol{r})\Big)\Big(-\nabla^2 G(\boldsymbol{r}-\boldsymbol{r}')\Big)\Big((\nabla'_a\theta_{\rm v} - A_a)(\boldsymbol{r}')\Big)\Big). \qquad (.5)$$

The two terms in this equation have similar structure, and integration by parts allows them to be expressed as

$$\frac{1}{2}\int d^2r\, d^2r' \Big(I_{ab}I_{cd} - I_{ad}I_{bc}\Big)\Big(\nabla_a\theta_{\rm v} - A_a\Big)(\boldsymbol{r})\, \Big(\nabla_b\nabla_c G(\boldsymbol{r}-\boldsymbol{r}')\Big)\, \Big(\nabla'_d\theta_{\rm v} - A_d)(\boldsymbol{r}')\Big) \qquad (.6)$$

Next, by using the elementary tensor identity

$$I_{ab}\, I_{cd} - I_{ad}\, I_{bc} = E_{ac}\, E_{bd} \qquad (.7)$$

and integrating by parts, the suprcurrent kinetic energy becomes

$$\frac{1}{2}\int d^2r\, d^2r' \left(E_{ab}\, \Big(\nabla_a(\nabla_b\theta_{\rm v} - A_a)(\boldsymbol{r})\Big)\, G(\boldsymbol{r}-\boldsymbol{r}')\, E_{cd}\, \Big(\nabla'_c(\nabla'_d\theta_{\rm v} - A_a)(\boldsymbol{r}')\Big)\right). \qquad (.8)$$

This form shows that the elimination of the smooth part of θ creates a long-ranged interaction for the curl of $\boldsymbol{\nabla}\theta_{\rm v} - \boldsymbol{A}$. This free energy can readily be shown to be equivalent to Eq. (4.11), and thus to describe the kinetic energy of the transverse part of the supercurrent. Equation (.8) features the curl of the gradient of the multi-valued function $\theta_{\rm v}$, which is a combination that isolates the δ-function contributions from the singularities in the vortex cores, so that

$$E_{ab}\nabla_a\nabla_b\theta_{\rm v} = 2\pi\, \rho_{\rm v}, \qquad (.9)$$

where $\rho_{\rm v}(\boldsymbol{r}) := \sum q_\nu \delta(\boldsymbol{r} - \boldsymbol{R}_\nu)$ defines the vortex density in terms of the vortex locations $\{\boldsymbol{R}_\nu\}$ and vorticity $\{q_\nu\}$. In particular, one sees that owing to the vortices the gradient of θ

can posses a transverse part, and this can partially relieve the frustration of $\boldsymbol{A}$ inherent in the London free energy.

To proceed further with the derivation of the effective free energy in terms of vortex variables, one now considers the full London free energy, Eq. (.2), which, in terms of the total magnetic field $B = E_{ab}\nabla_a A_b$, reads

$$\frac{1}{2}\int d^2r\, d^2r'\, (2\pi\rho_{\rm v} - B)(\boldsymbol{r})\, G(\boldsymbol{r}-\boldsymbol{r}')\, (2\pi\rho_{\rm v} - B)(\boldsymbol{r}') + \frac{1}{2}\int d^2r\, (B-H)^2. \quad (.10)$$

Note that we have omitted a constant contribution resulting from the suppression of the magnitude of the order parameter within the core of each vortex, as it is negligibly small, relative to the kinetic and field energies, in the London limit.

The next step is to eliminate the magnetic field from the free energy by setting it to its stationary value $\bar{B}$ which, from Eq. (.10), one sees is

$$\bar{B}(\boldsymbol{r}) = \int d^2r' \left(G+\delta\right)^{-1}(\boldsymbol{r}-\boldsymbol{r}') \left(H(\boldsymbol{r}') + 2\pi\int d^2r''\, G(\boldsymbol{r}'-\boldsymbol{r}'')\,\rho(\boldsymbol{r}'')\right), \quad (.11)$$

where $\left(G+\delta\right)^{-1}(\boldsymbol{r}-\boldsymbol{r}')$ is the inverse of the kernel $G(\boldsymbol{r}-\boldsymbol{r}') + \delta(\boldsymbol{r}-\boldsymbol{r}')$. It is convenient to adopt a schematic notation in which one suppresses integral signs and dependences on spatial variables, in which case the result for $\bar{B}$ reads

$$\bar{B} = (G+\delta)^{-1}(H + 2\pi\, G\,\rho). \quad (.12)$$

Replacing B by $\bar{B}$ in Eq. (.10) then yields the following expression for the free energy:

$$\frac{1}{2}\Big((2\pi\rho)\left(G - G(G+\delta)^{-1}G\right)(2\pi\rho) + H\left(\delta - (G+\delta)^{-1}\right)H \\ -H(G+\delta)^{-1}G(2\pi\rho) - (2\pi\rho)G(G+\delta)^{-1}H\Big). \quad (.13)$$

It is straightforward to see that each of the four integral kernels in this formula is the Green

function for the Helmholtz operator in two dimensions, which obeys $(-\nabla^2 + 1)\mathcal{G}(\boldsymbol{r}) = \delta(\boldsymbol{r})$, and is given by $\mathcal{G}(\boldsymbol{r}) = (2\pi)^{-1} K_0(|\boldsymbol{r}|)$, where $K_0(x)$ is a modified Bessel function. To exemplify this one can apply the following elementary manipulations to the kernel of the first term:

$$G - G(G+\delta)^{-1}\, G = G\left(\delta - \big(-\nabla^2(G+\delta)\big)^{-1}\right) = G\left((-\nabla^2+\delta)\mathcal{G} - \mathcal{G}\right) = G\left(-\nabla^2\right)\mathcal{G} = \mathcal{G} \tag{.14}$$

By similarly simplifying the remaining kernels in Eq. (.13) one completes the derivation of the effective free energy in terms of the vortex density $\rho_{\rm v}$ and the applied field H, arriving at the result

$$\frac{1}{4\pi}\int d^2r\, d^2r' \left(2\pi\rho_{\rm v} - H\right)(\boldsymbol{r})\, K_0(|\boldsymbol{r}-\boldsymbol{r}'|)\left(2\pi\rho_{\rm v} - H\right)(\boldsymbol{r}'), \tag{.15}$$

which is the analog for conventional superconductivity of the unconventional superconductivity formula Eq. (4.22).

References

[1] A. A. Abrikosov. On the lower critical field of thin layers of superconductors of the 2nd group. *JETP*, 19(4):988–991, 1964.

[2] J. F. Annett, B. L. Gyrffy, G. Litak, and K. I. Wysokiski. Magnetic field induced rotation of the d -vector in the spin-triplet superconductor Sr_2RuO_4. *Phys. Rev. B*, 78(5):054511, 2008.

[3] R. M. Arutunian and G. F. Zharkov. Behavior of a hollow superconducting cylinder in a magnetic field. *J. Low Temp. Phys.*, 52(5):409–431, 1983.

[4] P. E. C. Ashby and C. Kallin. Suppression of spontaneous supercurrents in a chiral p -wave superconductor. *Phys. Rev. B*, 79(22):224509, 2009.

[5] E. Babaev, A. Sudbo, and N. W. Ashcroft. A superconductor to superfluid phase transition in liquid metallic hydrogen. *Nature*, 431(7009):666–668, 2004.

[6] J. Bardeen, L. N. Cooper, and J. R. Schrieffer. Theory of superconductivity. *Phys. Rev.*, 108(5):1175, 1957.

[7] C. Bergemann, S. R. Julian, A. P. Mackenzie, S. NishiZaki, and Y. Maeno. Detailed topography of the fermi surface of Sr_2RuO_4. *Phys. Rev. Lett.*, 84(12):2662, 2000.

[8] P. G. Björnsson, Y. Maeno, M. E. Huber, and K. A. Moler. Scanning magnetic imaging of Sr_2RuO_4. *Phys. Rev. B*, 72(1):012504, 2005.

[9] H. Bluhm. Magnetic fields above the surface of a superconductor with internal magnetism. *Phys. Rev. B*, 76(14):144507, 2007.

[10] A. Bouhon and M. Sigrist. Influence of the domain walls on the josephson effect in Sr_2RuO_4. *N. Jo. Phys.*, 12(4):043031, 2010.

[11] S. B. Chung, H. Bluhm, and E.-A. Kim. Stability of half-quantum vortices in px+ipy superconductors. *Phys. Rev. Lett.*, 99(19):197002, 2007.

[12] M. C. Cross and W. F. Brinkman. Textural singularities in the superfluid A phase of ^{3}He. *J. Low Temp. Phys.*, 27(5):683–686, 1977.

[13] K. Deguchi, Z. Q. Mao, H. Yaguchi, and Y. Maeno. Gap structure of the spin-triplet superconductor Sr_2RuO_4 determined from the field-orientation dependence of the specific heat. *Phys. Rev. Lett.*, 92(4):047002, 2004.

[14] Vollhardt Dieter and P. Wlfle. *The superfluid phases of helium 3*. Taylor and Francis, New York, 1990.

[15] V. O. Dolocan, P. Lejay, D. Mailly, and K. Hasselbach. Observation of two species of vortices in the anisotropic spin-triplet superconductor Sr_2RuO_4. *Phys. Rev. B*, 74(14):144505, 2006.

[16] V. O. Dolocan, C. Veauvy, F. Servant, P. Lejay, K. Hasselbach, Y. Liu, and D. Mailly. Observation of vortex coalescence in the anisotropic spin-triplet superconductor Sr_2RuO_4. *Phys. Rev. Lett.*, 95(9):097004, 2005.

[17] D. S. Dummit and R. M. Foote. *Abstract algebra*. Wiley, Hoboken, NJ, 3rd edition, 2004.

[18] V. B. Geshkenbein, A. I. Larkin, and A. Barone. Vortices with half magnetic flux quanta in "heavy-fermion" superconductors. *Phys. Rev. B*, 36(1):235, 1987.

[19] V. Ginzburg and L. Landau. Phenomenological theory of superconductivity. *Zh. Eksper. Teor. Fiz*, 20:1064, 1950.

[20] E. Grosfeld, B. Seradjeh, and S. Vishveshwara. Proposed aharonov-casher interference measurement of non-abelian vortices in chiral p-wave superconductors. *Phys. Rev. B*, 83(10):104513, 2011.

[21] M. W. Haverkort, I. S. Elfimov, L. H. Tjeng, G. A. Sawatzky, and A. Damascelli. Strong spin-orbit coupling effects on the fermi surface of Sr_2RuO_4 and Sr_2RhO_4. *Phys. Rev. Lett.*, 101(2):026406, 2008.

[22] R. Heeb and D. F. Agterberg. Ginzburg-landau theory for a p-wave Sr_2RuO_4 superconductor: Vortex core structure and extended london theory. *Phys. Rev. B*, 59(10):7076, 1999.

[23] C. W. Hicks, J. R. Kirtley, T. M. Lippman, N. C. Koshnick, M. E. Huber, Y. Maeno, W. M. Yuhasz, M. B. Maple, and K. A. Moler. Limits on superconductivity-related magnetization in Sr_2RuO_4 and $PrOs_4Sb_{12}$ from scanning squid microscopy. *Phys. Rev. B*, 81(21):214501, 2010.

[24] M. Ichioka, Y. Matsunaga, and K. Machida. Magnetization process in a chiral p -wave superconductor with multidomains. *Phys. Rev. B*, 71(17):172510, 2005.

[25] K. Ishida, H. Mukuda, Y. Kitaoka, K. Asayama, Z. Q. Mao, Y. Mori, and Y. Maeno. Spin-triplet superconductivity in Sr_2RuO_4 identified by ^{17}O knight shift. *Nature*, 396(6712):658–660, 1998.

[26] D. A. Ivanov. Non-abelian statistics of half-quantum vortices in p-wave superconductors. *Phys. Rev. Lett.*, 86(2):268, 2001.

[27] Y. A. Izyumov and V. M. Laptev. Vortex structure in superconductors with a many-component order parameter. *Phase Transitions*, 20(1-2):95–112, 1990.

[28] R. Jackiw and C. Rebbi. Solitons with fermion number 1/2. *Phys. Rev. D*, 13(12):3398, 1976.

[29] J. Jang, R. Budakian, and Y. Maeno. Phase-locked cantilever magnetometry. *Applied Physics Letters*, 98(13):132510–3, 2011.

[30] J. Jang, D. G. Ferguson, V. Vakaryuk, R. Budakian, S. B. Chung, P. M. Goldbart, and Y. Maeno. Observation of half-height magnetization steps in Sr_2RuO_4. *Science*, 331(6014):186–188, 2011.

[31] C. Kallin and A. J. Berlinsky. Is Sr_2RuO_4 a chiral p-wave superconductor? *J. Phys. Cond. Mat.*, 21(16):164210, 2009.

[32] F. Kidwingira, J. D. Strand, D. J. Van Harlingen, and Y. Maeno. Dynamical superconducting order parameter domains in Sr_2RuO_4. *Science*, 314(5803):1267–1271, 2006.

[33] J. R. Kirtley, C. Kallin, C. W. Hicks, E. A. Kim, Y. Liu, K. A. Moler, Y. Maeno, and K. D. Nelson. Upper limit on spontaneous supercurrents in Sr_2RuO_4. *Phys. Rev. B*, 76(1):014526, 2007.

[34] A. Y. Kitaev. Fault-tolerant quantum computation by anyons. *Ann. Phys. (NY)*, 303(1):2–30, 2003.

[35] S. Kittaka, H. Taniguchi, S. Yonezawa, H. Yaguchi, and Y. Maeno. Higher- tc superconducting phase in Sr_2RuO_4 induced by uniaxial pressure. *Phys. Rev. B*, 81(18):180510, 2010.

[36] N. B. Kopnin and M. M. Salomaa. Mutual friction in superfluid ^{3}He: Effects of bound states in the vortex core. *Phys. Rev. B*, 44(17):9667, 1991.

[37] Y. Krockenberger, M. Uchida, K. S. Takahashi, M. Nakamura, M. Kawasaki, and Y. Tokura. Growth of superconducting Sr_2RuO_4 thin films. *Applied Physics Letters*, 97(8):082502–3, 2010.

[38] H.-J. Kwon, V. M. Yakovenko, and K. Sengupta. How to detect edge electron states in $(TMTSF)_2X$ and Sr_2RuO_4 experimentally. *Synthetic Metals*, 133-134:27–31, 2003.

[39] L. D. Landau and E. M. Lifshitz. *Quantum mechanics : non-relativistic theory*. Pergamon Press, New York, 3rd edition, 1977.

[40] L. D. Landau, E. M. Lifshitz, and L. P. Pitaevskii. *Electrodynamics of continuous media*. Course of theoretical physics. Pergamon, New York, 2nd edition, 1984.

[41] A. J. Leggett. Inequalities, instabilities, and renormalization in metals and other fermi liquids. *Ann. Phys. (NY)*, 46(1):76–113, 1968.

[42] A. J. Leggett. A theoretical description of the new phases of liquid ^{3}He. *Rev. Mod. Phys.*, 47(Copyright (C) 2010 The American Physical Society):331, 1975.

[43] A. J. Leggett. *Quantum liquids : Bose condensation and Cooper pairing in condensed-matter systems*. Oxford University Press, New York, 2006.

[44] A. J. Leggett. The ubiquity of superconductivity. *Annual Review of Condensed Matter Physics*, 2(1):11–30, 2011.

[45] N. A. Logoboy and E. B. Sonin. Domain walls in a tetragonal chiral p -wave superconductor. *Phys. Rev. B*, 79(9):094511, 2009.

[46] F. London. *Superfluids*. Dover, New York, 2nd edition, 1961.

[47] F. London and H. London. The electromagnetic equations of the supraconductor. *Proc. R. Soc. Lond. A*, 149:71–88, 1935.

[48] G. M. Luke, Y. Fudamoto, K. M. Kojima, M. I. Larkin, J. Merrin, B. Nachumi, Y. J. Uemura, Y. Maeno, Z. Q. Mao, Y. Mori, H. Nakamura, and M. Sigrist. Time-reversal symmetry-breaking superconductivity in Sr_2RuO_4. *Nature*, 394(6693):558–561, 1998.

[49] A. P. Mackenzie and Y. Maeno. The superconductivity of Sr_2RuO_4 and the physics of spin-triplet pairing. *Rev. Mod. Phys.*, 75(2):657, 2003.

[50] Y. Maeno, K. Yoshida, H. Hashimoto, S. Nishizaki, S. i. Ikeda, M. Nohara, T. Fujita, A. Mackenzie, nbsp, P, N. Hussey, E, J. Bednorz, Georg, and F. Lichtenberg. Two-dimensional fermi liquid behavior of the superconductor Sr_2RuO_4. *J. Phys. Soc. Jpn.*, 66(5):1405, 1997.

[51] Z. Q. Mao, Y. Maeno, S. NishiZaki, T. Akima, and T. Ishiguro. In-plane anisotropy of upper critical field in Sr_2RuO_4. *Phys. Rev. Lett.*, 84(5):991, 2000.

[52] M. Matsumoto and M. Sigrist. Quasiparticle states near the surface and the domain wall in a px $\pm$ i py-wave superconductor. *J. Phys. Soc. Jpn.*, 68(3):994, 1999.

[53] N. D. Mermin. The topological theory of defects in ordered media. *Rev. Mod. Phys.*, 51(3):591, 1979.

[54] V. P. Mineev and K. V. Samokhin. *Introduction to unconventional superconductivity*. Gordon and Breach, Amsterdam, 1999.

[55] H. Murakawa, K. Ishida, K. Kitagawa, H. Ikeda, Z. Q. Mao, and Y. Maeno. ^{101}Ru knight shift measurement of superconducting Sr_2RuO_4 under small magnetic fields parallel to the RuO_2 plane. *J. Phys. Soc. Jpn.*, 76:024716, 2007.

[56] H. Murakawa, K. Ishida, K. Kitagawa, Z. Q. Mao, and Y. Maeno. Measurement of the ^{101}Ru-knight shift of superconducting Sr_2RuO_4 in a parallel magnetic field. *Phys. Rev. Lett.*, 93(16):167004, 2004.

[57] C. Nayak, S. H. Simon, A. Stern, M. Freedman, and S. Das Sarma. Non-abelian anyons and topological quantum computation. *Rev. Mod. Phys.*, 80(3):1083, 2008.

[58] K. D. Nelson, Z. Q. Mao, Y. Maeno, and Y. Liu. Odd-parity superconductivity in Sr_2RuO_4. *Science*, 306(5699):1151–1154, 2004.

[59] A. M. Polyakov. *Gauge fields and strings*. Harwood Academic Publishers, New York, 1987.

[60] S. Raghu, A. Kapitulnik, and S. A. Kivelson. Hidden quasi-one-dimensional superconductivity in Sr_2RuO_4. *Phys. Rev. Lett.*, 105(13):136401, 2010.

[61] Y. Ran, Y. Zhang, and A. Vishwanath. One-dimensional topologically protected modes in topological insulators with lattice dislocations. *Nat. Phys.*, 5(4):298–303, 2009.

[62] N. Read and D. Green. Paired states of fermions in two dimensions with breaking of parity and time-reversal symmetries and the fractional quantum hall effect. *Phys. Rev. B*, 61(15):10267, 2000.

[63] T. M. Rice and M. Sigrist. Sr_2RuO_4: an electronic analogue of ^{3}He? *J. Phys. Cond. Mat.*, 7(47):L643, 1995.

[64] S. Das Sarma, C. Nayak, and S. Tewari. Proposal to stabilize and detect half-quantum vortices in strontium ruthenate thin films: Non-abelian braiding statistics of vortices in a px + i py superconductor. *Phys. Rev. B*, 73(22):220502, 2006.

[65] J. A. Sauls and M. Eschrig. Vortices in chiral, spin-triplet superconductors and superfluids. *N. Jo. Phys.*, 11(7):075008, 2009.

[66] K. Sengupta, H.-J. Kwon, and V. M. Yakovenko. Edge states and determination of pairing symmetry in superconducting Sr_2RuO_4. *Phys. Rev. B*, 65(10):104504, 2002.

[67] M. Sigrist and D. F. Agterberg. The role of domain walls on the vortex creep dynamics in unconventional superconductors. *Prog. Theor. Phys.*, 102(5):965, 1999.

[68] M. Sigrist, D. B. Bailey, and R. B. Laughlin. Fractional vortices as evidence of time-reversal symmetry breaking in high-temperature superconductors. *Phys. Rev. Lett.*, 74(16):3249, 1995.

[69] M. Sigrist, T. M. Rice, and K. Ueda. Low-field magnetic response of complex superconductors. *Phys. Rev. Lett.*, 63(16):1727, 1989.

[70] M. Sigrist and K. Ueda. Phenomenological theory of unconventional superconductivity. *Rev. Mod. Phys.*, 63(2):239, 1991.

[71] M. Stone and P. M. Goldbart. *Mathematics for physics : a guided tour for graduate students*. Cambridge University Press, New York, 2009.

[72] W. P. Su, J. R. Schrieffer, and A. J. Heeger. Soliton excitations in polyacetylene. *Phys. Rev. B*, 22(4):2099, 1980.

[73] T. A. Tokuyasu, D. W. Hess, and J. A. Sauls. Vortex states in an unconventional superconductor and the mixed phases of UPt_3. *Phys. Rev. B*, 41(13):8891, 1990.

[74] V. Vakaryuk. *Some properties of the magnetic response of mesoscopic superconducting rings*. PhD thesis, University of Illinois, Urbana-Champaign, 2010.

[75] V. Vakaryuk and A. J. Leggett. Spin polarization of half-quantum vortex in systems with equal spin pairing. *Phys. Rev. Lett.*, 103(5):057003, 2009.

[76] G. Volovik and L. Gor'kov. Superconducting classes in heavy-fermion systems. *JETP*, 61:843, 1985.

[77] G. E. Volovik. Monopoles and fractional vortices in chiral superconductors. *Proc. Nat. Acad. Sci. USA*, 97(6):2431–2436, 2000.

[78] G. E. Volovik and L. P. Gor'kov. An unusual superconductivity in UBe_{13}. *JETP Letters*, 39(12):674, 1984.

[79] G. E. Volovik and M. V.P. Line and point singularities in superfluid ^{3}He. *JETP Letters*, 24(11):561, 1976.

[80] J. Xia, Y. Maeno, P. T. Beyersdorf, M. M. Fejer, and A. Kapitulnik. High resolution polar kerr effect measurements of Sr_2RuO_4: Evidence for broken time-reversal symmetry in the superconducting state. *Phys. Rev. Lett.*, 97(16):167002, 2006.

[81] C. N. Yang. Concept of off-diagonal long-range order and the quantum phases of liquid he and of superconductors. *Rev. Mod. Phys.*, 34(4):694, 1962.

[82] K. Yoshida, Y. Maeno, S. Nishizaki, and T. Fujita. Anisotropic superconductivity of Sr_2RuO_4. *Physica C: Superconductivity*, 263(1-4):519–522, 1996.

[83] Y. Yoshioka and K. Miyake. Pairing mechanism and anisotropy of d-vector of spin-triplet superconductor Sr_2RuO_4. *J. Phys. Soc. Jpn.*, 78(7):074701, 2009.

[84] A. Zee. *Quantum field theory in a nutshell*. Princeton University Press, Princeton, 2003.

[85] J.-X. Zhu, C. S. Ting, J. L. Shen, and Z. D. Wang. Ginzburg-landau equations for layered p-wave superconductors. *Phys. Rev. B*, 56(21):14093, 1997.